scientific data

Check for updates

OPEN

DATA DESCRIPTOR

The PhanSST global database of Phanerozoic sea surface temperature proxy data

Emily J. Judd[1]✉, Jessica E. Tierney[2], Brian T. Huber[1], Scott L. Wing[1], Daniel J. Lunt[3], Heather L. Ford[4], Gordon N. Inglis[5], Erin L. McClymont[6], Charlotte L. O'Brien[7], Ronnakrit Rattanasriampaipong[8], Weimin Si[9], Matthew L. Staitis[10], Kaustubh Thirumalai[2], Eleni Anagnostou[11], Margot J. Cramwinckel[5,12], Robin R. Dawson[13], David Evans[14], William R. Gray[15], Ethan L. Grossman[16], Michael J. Henehan[17], Brittany N. Hupp[18], Kenneth G. MacLeod[19], Lauren K. O'Connor[20], Maria Luisa Sánchez Montes[21], Haijun Song[22] & Yi Ge Zhang[8]

Paleotemperature proxy data form the cornerstone of paleoclimate research and are integral to understanding the evolution of the Earth system across the Phanerozoic Eon. Here, we present PhanSST, a database containing over 150,000 data points from five proxy systems that can be used to estimate past sea surface temperature. The geochemical data have a near-global spatial distribution and temporally span most of the Phanerozoic. Each proxy value is associated with consistent and queryable metadata fields, including information about the location, age, and taxonomy of the organism from which the data derive. To promote transparency and reproducibility, we include all available published data, regardless of interpreted preservation state or vital effects. However, we also provide expert-assigned diagenetic assessments, ecological and environmental flags, and other proxy-specific fields, which facilitate informed and responsible reuse of the database. The data are quality control checked and the foraminiferal taxonomy has been updated. PhanSST will serve as a valuable resource to the paleoclimate community and has myriad applications, including evolutionary, geochemical, diagenetic, and proxy calibration studies.

[1]Smithsonian National Museum of Natural History, Department of Paleobiology, Washington, DC, 20560, USA. [2]University of Arizona, Department of Geosciences, Tuscon, AZ, 85721, USA. [3]University of Bristol, School of Geographical Sciences, Bristol, BS8 1SS, UK. [4]Queen Mary University of London, School of Geography, London, E1 4NS, UK. [5]University of Southampton, School of Ocean and Earth Science, National Oceanography Centre Southampton, Southampton, SO14 3ZH, UK. [6]Durham University, Department of Geography, Durham, DH1 3LE, UK. [7]University College London, Department of Geography, London, WC1E 6BT, UK. [8]Texas A&M University, Department of Oceanography, College Station, TX, 77843, USA. [9]Brown University, Department of Earth, Environmental and Planetary Sciences, Providence, RI, 02912, USA. [10]University of Edinburgh, School of Geosciences, Edinburgh, EH8 9XP, UK. [11]GEOMAR Helmholtz Centre for Ocean Research Kiel, 24148, Kiel, Germany. [12]Utrecht University, Department of Earth Sciences, Utrecht, 3584 CB, The Netherlands. [13]University of Massachusetts Amherst, Department of Geosciences, Amherst, MA, 01003, USA. [14]Goethe University Frankfurt, Institute of Geosciences, 60438, Frankfurt am Main, Germany. [15]Université Paris-Saclay, Laboratoire des Sciences du Climat et de l'Environnement, Gif-sur-Yvette, France. [16]Texas A&M University, Department of Geology and Geophysics, College Station, TX, 77843, USA. [17]GFZ German Research Centre for Geosciences, Section 3.3 Earth Surface Geochemistry, 14473, Potsdam, Germany. [18]Oregon State University, College of Earth, Ocean and Atmospheric Sciences, Corvallis, OR, 97331, USA. [19]University of Missouri, Department of Geological Sciences, Columbia, MO, 65211, USA. [20]University of Manchester, Department of Earth and Environmental Sciences, Manchester, M13 9PL, UK. [21]University of East Anglia, School of Environmental Sciences, Norwich, NR4 7TJ, UK. [22]China University of Geosciences, State Key Laboratory of Biogeology and Environmental Geology, School of Earth Sciences, Wuhan, 430074, China. ✉e-mail: ejjudd@syr.edu

Background & Summary

Geochemical proxy temperature data from ancient oceans are a key component of paleoclimate research[1–3]. High-resolution paleotemperature data from a single site can identify both long-term[4,5] and orbital-scale[6,7] climate variability, while multi-site comparisons from a given time slice provide insight into the spatial patterns of past climate change[8–12]. Additionally, such data are essential for validating Earth system models (ESMs)[13–16] and provide critical context for first-order temporal trends in other aspects of the Earth system, including evolution[17,18], geochemical cycling[19,20], and tectonics[21,22]. While single-proxy data sets that span the Phanerozoic[23–25] and multi-proxy compilations for select time slices[8–10,15] exist, a comprehensive, multi-proxy database of temperature data spanning the Phanerozoic has yet to be published.

PhanSST, a database of sea surface temperature (SST) proxy data spanning the Phanerozoic Eon, seeks to fill this gap. The compilation currently contains 150,691 discrete proxy values, which can be used to estimate past SST. These data come from five different proxies, amassed from 660 references, and represent more than 1,600 unique sampling locations. Each proxy value is associated with a suite of consistent and queryable metadata fields, and the database is available in a machine-readable format. To the best of our knowledge, this is the largest compilation of Phanerozoic paleotemperature proxy data to date. Our intention is to make PhanSST a living database, growing, improving, and evolving through time. Accordingly, we encourage the paleoclimate community to contribute their published data to the compilation going forward.

In addition to the initial purpose of the compilation outlined below, PhanSST is an invaluable resource to the paleoclimate community and can be used for a wide range of additional applications, including evolutionary and geochemical studies. The spatial and temporal reach of PhanSST facilitates paleoclimatic syntheses, including studies investigating climate sensitivity, the biotic and geochemical impacts of climate change, and the mechanisms driving large-scale global climate. The data are presented in their native proxy units, which permits flexibility in the choice of calibration model and additionally enables the compilation to be used in proxy calibration studies. Further, PhanSST includes data from known and suspected diagenetically altered material, with both expert-assigned binary diagenesis flags and additional metadata fields, allowing the database to be used in research investigating spatial and temporal trends in preservation.

Version 0.0.1 of PhanSST is presented in a tabular (csv) format. A static copy of Version 0.0.1 is archived in the NOAA-NCEI Paleoclimatology Database (https://www.ncei.noaa.gov/access/paleo-search/study/36813)[26], and dynamic versions of the most recent release can be found on Zenodo (https://doi.org/10.5281/zenodo.7049233)[27] and at the PhanSST website (https://www.paleo-temperature.org). In the following sections, we provide information regarding the data sources and selection criteria, review the definitions and decision-making behind the metadata fields associated with each proxy measurement, and outline the quality control process. We explore the broad spatial and temporal trends of the compilation, discuss future usage and limitations of the data set, and address the ongoing goals for the database to ensure that it remains a valuable asset to the paleoclimate community.

Methods

What is the primary purpose of the compilation? The PhanSST database is a part of the broader PhanTASTIC (Phanerozoic Technique Averaged Surface Temperature Integrated Curve) initiative[28], which aims to produce an internally consistent and statistically robust record of Earth's global mean surface temperature over the last 539 million years. Ultimately, these data will be integrated with ESMs[29] using data assimilation[10,30] to reconstruct relevant global climate fields and calculate the global mean surface temperature at the geochronologic age (i.e., stage) level across the Phanerozoic. Requisite to this goal is a compendium of paleotemperature proxy data.

PhanSST is a community-wide, collaborative effort. Each of the authors of this data descriptor contributed their time and expertise, entering data and quality control checking the records. Despite the more focused primary purpose of the compilation, we want to ensure that PhanSST will serve as a community-wide resource. The curated metadata fields, therefore, reflect a desire to maximize potential reuse of the database.

Why geochemical SST proxy data? We focused on compiling geochemical SST proxy data for several reasons. First, the ocean comprises approximately 70% of the Earth's surface, and SST proxies provide better long-term temporal coverage and generally more precise age control than terrestrial records due to more continuous deposition in marine environments. Second, the proxy types in PhanSST can be readily converted from proxy values into temperature units using established calibration models that propagate errors and account for seasonal biases[31–36]. Third, terrestrial air temperature proxies are a function of elevation and lapse rate, making interpretations of terrestrial data dependent upon paleogeographic and paleoaltimetric assumptions that are poorly constrained in deep time. SST proxies are still subject to assumptions, such as seawater chemistry, seasonality and depth of production, and temporal uniformity of proxy systems[34,35,37], and interpretations can be sensitive to the influence of plate movement or shifts in surface current positions[38,39]. However, the comparative richness of the marine record generally makes identifying anomalous sites or entries more straightforward. While beyond the scope of our current efforts, we hope that in the near future a parallel compilation of terrestrial temperature proxies will be developed.

Which SST proxy data? PhanSST included data from five SST proxies: oxygen isotopes of macro- and microfossil carbonate ($\delta^{18}O_{carbonate}$), oxygen isotopes of conodont phosphate ($\delta^{18}O_{phosphate}$), magnesium to calcium ratios (Mg/Ca) of planktonic foraminifera, the tetraether index of 86 carbons (TEX_{86}), and the alkenone unsaturation ratio ($U^{K'}_{37}$). While we did also collect marine carbonate clumped isotope data (Δ_{47}), those data are not included in the current release (Version 0.0.1) of PhanSST. Although laboratory-specific Δ_{47}-temperature calibrations are robust, interlaboratory differences in the way Δ_{47} data have been corrected raise concerns over the compatibility of the isotope values themselves[40]. Since PhanSST presents proxy values, rather than

paleotemperature estimates, we opted to omit the Δ_{47} data for now. With that said, a newly proposed reference frame[40] offers a promising way forward and we hope to include these data in the near future.

All of the proxy data included in the database have been previously published in peer-reviewed journal articles, theses and dissertations, book chapters, or public repositories (e.g., PANGAEA)[4–7,24,41–695]; the database does not include any unpublished data. The proxy values themselves, dominantly derive from either data tables contained within the original journal article, supplements, or public repositories. In general, data locked in PDF tables were extracted using Tabula (https://tabula.technology). Some dark data and missing metadata were obtained through personal communication with the original authors and, in very rare instances, data were digitized from figures. Details regarding the source of dark data can be found in the Quality Control logs (see *Compilation quality-control* for log availability).

PhanSST expands upon several existing compilations. The majority of oxygen isotope values from carbonate macrofossils come from Grossman and Joachimski[23] and the initial references of phosphate oxygen isotope values mostly derive from Grossman and Joachimski[23] and Song *et al.*[25]. Likewise, many of the Cretaceous data were originally collated by O'Brien *et al.*[696], Paleogene data by Hollis *et al.*[8] and Evans *et al.*[697], and Pliocene data by McClymont *et al.*[9]. To the extent possible, data sourced from these compilations were cross-checked with their initial publications to ensure completeness and avoid propagating any unintentional errors, and missing data or applicable metadata fields were filled in. The remaining data in PhanSST were scoured from the literature by the authors, who worked in teams based on their expertise with specific proxies and geologic time intervals. We used keyword queries in Google Scholar to identify missing references, and efforts were made to target literature from data-poor regions (e.g., South America) and time intervals (e.g., Silurian). While (quasi-) automated data discovery and entry methods show promise as a means of maximizing database completion and minimizing bias[698], given the broad nature of data sources and formats, such an approach was not tenable here.

Selection criteria varied slightly by proxy and time interval. Thanks to the initiatives of the International Ocean Discovery Program (IODP) and its predecessors, late Mesozoic and Cenozoic SST data are plentiful and data derived from cores often consist of high-resolution time series. In this case, we focused on compiling time series spanning at least one million years, recognizing that Quaternary data, for example, are compiled in more detail in other works[699,700]. Exceptions to this rule were made for data from undersampled regions (e.g., the Southern Ocean) or time periods (e.g., the Paleocene). In contrast to the high data density of the Cenozoic, data from the early Mesozoic and Paleozoic are comparatively scarce. Several proxies, such as $U^{K'}_{37}$, TEX_{86}, and foraminiferal-based records are limited to more recent times, and almost all ocean crust older than ~180 Ma has been recycled through subduction[701], removing a key sampling environment. As such, data availability is restricted by outcrop exposure, subject to more frequent and larger unconformities, and limited to fossiliferous horizons. Compared to core data, these records generally contain fewer measurements per site, lack a continuous time series, and have less precise age control or report relative rather than numeric ages. Therefore, we incorporated all available Paleozoic and Mesozoic proxy data, regardless of record duration. We did, however, require that all sites provide some level of age control; data that could not be assigned a relative age at the stage level were excluded.

Which metadata fields are included and why? The metadata fields included in PhanSST reflect a balance between the scope of the PhanTASTIC project and our intention to maximize the reuse potential of the database. Metadata fields were carefully curated to facilitate future updates to age models and proxy-, species- or methodological-specific corrections. For example, core information, sampling depth, and biostratigraphic information are included, permitting age model updates. On the other hand, we do not list age uncertainties because (1) age uncertainties are not consistently reported in the source publications, (2) it was not tractable to update all age models to a consistent timescale, and (3) the PhanTASTIC project focuses on temperature evolution at the stage level. Since we strive to make PhanSST a living database, we anticipate that updated age models, with uncertainties, may be added at a later date with assistance from the paleoclimate community.

To ensure a comprehensive and methodologically traceable compilation, we also opted to include diagenetically altered samples. Some samples can confidently be characterized as altered; however, diagenetic processes are gradual and criteria for what constitutes diagenetically altered material can be subjective and may change as new insights into diagenetic processes are gained. Consequently, rather than excluding such data, we have: (1) applied an expert-assigned binary diagenesis flag to make it clear which samples have been previously suggested or interpreted as altered, and (2) included relevant supplementary fields, such as elemental concentrations[702] and conodont color alteration index (CAI) values[703], allowing users to impose their own informed diagenetic assessments. This approach ensures that all data are available for future studies that may wish to adopt different alteration criteria or explore the spatial and temporal patterns of diagenesis.

Which metadata fields are excluded and why? The metadata fields currently provided have been carefully selected to help end users make informed decisions of which data to include in analyses and how best to correct them. However, two key metadata fields are omitted from PhanSST: paleotemperature estimates and paleocoordinates. Though we acknowledge that these fields are of particular interest, this was done deliberately to promote responsible and intentional reuse of the database.

Estimating SSTs from the proxy values involves applying and inverting a statistical model of how each proxy responds to environmental parameters; it is therefore a derived or modeled quantity subject to user-based decisions about how to treat each proxy system. In order to estimate SST for each of the more than 150,000 data points, we would need to make executive decisions regarding (1) which calibration to use for each proxy system, (2) what assumptions to use for non-thermal predictor variables (such as seawater chemistry), and (3) which (if any) taxon-specific or analytical corrections to apply. For any given proxy, there are a variety of proxy system models (PSMs) with which to estimate SST. For example, within the TEX_{86} proxy system, SSTs can be calculated

using the TEX_{86}^{H}[704], $TEX_{86\text{-linear}}$[696], or BAYSPAR[31] calibrations, among others, and exploration into region- and time-specific modifications to these calibrations is ongoing (e.g., Steinig *et al.*[574]). Holding all else constant, the difference in inferred temperatures across these calibrations can exceed 5 °C, and there is no consensus among the paleoclimate community on the most appropriate calibration(s) to use[8,705]. In fact, the choice of which calibration is most appropriate can vary based on the time interval and temporal resolution of the study, the taxon from which the data derive, the geographic breadth of the data, and the types of questions being investigated. Similarly, in order to calculate SST, many of these proxy systems require assumptions about non-thermal predictor variables (e.g., $\delta^{18}O_{seawater}$). Relating the proxy values to SST would therefore require decision making about these seawater chemistry values in the geologic past, which are largely unconstrained. Given the volume of data contained within PhanSST, these assumptions would need to be based on broad, first-order principles (e.g., a standardized $\delta^{18}O_{seawater}$ of −1‰ for ice-free times and 0‰ value during times of glaciation), but such simplifications are incorrect (e.g., we observe a >5‰ spatial spread in values in the modern ocean[706], a nuance that is wholly overlooked by assuming a single "ice-free" or "glaciated" value). Though there are better ways of estimating these values (e.g., extracting the local $\delta^{18}O_{seawater}$ values from an isotope-enabled ESM), such methods cannot be consistently applied across the entire database. And, in fact, the necessary resolution of these assumptions changes based on the scope of the study. Studies, for example, investigating Phanerozoic trends in oxygen isotopes may wish to apply a single calibration to all data points and use simplified assumptions for consistency, whereas studies investigating a specific time slice (e.g., the Cretaceous), may benefit from taking a more intricate approach (e.g., using taxa-specific PSMs and drawing $\delta^{18}O_{seawater}$ values from ESMs). It is therefore not possible for us to calculate SSTs for each data point while applying a traceable, scientifically sound, and ubiquitously appropriate methodology. Moreover, it is important that those who wish to calculate SSTs from the proxy data within PhanSST be fully aware of the decision making (and uncertainty) associated with the various PSMs and assumptions.

Likewise, we do not include paleogeographic information, which is also a derived quantity based on geophysical models. Here, we plot data using the plate rotation model of Scotese and Wright (2018)[707] for illustrative purposes, since it is one of the few rotations that extends back through the Phanerozoic. However, there are a variety of different plate rotation models available, particularly in more recent time intervals, and the projected paleocoordinates can vary significantly based on the rotation model used[38]. As with the SST estimates, the choice of which paleorotation is most appropriate to use is dependent upon the application of the data and the temporal resolution of the study. If, for example, a user is plotting data on existing ESM output, then they will want to use the same rotation that was used in the simulation so that the paleolongitudes (which are largely unconstrained) align. Alternatively, if they are testing a hypothesis about the timing or influence of a specific gateway opening, they may wish to use several different rotations and compare the results. Further, when aligning data in deep time, the time scale of the study matters, and the choice of time interval with which to align the data will again be dependent on the scope of the investigation. Time slice studies may wish to rotate all data to the same time frame (e.g., 56 Ma) despite the fact that the data may span a few million years in either direction. Other studies looking at changes in ocean dynamics from the same site across a 5-million-year window may wish to rotate each discrete data point to their precise numeric age. Given the variety of methods for estimating both SST and paleocoordinates, and the inherent complexity and uncertainty behind those singular discrete values, we believe that it is important for end users to go through the decision making process themselves to ensure that the values are best tailored toward their respective application. We do, however, recognize that users who wish to calculate SSTs or paleocoordinates may benefit from guidance. We offer some broad recommendations on how to select and apply temperature calibrations and rotation models below in the *Applying the database in deep time* section.

Data Records

In addition to the proxy value itself, each entry is associated with an array of relevant metadata fields, which vary depending on the nature of the record and the proxy. In total, there are more than 40 metadata fields that can broadly be grouped into six categories: (1) sample site and other identifying information, (2) age information, (3) proxy information, (4) taxonomic and environmental information, (5) proxy-specific information, and (6) reference metadata. Basic descriptions of these fields can be found in Table 1 and specifics on how and why each field is assigned are provided below.

For clarity and consistency while reading this data descriptor, ***entries*** refer to each discrete proxy value and its associated metadata (i.e., a row), ***fields*** refer to the metadata collected for each entry (i.e., a column), and ***sampling sites*** refer to the unique geographic coordinates of entries, independent of the number entries from that location. Unique sampling sites can be parsed temporally (e.g., by stage, period, 2.5 myr bins, etc.), by proxy type, or a combination of the two.

Sample ID and location fields. The first field is the *SampleID*, which reflects the unique (often alphanumeric) identification code associated with each entry, as originally published. Currently, the *SampleID* field only applies to samples collected in outcrop; however, in the future, we plan to also include the unique drill core sample IDs. The remaining sample site fields provide information on the geographic and stratigraphic position of each entry. Data that come from drill cores, such as those from IODP, list the *SiteName*, referencing the expedition site, and also include sampling depth information (i.e., *SiteHole*, *MBSF*, and/or *MCD*) to allow age models to be updated in the future. Data collected in outcrop similarly include a *SiteName* and *SampleDepth*, as well as the geologic *Formation* from which the data were collected, when available.

Each entry is also associated with the modern coordinates of the sampling site (*ModLat* and *ModLon*) and tags indicating the *ContinentOcean* and *Country* of collection for easy filtering. For consistency, the coordinates of sample sites were rounded to two decimal degrees. In some cases (predominantly Paleozoic data collected in outcrop and published in older journal articles) precise coordinates were not provided[423,483,501]. In

Field name	When applicable	Description of field (units)
Sample ID and location fields		
SampleID	All data	Unique sample identification code, as originally published
SiteName	All data	Name of the drill core site or section
SiteHole	Drill core data	The alphabetic hole specifier
MBSF	Drill core data	Depth below the sea floor (m)
MCD	Drill core data	The mean composite depth (m)
SampleDepth	Outcrop data	Stratigraphic height or depth (m)
Formation	Outcrop data	Geologic formation name
Country	All data	The country or ocean of the data collection site
ContinentOcean	All data	The continent or ocean basin of the data collection site
ModLat	All data	Modern latitude of collection site rounded to two decimals; negative values indicate the Southern Hemisphere (decimal degrees)
ModLon	All data	Modern longitude of the collection site rounded to two decimals; negative values indicate the Western Hemisphere (decimal degrees)
Age fields		
Age	All data	Age, in reference to GTS2020 [710] (Ma)
Period	All data	The geologic period
Stage	All data	The geologic stage (i.e., geochronologic age)
StagePosition	All data (barring those only assigned to a stage)	Further specification of relative age (Early, Middle, or Late)
Biozone	Outcrop data	Conodont, graptolite, and/or ammonite biozone
AgeFlag	All data	Flag indicating if relative age fields were autofilled from numeric age values (0), age values were autofilled from relative age fields (1), or both relative and numeric age values were provided (2)
Proxy fields		
ProxyValue	All data	Reported proxy value (native proxy units)
ProxyType	All data	Reference to the proxy type; see Table 2
ValueType	All data	Reference to the averaging of the data (see text)
DiagenesisFlag	$\delta^{18}O$ and Mg/Ca data	Binary expert-assigned flag indicating good (0) or questionable (1) preservation
Taxonomic, environmental, and ecological fields		
Taxon1	All data	First-order taxonomic classification (see Table 3)
Taxon2	$\delta^{18}O$ data	Second-order (class) classification of mollusks (see Table 3)
Taxon3	All $\delta^{18}O$ and Mg/Ca data	Third-order (genus or species) classification (see Table 3)
Environment	Outcrop data	Depositional environment (e.g., mid-shelf, epeiric)
Ecology	All $\delta^{18}O$ and Mg/Ca data	Ecological preference of the sampled taxon (e.g., surface, benthic)
Proxy-specific fields		
AnalyticalTechnique	All $\delta^{18}O$ data	The analytical technique used to obtain the data (IRMS vs SIMS)
CL	Macrofossil $\delta^{18}O_{carbonate}$ data	Cathodoluminescence microscopy assessment
Elemental Suite	Macrofossil $\delta^{18}O_{carbonate}$ data	All reported elemental concentrations (i.e., Fe, Mn, Mg, Sr, Ca) or ratios (i.e., Sr/Ca, Mg/Ca, Mn/Sr)
NBS120c	$\delta^{18}O_{phosphate}$ data	The NBS120c standard value used to correct the data (‰)
Durango	$\delta^{18}O_{phosphate}$ data	The Durango standard value used to correct SIMS data (‰)
MaximumCAI	$\delta^{18}O_{phosphate}$ data	The maximum reported conodont color alteration index value for that sample or horizon
ModWaterDepth	Mg/Ca data	The modern water depth of the sampling site
CleaningMethod	Mg/Ca data	A binary flag to indicate either oxidative-only cleaning (0) or inclusion of a reductive cleaning step (1)
Fractional abundances	TEX_{86} data	Fields to indicate the fractional abundances of the GDGTs
Index values	TEX_{86} data	Branched and isoprenoid tetraether (BIT), methane (MI), and delta ring (dRI) index values
Reference metadata		
LeadAuthor	All data	The last name of the first author of the original publication
Year	All data	The year of the original publication
PublicationDOI	All data	The DOI of the original publication
DataDOI	All data	The DOI of the online repository hosting the data

Table 1. Field names and descriptions.

these instances, locations were estimated using context from the original publication, outcrop information from Macrostrat[708], and occurrence data from the Paleobiology Database[709].

Age fields. Six age fields provide information related to the age of each sample, including numeric *Age* (in Ma) as well as the *Period* and *Stage*, which provide relative age information. We use the chronostratigraphic term "stage" as a synonym for the geochronologic "age" to mitigate confusion between numeric ages and geochronologic ages. Biostratigraphic information (e.g., conodont zone), when provided, is retained in the *Biozone* field, permitting future age model updates for data collected in outcrop with each new iteration of the Geologic Time Scale (GTS). We did not divide data from the Holocene Epoch into their respective stages; all data younger than 0.0117 Ma were assigned to the "Holocene" in the *Stage* field. Likewise, all data from the unnamed stage of the Pleistocene were assigned to the "Upper Pleistocene" and all data from the Pridoli Epoch are assigned to the "Pridoli".

Given the broad nature of this compilation and the variety of time scales and proxies incorporated, constraining entry ages in a consistent and traceable way required a multifaceted approach. Data coming from IODP cores, for example, often have higher precision age models tied to sampling depth. In contrast, data from outcrops are frequently more challenging to date precisely and quantitatively. Thus, ages were assigned in one of three ways: by entering a numeric age and auto-filling the relative age information, by entering relative age information and auto-filling the numeric age information, or by retaining both the manually entered numeric and relative age information. The *AgeFlag* field identifies which approach was taken (indicated by a 0, 1, or 2, respectively).

Numeric age assignments with auto-filled relative ages. If the original paper provided a precise numeric age, the period and stage fields were automatically filled in using age boundaries from GTS 2020[710]. We made efforts to use recent drill core age models, but given the size of the data compilation, updating all of the age models was not feasible. When available, we compiled sampling depth information (i.e., *SiteHole*, *MBSF*, and/or *MCD*) so that age models may be updated in the future. If the data came from an existing compilation, we deferred to their reported age unless a more recent age model was readily available. Data with precise numeric ages are denoted by a zero (0) in the *AgeFlag* field.

Relative age assignments with auto-filled numeric age. Some data can only be relatively dated. In the absence of precise numeric ages, the *Stage* field was entered manually. Stage duration is highly variable, with a median length of 4.65 myr. In general, stage duration scales with availability of material and scientific interest in the time interval, with a maximum duration of 21.56 myr (Norian) and a minimum of 11.7 kyr (Holocene, though not a defined stage as discussed above).

The stage assignments are largely based on the divisions reported in the original publication, though some data points have been updated based on the biostratigraphic information contained in the *Biozone* field based on the divisions in GTS 2020[710]. Relative ages were further qualified using the *StagePosition* field (i.e., early, middle, or late), if such information was available or could be realistically constrained using the biozonations. A numeric age was then estimated based on the stage boundaries of GTS 2020[710]. Entries constrained only at the stage level were assigned numeric ages based on the arithmetic mean of the upper and lower stage boundaries. Numeric ages of entries tied to a specific stage position (early, middle, or late) were estimated by dividing the stage into three equal time slices and assigning a numeric age based on the midpoint of that entry's respective third. Data with numeric age assignments extrapolated from relative age information are denoted by a one (1) in the *AgeFlag* field.

Note that assigning ages in this manner means that high(er)-resolution relative time series information is not retained in the auto-filled numeric ages. For example, in some original publications, authors constructed their own relative age model and assigned sequential relative ages to stratigraphically successive data points. However, it was not feasible to convert these relative time series into numeric ages using a consistent and traceable methodology. For the purposes of the PhanTASTIC project, stage-level temporal resolution is sufficient. Regardless, stratigraphic position, when available, was recorded in the *MBSF*, *MCD*, and/or *SampleDepth* fields, which allows users to construct relative time series if desired.

Proxy fields. The four proxy fields consist of the proxy value, the proxy type, value type, and preservation state. Table 2 provides a list of all *ProxyType* options. *ValueType* options include: (1) 'im', indicating the proxy value represents an individual measurement from an individual specimen, (2) 'ia', indicating the proxy value reflects the average of replicate measurements from a single individual specimen, and (3) 'pa', indicating the measurement reflects a population average from multiple specimens. All TEX_{86} and $U^{K'}_{37}$ entries, by definition, are listed as 'pa'.

The *DiagenesisFlag* field is a binary flag specifying preservation state. We generally deferred to the expert opinion of the authors responsible for entering and/or quality-control checking the data and were as conservative as possible, flagging both known and suspected alteration. Both $\delta^{18}O$ and Mg/Ca foraminiferal data were flagged based on the preservation of the tests themselves (e.g., glassy vs. frosty)[466] rather than an assessment of the fidelity of the proxy value. Unlike foraminifera, there is currently no method for assessing the preservational state of the macrofossil $\delta^{18}O_{carbonate}$ and $\delta^{18}O_{phosphate}$ that is consistently applied across the literature. The diagenetic flags provided here, therefore, generally reflect the interpretation of the original authors. We also flagged any $\delta^{18}O_{carbonate}$ entries lower than −10‰ as these values would yield unrealistically warm SSTs, suggesting that either diagenesis or non-marine seawater compositions affected the measurement. We appreciate that diagenesis is a spectrum and applying a subjective binary flag both overlooks the nuance of the processes involved and is inherently not reproducible. To that end, we have also provided additional diagenetic fields specific to

Field value	Proxy type	Units
d18a	$\delta^{18}O$ of aragonite	‰; VPDB
d18c	$\delta^{18}O$ of calcite	‰; VPDB
d18p	$\delta^{18}O$ of phosphate	‰; VSMOW
mg	Mg/Ca ratio	mmol/mol
tex	TEX_{86}	unitless ratio
uk	$U_{37}^{K'}$	unitless ratio

Table 2. Proxy types.

$\delta^{18}O_{carbonate}$ and $\delta^{18}O_{phosphate}$ data, such as trace and major element ratios and concentrations of macrofossils, cathodoluminescence assessments, and maximum CAI of conodonts. End users can define their own diagenetic thresholds (e.g., Mn/Sr <0.5) and use these fields to consistently filter or flag suspect data.

We have not indicated the preservation state of TEX_{86} nor $U_{37}^{K'}$ entries because although methods for assessing preservation and thermal maturity exist[8,711], they are not consistently reported in the literature. Nevertheless, as with the oxygen isotope data, we have included some proxy-specific fields to help filter TEX_{86} data for non-thermal influences (see below).

Taxonomic and environmental fields. The taxonomic and environmental fields provide information about the organism from which the proxy data derive (Table 3), as well as the depositional environment and ecology of the sampled taxon. The *Taxon1* field refers to the first-order taxonomic affiliation of the organism, primarily classified at the phylum level. The *Taxon2* field, applicable only to mollusk $\delta^{18}O_{carbonate}$ data, further specifies the class, and the *Taxon3* field specifies the binomial species name of the sampled organism, when available. These fields help characterize the paleoenvironment from which the data come, permit the compilation to be filtered by taxon, and contain information pertinent to species-specific calibrations[34,35].

While most of the entries in PhanSST are reported as representing SST, in reality very few of the taxa from which the data derive genuinely lived at the sea surface. Some PSMs, such as BAYSPAR[31] for TEX_{86} and BAYSPLINE[33] for $U_{37}^{K'}$, are based on calibrations between core tops and modern SST, partly (but not completely, since organisms might migrate vertically through time) alleviating this limitation. However, it can be difficult to interpret data that come from (1) proxies that do not have modern core top calibrations, (2) extinct taxa, or (3) intervals with substantially different environmental conditions than today that may have promoted vertical migration within the water column. When available and applicable, we have therefore included metadata pertaining to the depositional environment of the source material (e.g., marginal, mid-shelf, slope) in the *Environment* field and the lifestyle or depth habitat of the organism in the *Ecology* field. The ecology of carbonate macrofossils and conodonts are classified as either benthic, nektic, planktic, or some combination therein, while planktic foraminifera are classified as either surface/mixed layer or (sub-)thermocline. These fields allow users to easily filter or index entries within the compilation to fit their needs. For example, depending on the scope of the study, it may be germane to filter out benthic brachiopods deposited in slope environments while retaining brachiopods from inner shelf environments, as they are more likely to record temperatures closer to sea surface values. Alternatively, comparing data from surface- and thermocline-dwelling species of foraminifera with benthic bivalve data from the same site could elucidate vertical temperature gradients of ancient oceans.

Proxy-specific fields. Certain proxy-specific fields were added to the compilation to permit data corrections, facilitate the implementation of PSMs, aid in diagenetic assessments, and improve the overall utility of the database. For traceability purposes (i.e., to ensure that our records reflect the original data tables) we have not corrected any of the proxy values, but we do provide the information required to enable a correction. For example, the $\delta^{18}O$ data from both carbonates and phosphates include information about the *AnalyticalTechnique* (i.e., IRMS or SIMS), as evidence suggests there may be methodological offsets in the isotope values[148,712]. The NBS-120c value used to standardize the $\delta^{18}O_{phosphate}$ data is reported in the *NBS120c* field. The consensus value of 21.7‰ is now generally applied, but the value of the standard varies significantly in older literature. Additionally, in the case of SIMS data, we also report the *Durango* standard value. Reporting the "uncorrected" published values, while also specifying the method, permits end-user autonomy of how to treat data derived by different means.

To assist in assessments of sample preservation, we have included available trace, minor, and major element concentrations and ratios associated with $\delta^{18}O_{carbonate}$ macrofossil data (e.g., Fe, Mn, Mg, Sr, Sr/Ca, Mg/Ca). Diagenetic processes yield predictable directional changes to these concentrations and ratios; by comparing fossil values to modern taxon- or site-specific ranges, informed threshold values can thus be used to further assess the preservation state of samples[713,714]. For the same reason, when reported, we have also included categorical diagenetic assessments using cathodoluminescence microscopy[702] (*CL*; L, luminescent; SL, slightly luminescent; NL, non-luminescent).

When available, $\delta^{18}O_{phosphate}$ entries are associated with the maximum reported conodont color alteration index (*MaximumCAI*) value[703] for that sample or horizon. Phosphate is generally considered to be more resistant to diagenetic alteration than carbonate, but there remains some debate as to when data from conodont elements should be considered altered[148,312]. Inclusion of this field allows users to impose their own CAI threshold criteria for assessing preservation or to analyze relationships between isotope values and CAI.

Taxon1	Taxon2	Taxon3	Description
br		Binomial species name	Brachiopod
m			Mollusk
	bi	Binomial species name	Bivalve
	ce	Binomial species name	Cephalopod
	ga	Binomial species name	Gastropod
	ot	Binomial species name	Other
co		Binomial species name	Conodonts
ha			Haptophyte
pf		Binomial species name	Planktonic foraminifera
th			Thaumarchaeota

Table 3. Taxonomic specifiers.

Additional fields are included for foraminiferal Mg/Ca data to provide information needed for using the Bayesian Mg/Ca forward model, BAYMAG[35]. Previous studies have demonstrated that Mg/Ca values are dependent upon both the bottom water calcite saturation state[715] (Ω) and the cleaning method used prior to analysis[716], and, as such, are included as predictor variables in BAYMAG. All Mg/Ca entries, therefore, include the water depth of the modern sampling site (*ModWaterDepth*), which can be used in tandem with the geographic information to inform paleodepth estimates (and thus constrain Ω), and a binary *CleaningMethod* field to indicate whether the cleaning omitted (0) or included (1) a reductive step.

TEX_{86} entries include the fractional abundances of the isoprenoidal glycerol dialkyl glycerol tetraethers (GDGTs), if available, following the recommendation of Hollis *et al.*[8]. Additionally, we have included the branched and isoprenoid tetraether index[717] (BIT), the methane index[718] (MI), and the delta ring index[719] (ΔRI), which can all be used to assess the extent to which TEX_{86} values may be affected by non-thermal factors. These fields allow the end-user to screen data by the indices and threshold values of their choice.

Reference metadata. The reference fields contain the publication metadata, including the lead (first) author, publication year, and the DOI to the publication where the data were originally reported (*PublicationDOI*). We also recognize that many of these data are available in online repositories (e.g., PANGAEA). While Version 0.0.1 of PhanSST only provides the *PublicationDOI*, in future releases we plan to also utilize the *DataDOI* to direct users to any online repository hosting the data. To aid in ease of machine readability, accents and special characters in the *LeadAuthor* and other applicable fields were removed. However, the full and unaltered database citations, including the article title and journal name, can be found in a supplementary Excel (.xlsx) file available on Zenodo and the PhanSST website.

Technical Validation

Compilation quality-control. Data were quality-control (QC) checked by the authors of this data descriptor. For data deriving from drill cores, we generated a PDF file for each unique sampling site, parsed by the *SiteName* and *ProxyType* fields (Fig. 1). The QC PDFs included relevant metadata, such as the reference fields (*LeadAuthor, Year, DOI*) and the sample site coordinates. All data for a given site were plotted versus both time and core depth and colored by reference, with different symbols to indicate the *DiagenesisFlag* and *AgeFlag* assignments of each data point. QC PDFs of data derived from planktic foraminifera ($\delta^{18}O_{carbonate}$ and Mg/Ca) contained plots colored by species. Using shared Google spreadsheets for each proxy, we verified that the information in each QC PDF matched the publication values, working in teams based on expertise (Fig. 2a). Each unique site, proxy, and reference was evaluated based on a standardized suite of criteria to ensure consistency throughout the process (Fig. 3). Those assisting in the QC process checked boxes to confirm the fidelity of the journal metadata, modern coordinates, age model, depth information, proxy value, preservation state, taxa, cleaning method (for Mg/Ca), and fractional abundances (for TEX_{86}). We corrected any issues identified and maintained a detailed log of comments, providing a record of our QC process. Links to read-only versions of these QC logs are available on the PhanSST website and in the "Read Me" documentation on Zenodo.

Given the large number of foraminiferal species in the database and the potential for outdated taxonomy, we conducted a systematic QC of the listed species. Species names were checked for outdated taxonomic assignments and misspellings (Fig. 2b), using databases like Mikrotax. We added an expert-assigned *Ecology* field to help distinguish surface or mixed layer dwelling species from (sub-)thermocline species.

The macrofossil $\delta^{18}O_{carbonate}$ and $\delta^{18}O_{phosphate}$ data were QC checked separately. These data generally come from outcrops, with many studies reporting multiple sampling sites but only a few measurements at each site. These differences inhibited straightforward parsing of the carbonate macrofossil and phosphate records into site-level QC PDFs, so instead these data were inspected manually. Records were checked by comparing proxy values and metadata between existing compilations[23] and original publications. As with the core data, a detailed log of the changes made was retained.

In addition to the manual quality-control checks described above, we also performed automated analyses for each field to identify any missing or erroneous metadata (available on GitHub; see *Code Availability*). For example, the *ModLat* and *ModLon* fields were screened to ensure that latitude and longitude values were in decimal degrees and fall between −90 to 90 and −180 to 180, respectively. Country names and sample coordinates were further crosschecked against publicly available country shapefiles data, to ensure accuracy and consistency in

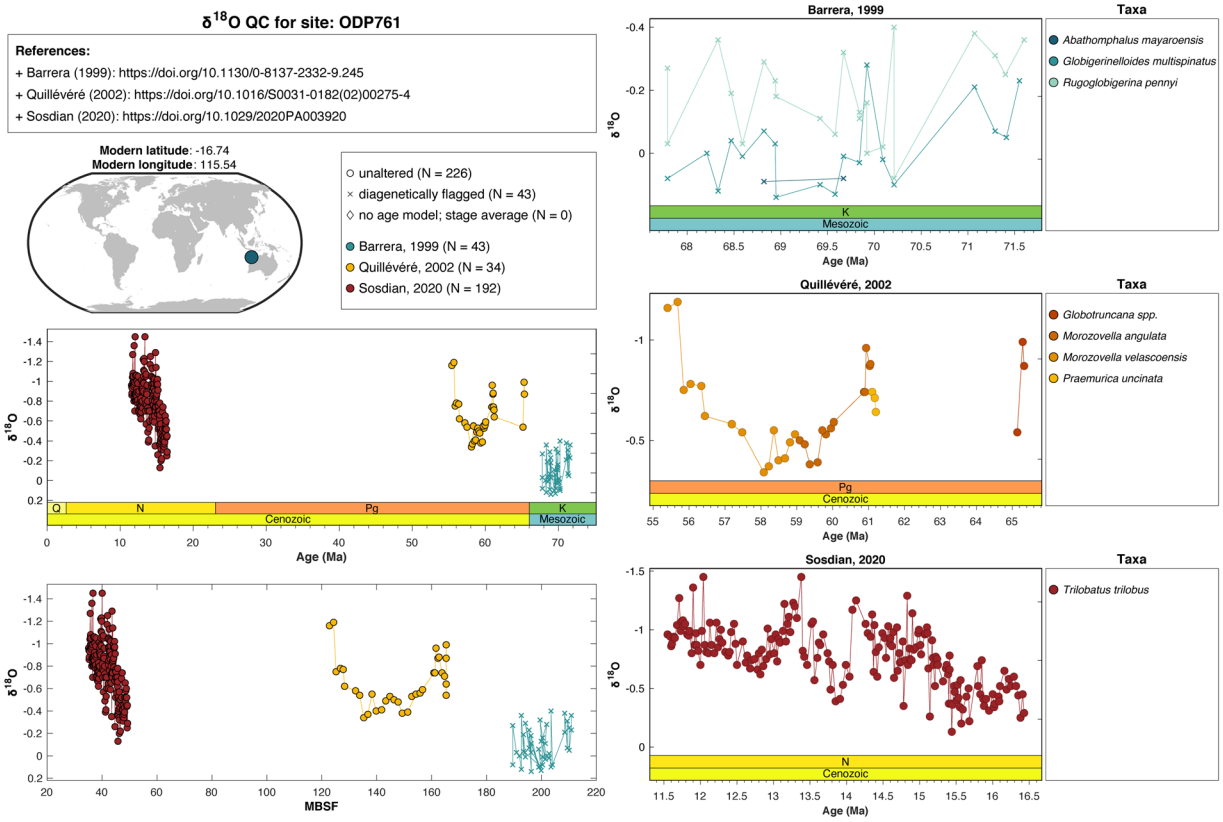

Fig. 1 Example QC PDF for the foraminiferal $\delta^{18}O_{carbonate}$ data from ODP Site 761.

the assignment. *ContinentOcean* assignments were verified by indexing all categorical responses (e.g., NA, North America; SO, Southern Ocean) and mapping each data point tagged to each respective geographic region. Stage and period names were compared to the list of accepted names from GTS 2020[710], and checked for agreement between numeric age, period, and stage. We also printed lists of the unique period, stage, proxy type, value type, and taxonomic names to ensure they each respectively conformed to our accepted convention. Lists of all unique values for each categorical field (e.g., *ProxyType, ValueType, AnalyticalMethod*) were printed to identify any inconsistencies, and every field was queried to identify missing values.

General database statistics. Version 0.0.1 of PhanSST contains 150,691 entries, drawn from 660 different references, representing 1,643 unique sampling sites and 93 of the 100 Phanerozoic stages. Of these, 25,782 have been flagged as diagenetically altered, though this flag does not apply to the TEX_{86} or $U^{K'}_{37}$ entries; there remain nearly 120,000 unflagged data points after applying a conservative screening of these latter proxies to ensure fidelity of their values (i.e., excluding TEX_{86} data whose BIT, MI, or ΔRI values are greater than 0.5 and $U^{K'}_{37}$ data whose paleolatitude is greater than 70°N, since these data are considered compromised by alkenone production in sea ice[33,720,721]). Across the database, $\delta^{18}O_{carbonate}$ data are the most common, constituting over half of all entries (Table 4). This prevalence reflects the fact that carbonate oxygen isotope data (1) are the oldest quantitative paleotemperature proxy, with its origins dating back to 1947[722], (2) represent one of only two SST proxies available across the entirety of the Phanerozoic, and (3) are commonly measured on foraminifera from drill cores. However, the $\delta^{18}O_{carbonate}$ data are commonly affected by diagenesis, with ~30% of the 81,633 entries flagged as altered. Despite their limited temporal availability, $U^{K'}_{37}$ data account for a quarter of all entries, and all data, barring those from regions prone to sea ice, are considered to reflect a primary SST signal. The high volume of $U^{K'}_{37}$ data is likely a result of the ease of analysis and straightforward relationship between temperature and proxy value. The remaining three proxies collectively contribute to the remaining quarter of the entries in PhanSST, with conodont $\delta^{18}O_{phosphate}$ being the least common.

Below, we highlight some of the first-order spatial and temporal trends in data density, sampling locations, and proxy values of PhanSST. The syntheses presented illustrate just a small fraction of the spatio-temporal patterns uniquely elucidated by a compilation of this size and demonstrate the potential of the database to facilitate paleoclimatic, geochemical, and paleoecological research.

Temporal trends in data density. The Cenozoic accounts for just 12% of Phanerozoic time, while the Mesozoic accounts for 35% and the Paleozoic, 53%. The number of PhanSST entries and sampling sites per era, however, follow a different distribution (Table 5), reflecting fundamental differences in the availability, density, and nature of paleo-SST archives across geologic time. Cenozoic entries account for 79% of the data in PhanSST, while

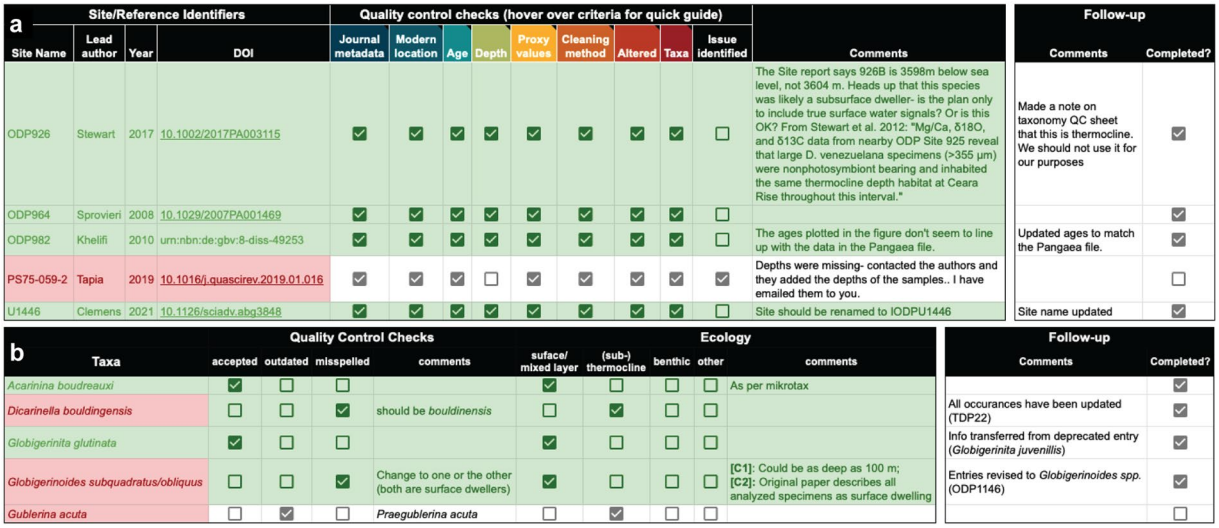

a

Site/Reference Identifiers				Quality control checks (hover over criteria for quick guide)										Follow-up	
Site Name	Lead author	Year	DOI	Journal metadata	Modern location	Age	Depth	Proxy values	Cleaning method	Altered	Taxa	Issue identified	Comments	Comments	Completed?
ODP926	Stewart	2017	10.1002/2017PA003115	☑	☑	☑	☑	☑	☑	☑	☑	☐	The Site report says 926B is 3598m below sea level, not 3604 m. Heads up that this species was likely a subsurface dweller- is the plan only to include true surface water signals? Or is this OK? From Stewart et al. 2012: "Mg/Ca, δ18O, and δ13C data from nearby ODP Site 925 reveal that large D. venezuelana specimens (>355 μm) were nonphotosymbiont bearing and inhabited the same thermocline depth habitat at Ceara Rise throughout this interval."	Made a note on taxonomy QC sheet that this is thermocline. We should not use it for our purposes	☑
ODP964	Sprovieri	2008	10.1029/2007PA001469	☑	☑	☑	☑	☑	☑	☑	☑	☐			☑
ODP982	Khelifi	2010	urn:nbn:de:gbv:8-diss-49253	☑	☑	☑	☑	☑	☑	☑	☑	☐	The ages plotted in the figure don't seem to line up with the data in the Pangaea file.	Updated ages to match the Pangaea file.	☑
PS75-059-2	Tapia	2019	10.1016/j.quascirev.2019.01.016	☑	☑	☑	☐	☑	☑	☑	☑	☑	Depths were missing- contacted the authors and they added the depths of the samples.. I have emailed them to you.		☐
U1446	Clemens	2021	10.1126/sciadv.abg3848	☑	☑	☑	☑	☑	☑	☑	☑	☐	Site should be renamed to IODPU1446	Site name updated	☑

b

Quality Control Checks					Ecology				Follow-up	
Taxa	accepted	outdated	misspelled	comments	suface/ mixed layer	(sub-) thermocline	benthic	other	Comments	Completed?
Acarinina boudreauxi	☑	☐	☐		☑	☐	☐	☐	As per mikrotax	☑
Dicarinella bouldingensis	☐	☐	☑	should be *bouldinensis*	☐	☑	☐	☐	All occurances have been updated (TDP22)	☑
Globigerinita glutinata	☑	☐	☐		☑	☐	☐	☐	Info transferred from deprecated entry (*Globigerinita juvenillis*)	☑
Globigerinoides subquadratus/obliquus	☐	☐	☑	Change to one or the other (both are surface dwellers)	☑	☐	☐	☐	Entries revised to *Globigerinoides spp.* (ODP1146)	☑
Gublerina acuta	☐	☑	☐	*Praegublerina acuta*	☐	☑	☐	☐		☐

Fig. 2 (**a**) Example QC Google spreadsheet for foraminiferal Mg/Ca data, parsed by site and publication. The fidelity of the entered data was checked based on eight suites of standardized criteria (see Fig. 3). (**b**) Example of the foraminifera taxonomy QC Google spreadsheet. Foraminiferal species were checked separately for outdated or misspelled names and flagged by environment.

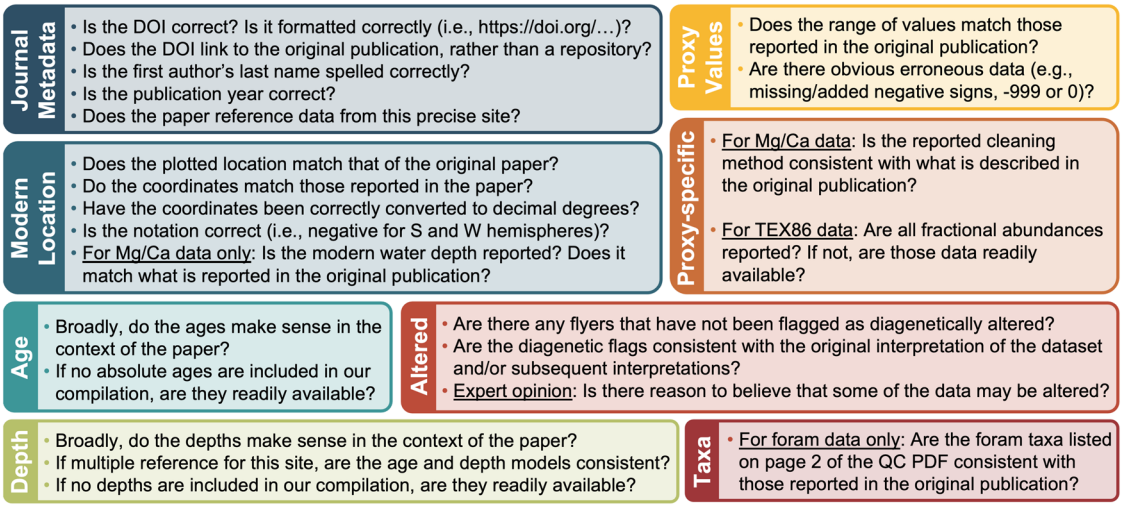

Fig. 3 The QC criteria under which each site and reference was evaluated. Checking the boxes of the same color and heading in Fig. 2a confirms that all of the criteria for a given category have been met.

Cenozoic sampling sites account for a quarter of the unique sites. The over-representation of Cenozoic entries reflects the fact that the majority of these data come from drill cores, with long and often high-resolution records, and many of these cores have SST data from multiple proxies. Additionally, several of the proxies, such as $U_{37}^{K'}$[723], are restricted to more recent times. Collectively, these factors influence both the number of entries and unique sampling sites from each proxy type through time (Figs. 4,5). While carbonate oxygen isotope data, largely from planktonic foraminifera, dominate the Cenozoic record, many of these data have been flagged as altered due to pervasive secondary bottom water calcite precipitation overprinting the SST signal[466,724]. TEX_{86} data are common throughout the Cenozoic, while both the number of entries and sampling sites of the $U_{37}^{K'}$ data grow rapidly across the late Neogene through Holocene. Overall, despite rising numbers of entries across the era, the number of unique sampling sites at the stage level remains fairly consistent within each proxy, with only the $U_{37}^{K'}$ sites showing a large increase towards the present (Fig. 4). The abundance of multi-proxy records from the same cores further moderates the total number of unique sites across all proxies.

Mesozoic entries account for just 12% of the compilation but contribute over a third of all sampling sites (Table 5). The Mesozoic marks a transition in both depositional environment and proxy availability. In the Cretaceous, IODP data are still available, as are foraminiferal-based and TEX_{86} records. However, the the lack of pelagic calcifiers and preserved biomarkers in sediments predating the mid to late Mesozoic limits both the

Proxy	All entries		Unaltered entries	
	N	Proportion	N	Proportion
$\delta^{18}O_{carbonate}$	81,633	54%	56,691	48%
$\delta^{18}O_{phosphate}$	6,358	4%	6,014	5%
Mg/Ca	13,249	9%	9,846	8%
TEX_{86}	14,091	9%	11,176	9%
$U^{K'}_{86}$	35,360	24%	35,324	30%
Total	150,691		119,051	

Table 4. Summary of entries by proxy. See text and caption of Fig. 5 for details regarding how preservation was assessed.

Era	Proportion of...		
	Phanerozoic	Entries	Sites
Cenozoic	12%	79%	24%
Mesozoic	35%	12%	35%
Paleozoic	53%	9%	41%

Table 5. Summary of the proportion of entries and sites by geologic era, with the proportion of Phanerozoic time encompassed within each era for comparison.

materials and proxies available. Further, nearly all seafloor older than the late Jurassic has been subducted[701], which fundamentally restricts the temporal reach of ocean drill cores. Therefore, records from the early portion of the Mesozoic dominantly come from shelf deposits or epeiric seas. These data are generally collected from outcrops and thus lack the high-resolution, high sampling density of core data. Additionally, the early Mesozoic marks the initial breakup of Pangaea; the supercontinent reduced continental margin area and prohibited widespread continental flooding[725,726] and so compared to other intervals in Earth's history, there are very few marine environments preserved[727]. The reduction in early Mesozoic marine sedimentary occurrences is mirrored in PhanSST by the dearth of Triassic and early Jurassic sampling sites (Fig. 4b). Overall, the era is dominated by carbonate isotope data. Phosphate isotope data are common in the Triassic, but disappear at the close of the period, reflecting the extinction of conodonts[728]. Conversely, TEX_{86} data make an appearance in the latter half of the Mesozoic, and foraminiferal Mg/Ca data, though present in the Cretaceous, are infrequent, both in terms of entries and sampling sites.

Despite comprising more than half of the Phanerozoic Eon, Paleozoic entries account for just 9% of all data but constitute 40% of sampling sites (Table 5). All Paleozoic entries come from marine sediments deposited on continental margins or interiors. Paleozoic studies often report multiple sample sites, with only a small number of measurements from each site[67,252,616]. Thus, the number of sampling sites remains high, but the data density at each site is drastically reduced (Fig. 5). Only carbonate and phosphate oxygen isotope data are available for the Paleozoic (Fig. 4). Notable declines in data density in the Cambrian, Silurian, and Permian (Figs. 4 and 5) can be ascribed to a combination of preservation and eustasy, limiting the number of sites and material available for analysis.

Spatial trends in data density. The spatial distribution of PhanSST sampling sites are inherently uneven, both with respect to their modern (Fig. 6) and paleo-locations (Fig. 7). Paleo-latitude and -longitude of each entry was estimated using the plate model of Scotese and Wright[707], implemented in G-Plates (Version 2.2.0)[729]. In terms of their modern distributions, Cenozoic data are the most spatially widespread and entry numbers at each site are high, owing to the availability of ocean core data and the high-resolution, multi-proxy studies they permit. Mesozoic sampling sites reflect the mix of high sample densities at the few ocean cores that extend back into the Cretaceous and lower sample density associated with outcrop data. By the Paleozoic, all samples are situated on land and heavily weighted toward the Northern Hemisphere, with most data coming from a few key regions (i.e., North America, Europe, Australia, and China). The Southern Hemisphere is consistently underrepresented across all three eras and five proxies and spanning both marine and continental deposits. The paucity of data from South America and Africa, as well as the southern sectors of the Indian and Pacific oceans, mirrors patterns in paleontological data[709,730] and highlights the tectonic, depositional, and colonial biases in paleoclimate data.

Viewing the paleogeographic distribution of the data by period (Fig. 7) further accentuates depositional and latitudinal biases. The Cambrian through Jurassic data overwhelmingly come from epeiric sea settings, while the Cretaceous through Quaternary records are biased toward continental margins. Likewise, the Paleozoic records, which dominantly come from modern-day North America and Europe, are weighted toward the tropics; as these continents migrate northward through the Mesozoic and into the Cenozoic, the records begin to favor the Northern Hemisphere mid latitudes. The Cenozoic data are more evenly distributed across latitudes due to the availability of core data; however, the Southern Hemisphere remains underrepresented.

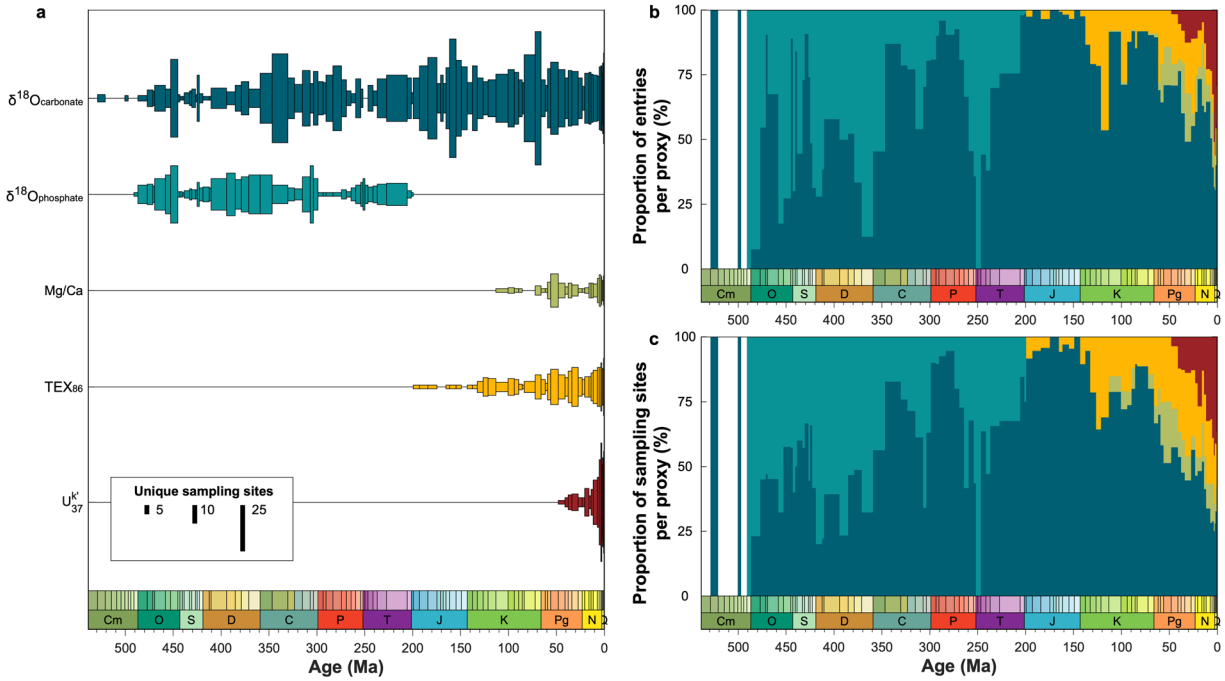

Fig. 4 Summary of the (**a**) number of unique sampling locations through geologic time, (**b**) proportion of entries, and (**c**) proportion of unique sampling sites separated by proxy type and binned by geologic stage. Colors in panels **b** and **c** follow the convention of panel **a**.

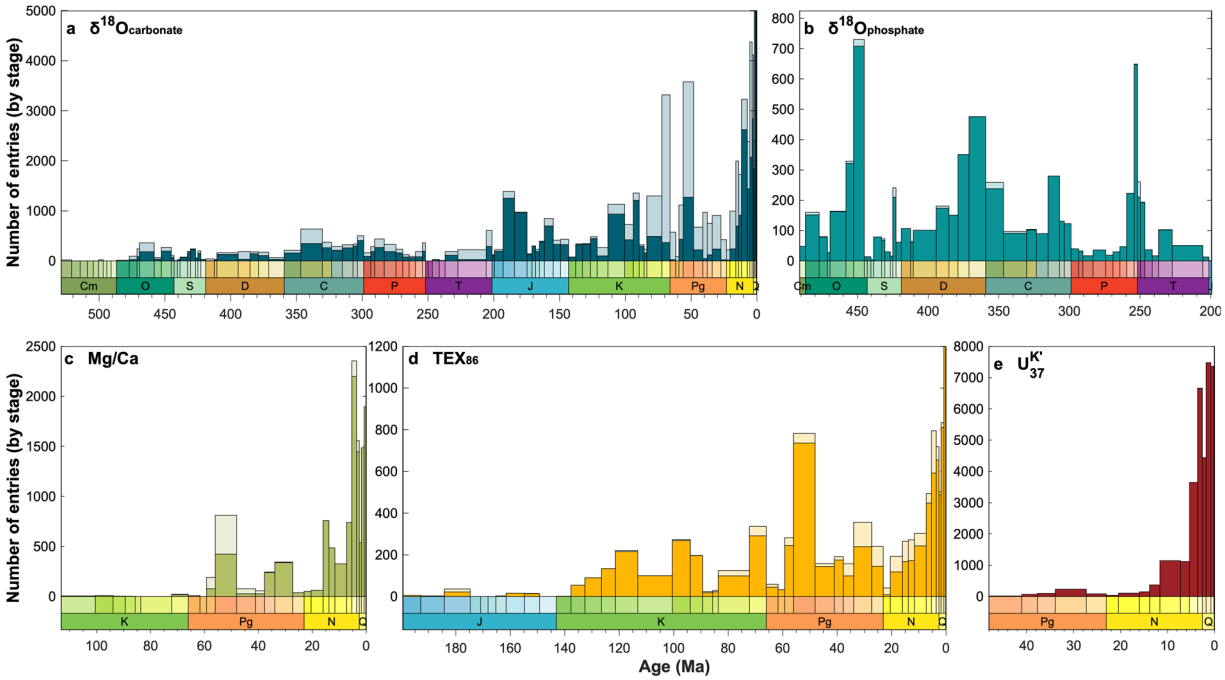

Fig. 5 Number of entries from unaltered (opaque) and total (transparent) material, separated by proxy type and binned by geologic stage. The diagenetic determinations in panels **a-c** are based on the expert-assigned *DiagenesisFlag* field. This flag applies to all proxies barring TEX_{86} and $U^{K'}_{37}$; here, TEX_{86} fidelity is based on entries with BIT, MI, and ΔRI values all below 0.5, while $U^{K'}_{37}$ data whose paleolatitude is greater than 70°N are considered compromised by alkenone production in sea ice. Due to a large increase in the number of entries approaching the Holocene, the y-axis has been scaled in panels **a** and **d**, cropping the upper limits of the Quaternary data from these plots.

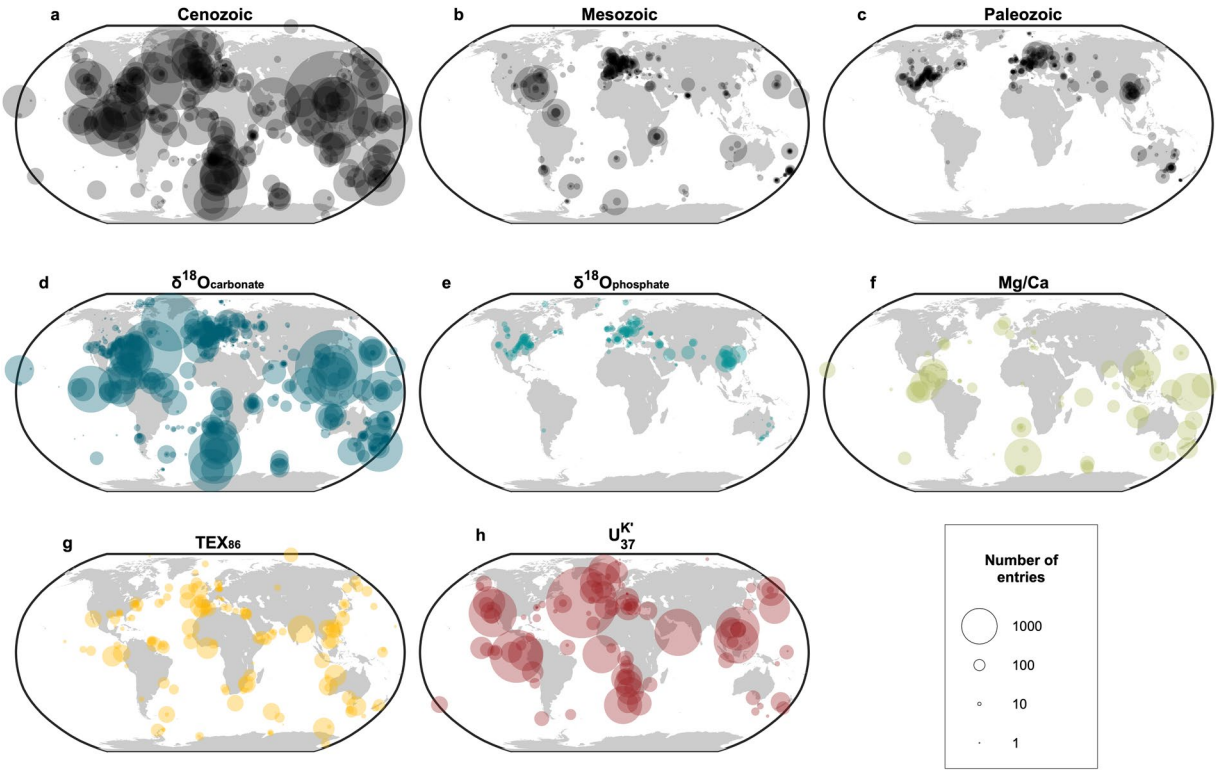

Fig. 6 Summary of the modern spatial distribution of sampling sites by (**a**–**c**) era and (**d**–**h**) proxy type, with the size of each point scaled to the number of entries at each site. All panels are plotted on the same scale.

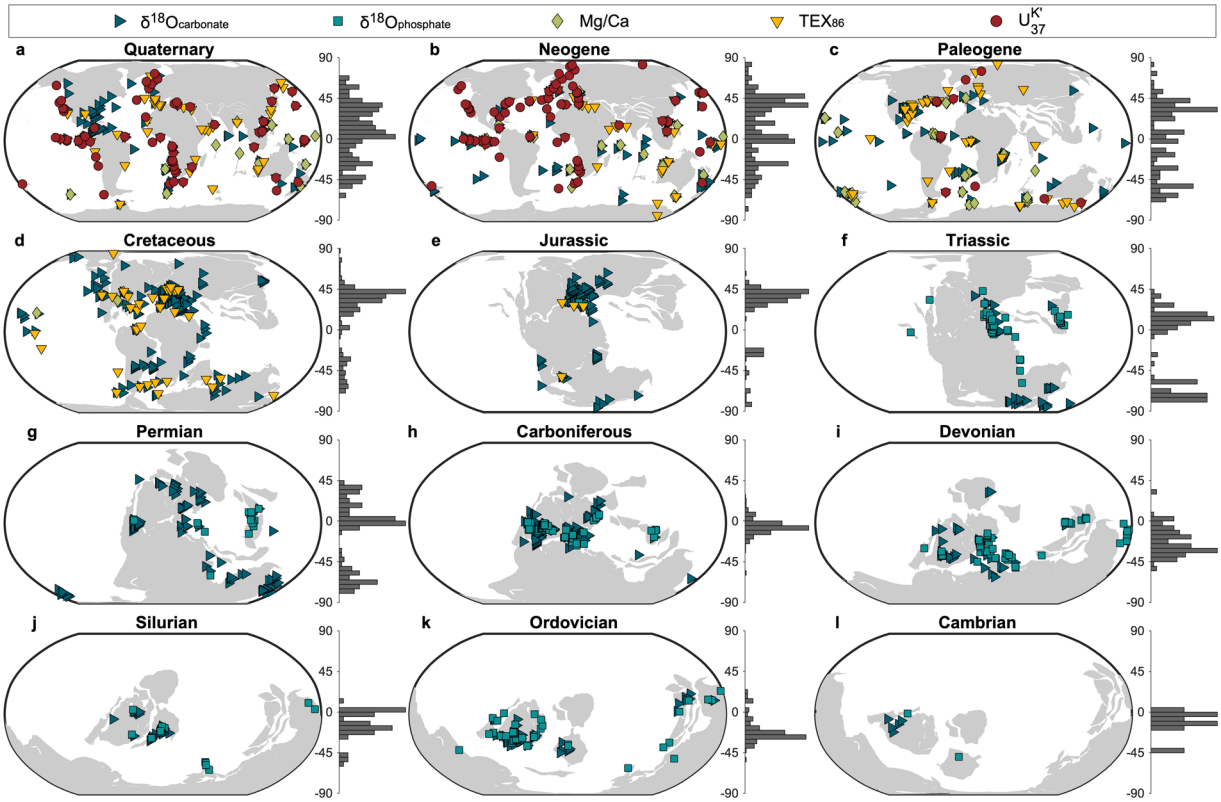

Fig. 7 Summary of the paleogeographic spatial distribution of sampling sites, colored by proxy type and separated by geologic period. Histograms to the right of each map show the relative latitudinal distribution of all unique sampling sites within 5° bins.

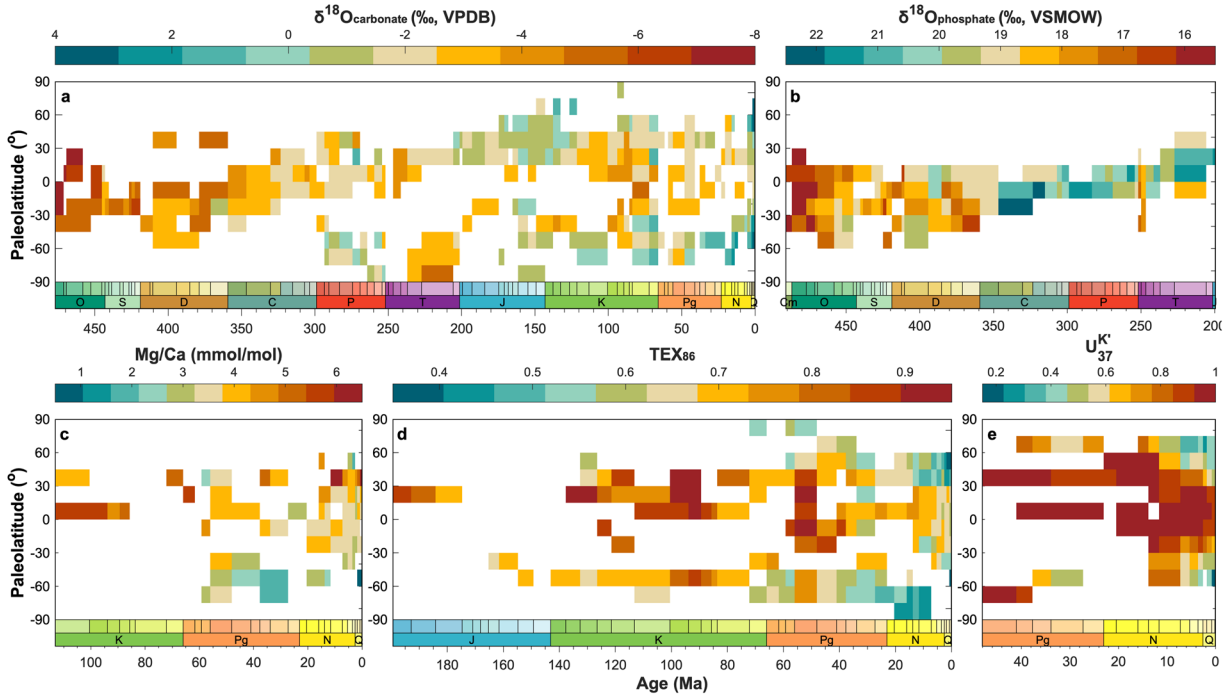

Fig. 8 Summary of the spatio-temporal trends in proxy values from unaltered materials, separated by proxy type and binned temporally by stage and spatially by 15° paleolatitudinal bins. The scale of each color bar is unique to each proxy type, but for all panels, cooler colors correspond with proxy values associated with cooler temperatures and vice versa.

Spatio-temporal trends in proxy values. The volume of data contained within PhanSST and the consistent and queryable metadata fields permit a large-scale view of the evolution of proxy information through geological time. Figure 8 shows heat maps of proxy values from unaltered material across the temporal range of each proxy, with data temporally averaged by stage and spatially averaged into 15° paleolatitudinal bins. Vertical trends show the latitudinal proxy gradient at any given stage, while the horizontal trends show temporal evolution of proxy values within a latitudinal bin.

The $\delta^{18}O_{carbonate}$ data (Fig. 8a) exhibit a clear trend toward higher values towards modern day. This trend has long been recognized and interpreted to reflect either a secular evolution in the oxygen isotopic evolution of seawater through geologic time, a true temperature signal from a much warmer ancient world, or an increased influence of diagenetic alteration with age[24,312,731,732]. Viewing the data as a function of both space and time importantly highlights that very few early Paleozoic records extend beyond the tropics, while tropical Mesozoic and (unaltered) Cenozoic data are less common. Thus, to some extent the observed shift toward higher values should logically follow based on the differences in the latitudinal extent of the data, regardless of the prevailing climate regime. The end of the Paleozoic also marks a transition from data sourced from warmer epeiric environments to continental margins, where temperatures are more likely to resemble zonal mean values[39]. Differences in the geographic and environmental spread of data between eras may therefore partly explain the long-term temporal trend.

The $\delta^{18}O_{phosphate}$ data are restricted mainly to the low latitudes in the Paleozoic, boreal mid latitudes in the Mesozoic, and absent in the Cenozoic (Fig. 8b). While there is a long-term temporal trend toward higher values across the Paleozoic, the enrichment observed in the tropics during the Carboniferous and Permian is consistent with cooling during the Late Paleozoic Icehouse[733].

The Mg/Ca data have a sporadic temporal and spatial distribution (Fig. 8c). Even during more data dense intervals, such as the late Neogene, latitudinal gradients deviate from a temperature-driven expectation. The Mg/Ca proxy is sensitive to several non-thermal factors, such as the magnesium to calcium ratio of the seawater at the time of precipitation, the bottom water calcite saturation state at the time of burial, surface ocean pH and salinity, and the cleaning method used during analysis[35–37]. Cumulatively, these factors inhibit straightforward interpretation of the raw proxy values.

Compared to the other data types, $U^{K'}_{37}$ data have a short temporal span but a wide spatial distribution. Nearly all latitudinal bins from the mid-Neogene through modern are represented (Fig. 8e). Unencumbered by non-thermal influences, the alkenone data exhibit well developed latitudinal gradients. However, because $U^{K'}_{37}$ is a ratio bounded on a 0 (cold) to 1 (hot) scale, tropical locations consistently approach the limit of the proxy, making it challenging to discern temporal trends in these regions. Though lacking the spatial coverage of the $U^{K'}_{37}$ data, the TEX_{86} data exhibit spatial and temporal trends broadly consistent with the current understanding of Cenozoic climate[3] and have the most consistent high latitude southern hemisphere coverage (Fig. 8d).

Proxy system	Non-thermal assumptions	Calibrations
$\delta^{18}O_{carbonate}$	$\delta^{18}O$ of the seawater	Bemis *et al.*[734]
	pH of the seawater	Grossman and Ku, 1986[735]
		Kim and O'Niel, 1997[736]
		Malevich *et al.*[34]
		See also Grossman, 2012[737] for more
$\delta^{18}O_{phosphate}$	$\delta^{18}O$ of the seawater	Lécuyer *et al.*[366]
		Pucéat *et al.*[738]
Mg/Ca	Mg/Ca of the seawater	Anand *et al.*[739]
	pH of the seawater	Gray and Evans, 2019[36]
	Bottom water saturation state (Ω)	Tierney *et al.*[35]
	Salinity	
	Cleaning method (oxidative or reductive)	
TEX_{86}		Schouten *et al.*[740]
		Kim *et al.*[704]
		O'Brien *et al.*[696]
		Tierney and Tingley, 2014[31]
$U^{K'}_{37}$		Müller *et al.*[741]
		Conte *et al.*[742]
		Tierney and Tingley, 2018[33]

Table 6. Non-exhaustive list of non-thermal predictor variables associated with each proxy system in PhanSST, and some commonly-used calibrations. Note that in addition to the listed non-thermal assumptions, some calibrations may also take into account other factors, such as the paleolatitude or the ocean basin from which the data derive.

The paleogeographic maps (Fig. 7) and heatmaps (Fig. 8) demonstrate that all proxies have discontinuous spatial and temporal coverage, but that collectively the Cenozoic is well represented. Geographic coverage diminishes in the Mesozoic and is extremely limited in the Paleozoic. Differences in the distribution of data, both between eras and proxies, likely bias our collective understanding of Phanerozoic climate. Identifying and acknowledge these patterns can aid in the interpretation of global climate trends and inform decisions regarding where to target future data acquisition efforts, with respect to both geography and proxy type.

Usage Notes

Informed user notice. Although PhanSST has many applications beyond its initial intended purpose, several sources of uncertainty are not constrained in the current version of the compilation. As noted above, the database does not include age uncertainty. Additionally, while specific screening procedures (e.g., XRD, SEM) can help identify altered material, the assessment of preservation is subjective, particularly in a binary sense. We have taken a conservative approach, flagging everything that was either (1) interpreted as altered in the original publication, (2) was deemed suspect based on the expert opinion of the co-authors or (3) was beyond the reasonable range of values for any given proxy. As discussed above, since there are a wide range of metrics and thresholds used to evaluate the fidelity of different proxy values, we have chosen to include proxy-specific fields that can aid in diagenetic assessments. We recommend that end-users utilize these fields, in tandem with the binary *DiagenesisFlag*, to make their own informed diagenetic determinations.

All entries in PhanSST contain raw proxy values. This decision was intentional to ensure consistency between PhanSST and the original data tables from which the data were drawn and to ensure traceability. However, where appropriate, the database includes relevant information to assist in species- or methodological-specific corrections (e.g., *AnalyticalTechnique, NBS120c, Durango, CleaningMethod*). We encourage users to make use of these fields to guarantee appropriate reuse.

Finally, we would like to recognize that the data contained within PhanSST represent the collective work of countless researchers and required an enormous amount of time, effort, and resources to generate. PhanSST has compiled these disparate data sets, but can stake no claim in their generation. Upon reuse (and when realistically feasible), we recommend users to cite both PhanSST and the original data references to ensure appropriate attribution.

Applying the database in deep time. When applying these data in the deep time, it will often be necessary to (1) convert the proxy values to temperature estimates and (2) estimate their paleogeographic position. In addition to the considerations outline above in the *Informed user notice*, it is important to make deliberate and justifiable decisions regarding the choice of temperature calibration and plate rotation model.

For any given proxy system, there are a variety of different PSMs available with which to estimate SST. There is justification to use different calibrations under different circumstances (e.g., based on the location, age, or taxon from which the data derive) and in many instances it may also be useful to report estimates of SSTs using multiple calibrations (see the *Which metadata fields are excluded and why?* section for specific examples). Similarly, in order to calculate SST, many of these proxies require assumptions about the seawater chemistry of

ancient oceans and other non-thermal variables. In Table 6 we have provided a non-exhaustive list of calibration references and potential non-thermal predictor variables for each proxy system. Some of the PSMs are straightforward transfer functions[366,704,734], allowing SSTs to be calculated by hand or, e.g., in Excel, while others involve a system of equations[31,34,35] that can be implemented in various coding languages (e.g., Python, R, or Matlab). It is important to be aware that different PSMs also handle uncertainty differently, with some providing 1σ calibration uncertainty, some providing 95% confidence intervals, and others providing no means of estimating error.

There are, similarly, myriad plate rotation models to choose from and the choice of which model is most appropriate depends upon several factors. The most important consideration is how the paleogeographic information will be used. If the data will be plotted on top of an ESM output, then to ensure the data are placed correctly the user will want to use the same rotation model as the simulation. This is particularly true in deeper time, when paleolongitudes are unconstrained[38]. Once the user has determined the appropriate plate model, rotation of the data can be implemented using G-Plates[729], either through the command line in Python or via a graphical user interface. Conversely, if the data are being used to investigate latitudinal temperature gradients during a specific time slice, then it may be prudent to try several rotation models to get a sense of the uncertainty in the values. If only paleolatitude is needed, we recommend using the Paleolatitude Calculator[38], which provides estimates–and uncertainties–from several different plate rotation models.

Data availability and nature of a living database. A static copy of PhanSST Version 0.0.1 is archived in the NOAA-NCEI Paleoclimatology Database (https://www.ncei.noaa.gov/access/paleo-search/study/36813)[26]. Version controlled releases of the database and additional reference and database metadata can be found on Zenodo (https://doi.org/10.5281/zenodo.7049233)[27] and at the PhanSST website (https://www.paleo-temperature.org). We chose to host the data on Zenodo because it (1) permits version control and (2) interfaces directly with GitHub, which will allow us to release new versions of the database under the same DOI. Despite our best efforts to identify data from the literature and QC each entry, given the sheer volume of data contained within PhanSST, there are undoubtedly errors or data sets that we have overlooked. Any issues or omissions identified by end-users can be reported on the PhanSST website and the erroneous information will be updated in future releases of the database. Likewise, the website contains a blank data entry template and instructions for entering and submitting missing or newly published data. Completed data entry forms can be submitted via the PhanSST website or emailed directly to PhanSST@outlook.com. We encourage the community to contribute newly published data so that the database can continue to grow. Through continued crowd-sourcing of data entry and QC, PhanSST will remain a useful resource for the paleoclimate community for years to come.

Code availability

Figures 4–8 were produced in Matlab. Example code and auxiliary functions to (1) reproduce Figs. 4–6 and (2) run the automated QC checks on the database are available on GitHub (https://github.com/EJJudd/SciDataSupplement). The paleocoordinates used to produce Figs. 7,8 were estimated using the plate model of Scotese and Wright[707], implemented in G-Plates (Version 2.2.0)[729].

Received: 1 March 2022; Accepted: 8 November 2022;
Published online: 06 December 2022

References

1. Emiliani, C. Pleistocene temperatures. *J. Geol.* **63**, 538–578 (1955).
2. Zachos, J. C., Pagani, M., Sloan, L., Thomas, E. & Billups, K. Trends, rhythms, and aberrations in global climate 65 Ma to present. *Science* **292**, 686–693, https://doi.org/10.1126/science.1059412 (2001).
3. Westerhold, T. *et al.* An astronomically dated record of Earth's climate and its predictability over the last 66 million years. *Science* **369**, 1383–1387, https://doi.org/10.1126/science.aba6853 (2020).
4. Falzoni, F., Petrizzo, M. R., Clarke, L. J., MacLeod, K. G. & Jenkyns, H. C. Long-term Late Cretaceous oxygen- and carbon-isotope trends and planktonic foraminiferal turnover: A new record from the southern midlatitudes. *Geol. Soc. Am. Bull.* **128**, 1725–1735, https://doi.org/10.1130/B31399.1 (2016).
5. Cramwinckel, M. J. *et al.* Synchronous tropical and polar temperature evolution in the Eocene. *Nature* **559**, 382–386, https://doi.org/10.1038/s41586-018-0272-2 (2018).
6. Hodell, D. *et al.* A reference time scale for Site U1385 (Shackleton Site) on the SW Iberian Margin. *Glob. Planet. Change* **133**, 49–64, https://doi.org/10.1016/j.gloplacha.2015.07.002 (2015).
7. Naafs, B., Hefter, J. & Stein, R. Millennial-scale ice rafting events and Hudson Strait Heinrich (-like) Events during the late Pliocene and Pleistocene: a review. *Quaternary Sci. Rev.* **80**, 1–28 (2013).
8. Hollis, C. J. *et al.* The DeepMIP contribution to PMIP4: Methodologies for selection, compilation and analysis of latest Paleocene and early Eocene climate proxy data, incorporating version 0.1 of the DeepMIP database. *Geoscientific Model. Dev.* **12**, 3149–3206, https://doi.org/10.5194/gmd-12-3149-2019 (2019).
9. McClymont, E. L. *et al.* Lessons from a high-CO_2 world: An ocean view from ~3 million years ago. *Clim. Past.* **16**, 1599–1615, https://doi.org/10.5194/cp-16-1599-2020 (2020).
10. Tierney, J. E. *et al.* Glacial cooling and climate sensitivity revisited. *Nature* **584**, 569–573, https://doi.org/10.1038/s41586-020-2617-x (2020).
11. Lawrence, K. T., Coxall, H. K., Sosdian, S. & Steinthorsdottir, M. Navigating Miocene ocean temperatures for insights into the future. *EOS: Transactions* **102**, https://doi.org/10.1029/2021EO210528 (2021).
12. Lawrence, K. T., Coxall, H. K. & Sosdian, S. Miocene temperature portal. *Dataset version 2. Bolin Cent. Database* https://doi.org/10.17043/miocene-temperature-portal-2 (2021).
13. Lunt, D. J. *et al.* DeepMIP: Model intercomparison of early Eocene climatic optimum (EECO) large-scale climate features and comparison with proxy data. *Clim. Past.* **17**, 203–227, https://doi.org/10.5194/cp-17-203-2021 (2021).
14. Zhu, J. *et al.* Assessment of equilibrium climate sensitivity of the Community Earth System Model version 2 through simulation of the Last Glacial Maximum. *Geophysical Research Letters* **48**, https://doi.org/10.1029/2020GL091220 (2021).
15. Burls, N. J. *et al.* Simulating Miocene warmth: Insights from an opportunistic multi-model ensemble (MioMIP1). *Paleoceanogr. Paleoclimatol.* https://doi.org/10.1029/2020PA004054 (2021).

16. Haywood, A. M. *et al*. The Pliocene Model Intercomparison Project Phase 2: Large-scale climate features and climate sensitivity. *Clim. Past.* **16**, 2095–2123, https://doi.org/10.5194/cp-16-2095-2020 (2020).
17. Mayhew, P. J., Jenkins, G. B. & Benton, T. G. A long-term association between global temperature and biodiversity, origination and extinction in the fossil record. *Proc. R. Soc. B: Biol. Sci.* **275**, 47–53, https://doi.org/10.1098/rspb.2007.1302 (2008).
18. Saupe, E. *et al*. Macroevolutionary consequences of profound climate change on niche evolution in marine molluscs over the past three million years. *Proceedings of the Royal Society B: Biological Sciences* **281**, https://doi.org/10.1098/rspb.2014.1995 (2014).
19. Berner, R. A., Lasaga, A. C. & Garrels, R. M. The carbonate-silicate geochemical cycle and its effect on atmospheric carbon dioxide over the past 100 million years. *Am. J. Sci.* **283**, 641–683, https://doi.org/10.2475/ajs.283.7.641 (1983).
20. Mills, B. J., Donnadieu, Y. & Goddéris, Y. Spatial continuous integration of Phanerozoic global biogeochemistry and climate. *Gondwana Res.* https://doi.org/10.1016/j.gr.2021.02.011 (2021).
21. Hay, W. W. Tectonics and climate. *Geologische Rundsch.* **85**, 409–437, https://doi.org/10.1007/BF02369000 (1996).
22. Spicer, R. A. *et al*. Constant elevation of southern Tibet over the past 15 million years. *Nature* **421**, 622–624, https://doi.org/10.1038/nature01356 (2003).
23. Grossman, E. L. & Joachimski, M. M. Chapter 10 - Oxygen isotope stratigraphy. In Gradstein, F. M., Ogg, J. G., Schmitz, M. D. & Ogg, G. M. (eds.) *Geologic Time Scale 2020*, 279-307, https://doi.org/10.1016/B978-0-12-824360-2.00010-3 (Elsevier, 2020).
24. Henkes, G. A. *et al*. Temperature evolution and the oxygen isotope composition of Phanerozoic oceans from carbonate clumped isotope thermometry. *Earth Planet. Sci. Lett.* **490**, 40–50, https://doi.org/10.1016/j.epsl.2018.02.001 (2018).
25. Song, H., Wignall, P. B., Song, H., Dai, X. & Chu, D. Seawater temperature and dissolved oxygen over the past 500 million years. *J. Earth Sci.* **30**, 236–243, https://doi.org/10.1007/s12583-018-1002-2 (2019).
26. Judd, E. J. *et al*. PhanSST - A global database of Phanerozoic sea surface temperature proxy data (v.0.0.1). *NOAA National Centers for Environmental Information* https://doi.org/10.25921/b420-jp55 (2022).
27. Judd, E. J. *et al*. Phansst - a global database of phanerozoic sea surface temperature proxy data *Zenodo* https://doi.org/10.5281/zenodo.7049233 (2022).
28. Voosen, P. A 500-million-year survey of Earth's climate reveals dire warning for humanity. *Science* https://doi.org/10.1126/science.aay1323 (2019).
29. Valdes, P. J., Scotese, C. R. & Lunt, D. J. Deep ocean temperatures through time. *Clim. Past.* **17**, 1483–1506, https://doi.org/10.5194/cp-17-1483-2021 (2021).
30. Hakim, G. J. *et al*. The last millennium climate reanalysis project: Framework and first results. *J. Geophys. Research: Atmospheres* **121**, 6745–6764, https://doi.org/10.1002/2016JD024751 (2016).
31. Tierney, J. E. & Tingley, M. P. A Bayesian, spatially-varying calibration model for the TEX_{86} proxy. *Geochim. Cosmochim. Acta* **127**, 83–106, https://doi.org/10.1016/j.gca.2013.11.026 (2014).
32. Thirumalai, K., Quinn, T. M. & Marino, G. Constraining past seawater $\delta^{18}O$ and temperature records developed from foraminiferal geochemistry. *Paleoceanography* **31**, 1409–1422, https://doi.org/10.1002/2016PA002970 (2016).
33. Tierney, J. E. & Tingley, M. P. BAYSPLINE: A new calibration for the alkenone paleothermometer. *Paleoceanogr. Paleoclimatol.* **33**, 281–301, https://doi.org/10.1002/2017PA003201 (2018).
34. Malevich, S. B., Vetter, L. & Tierney, J. E. Global core top calibration of $\delta^{18}O$ in planktic foraminifera to sea surface temperature. *Paleoceanogr. Paleoclimatol.* **34**, 1292–1315, https://doi.org/10.1029/2019PA003576 (2019).
35. Tierney, J. E., Malevich, S. B., Gray, W., Vetter, L. & Thirumalai, K. Bayesian calibration of the Mg/Ca paleothermometer in planktic foraminifera. *Paleoceanogr. Paleoclimatol.* **34**, 2005–2030, https://doi.org/10.1029/2019PA003744 (2019).
36. Gray, W. R. & Evans, D. Nonthermal influences on Mg/Ca in planktonic foraminifera: A review of culture studies and application to the last glacial maximum. *Paleoceanogr. Paleoclimatol.* **34**, 306–315, https://doi.org/10.1029/2018PA003517 (2019).
37. Evans, D., Brierley, C., Raymo, M. E., Erez, J. & Müller, W. Planktic foraminifera shell chemistry response to seawater chemistry: Pliocene-Pleistocene seawater Mg/Ca, temperature and sea level change. *Earth Planet. Sci. Lett.* **438**, 139–148, https://doi.org/10.1016/j.epsl.2016.01.013 (2016).
38. van Hinsbergen, D. J. *et al*. A paleolatitude calculator for paleoclimate studies. *PloS one* **10**, https://doi.org/10.1371/journal.pone.0126946 (2015).
39. Judd, E. J., Bhattacharya, T. & Ivany, L. C. A dynamical framework for interpreting ancient sea surface temperatures. *Geophysical Research Letters* **47**, https://doi.org/10.1029/2020GL089044 (2020).
40. Bernasconi, S. M. *et al*. InterCarb: A community effort to improve interlaboratory standardization of the carbonate clumped isotope thermometer using carbonate standards. *Geochemistry, Geophysics, Geosystems* **22**, https://doi.org/10.1029/2020GC009588 (2021).
41. Abramovich, S., Keller, G., Stüben, D. & Berner, Z. Characterization of late Campanian and Maastrichtian planktonic foraminiferal depth habitats and vital activities based on stable isotopes. *Palaeogeography, Palaeoclimatology, Palaeoecology* **202**, 1–29, https://doi.org/10.1016/s0031-0182(03)00572-8 (2003).
42. Abramovich, S. & Keller, G. Planktonic foraminiferal response to the latest Maastrichtian abrupt warm event: A case study from South Atlantic DSDP Site 525A. *Mar. Micropaleontology* **48**, 225–249, https://doi.org/10.1016/s0377-8398(03)00021-5 (2003).
43. Aguirre-Urreta, M. B. *et al*. Southern Hemisphere Early Cretaceous (Valanginian-Early Barremian) carbon and oxygen isotope curves from the Neuquén Basin, Argentina. *Cretac. Res.* **29**, 87–99, https://doi.org/10.1016/j.cretres.2007.04.002 (2008).
44. Ai, X. E. *et al*. Southern Ocean upwelling, Earth's obliquity, and glacial-interglacial atmospheric CO_2 change. *Science* **370**, 1348–1352, https://doi.org/10.1126/science.abd2115 (2020).
45. Aharon, P. & Chappell, J. Carbon and oxygen isotope probes of reef environment histories. In Barnes, D. J. (ed.) *Perspectives on Coral Reefs*, 1-15 (Australian Institute of Marine Science, 1983).
46. Albanesi, G. L., Barnes, C. R., Trotter, J. A., Williams, I. S. & Bergström, S. M. Comparative Lower-Middle Ordovician conodont oxygen isotope palaeothermometry of the Argentine Precordillera and Laurentian margins. *Palaeogeography, Palaeoclimatology, Palaeoecology* **549**, 109115, https://doi.org/10.1016/j.palaeo.2019.03.016 (2020).
47. Alberti, M., Fürsich, F. T., Pandey, D. K. & Ramkumar, M. Stable isotope analyses of belemnites from the Kachchh Basin, western India: Paleoclimatic implications for the Middle to Late Jurassic transition. *Facies* **58**, 261–278, https://doi.org/10.1007/s10347-011-0278-9 (2011).
48. Alberti, M., Fürsich, F. T. & Pandey, D. K. The Oxfordian stable isotope record ($\delta^{18}O$, $\delta^{13}C$) of belemnites, brachiopods, and oysters from the Kachchh Basin (western India) and its potential for palaeoecologic, palaeoclimatic, and palaeogeographic reconstructions. *Palaeogeography, Palaeoclimatology, Palaeoecology* **344-345**, 49–68, https://doi.org/10.1016/j.palaeo.2012.05.018 (2012).
49. Alberti, M., Fürsich, F. T., Abdelhady, A. A. & Andersen, N. Middle to Late Jurassic equatorial seawater temperatures and latitudinal temperature gradients based on stable isotopes of brachiopods and oysters from Gebel Maghara, Egypt. *Palaeogeography, Palaeoclimatology, Palaeoecology* **468**, 301–313, https://doi.org/10.1016/j.palaeo.2016.11.052 (2017).
50. Alberti, M., Fürsich, F. T. & Andersen, N. First steps in reconstructing Early Jurassic sea water temperatures in the Andean Basin of northern Chile based on stable isotope analyses of oyster and brachiopod shells. *J. Palaeogeogr.* **8**, https://doi.org/10.1186/s42501-019-0048-0 (2019).
51. Alsenz, H. *et al*. Sea surface temperature record of a Late Cretaceous tropical Southern Tethys upwelling system. *Palaeogeography, Palaeoclimatology, Palaeoecology* **392**, 350–358, https://doi.org/10.1016/j.palaeo.2013.09.013 (2013).
52. Anagnostou, E. *et al*. Changing atmospheric CO_2 concentration was the primary driver of early Cenozoic climate. *Nature* **533**, 380–384, https://doi.org/10.1038/nature17423 (2016).

53. Anagnostou, E. *et al.* Proxy evidence for state-dependence of climate sensitivity in the Eocene greenhouse. *Nature Communications* **11**, https://doi.org/10.1038/s41467-020-17887-x (2020).
54. Anderson, T. F., Popp, B. N., Williams, A. C., Ho, L. & Hudson, J. D. The stable isotopic records of fossils from the Peterborough Member, Oxford Clay Formation (Jurassic), UK: Palaeoenvironmental implications. *J. Geol. Soc.* **151**, 125–138, https://doi.org/10.1144/gsjgs.151.1.0125 (1994).
55. Ando, A., Huber, B. T., MacLeod, K. G., Ohta, T. & Khim, B.-K. Blake Nose stable isotopic evidence against the mid-Cenomanian glaciation hypothesis. *Geology* **37**, 451–454, https://doi.org/10.1130/g25580a.1 (2009).
56. Ando, A., Huber, B. T., MacLeod, K. G. & Watkins, D. K. Early Cenomanian "hot greenhouse" revealed by oxygen isotope record of exceptionally well-preserved foraminifera from Tanzania. *Paleoceanography* **30**, 1556–1572, https://doi.org/10.1002/2015pa002854 (2015).
57. Andreasson, F. P. & Schmitz, B. Winter and summer temperatures of the early middle Eocene of France from *Turritella* $\delta^{18}O$ profiles. *Geology* **24**, 1067–1070, 10.1130/0091-7613(1996)024<1067:wastot>2.3.co;2 (1996).
58. Andreasson, F. P. & Schmitz, B. Tropical Atlantic seasonal dynamics in the Early Middle Eocene from stable oxygen and carbon isotope profiles of mollusk shells. *Paleoceanography* **13**, 183–192, https://doi.org/10.1029/98pa00120 (1998).
59. Andreasson, F. P. & Schmitz, B. Temperature seasonality in the early middle Eocene North Atlantic region: Evidence from stable isotope profiles of marine gastropod shells. *Geological Society of America Bulletin* **112**, 628–640, 10.1130/0016-7606(2000)112<628:tsitem>2.0.co;2 (2000).
60. Angiolini, L. *et al.* Lower Permian brachiopods from Oman: Their potential as climatic proxies. *Earth Environ. Sci. Trans. R. Soc. Edinb.* **98**, 327–344, https://doi.org/10.1017/s1755691008075634 (2007).
61. Angiolini, L. *et al.* How cold were the Early Permian glacial tropics? Testing sea-surface temperature using the oxygen isotope composition of rigorously screened brachiopod shells. *J. Geol. Soc.* **166**, 933–945, https://doi.org/10.1144/0016-76492008-096r (2009).
62. Armendáriz, M., Rosales, I. & Quesada, C. Oxygen isotope and Mg/Ca composition of Late Viséan (Mississippian) brachiopod shells from SW Iberia: Palaeoclimatic and palaeogeographic implications in northern Gondwana. *Palaeogeography, Palaeoclimatology, Palaeoecology* **268**, 65–79, https://doi.org/10.1016/j.palaeo.2008.07.008 (2008).
63. Armendáriz, M. *et al.* High-resolution chemostratigraphic records from Lower Pliensbachian belemnites: Palaeoclimatic perturbations, organic facies and water mass exchange (Asturian basin, northern Spain). *Palaeogeography, Palaeoclimatology, Palaeoecology* **333-334**, 178–191, https://doi.org/10.1016/j.palaeo.2012.03.029 (2012).
64. Auderset, A. *et al.* Gulf Stream intensification after the early Pliocene shoaling of the Central American Seaway. *Earth Planet. Sci. Lett.* **520**, 268–278, https://doi.org/10.1016/j.epsl.2019.05.022 (2019).
65. Avila, T. D. *et al.* Role of seafloor production versus continental basalt weathering in Middle to Late Ordovician seawater $^{87}Sr/^{86}Sr$ and climate. *Earth and Planetary Science Letters* **593**, 117641, https://doi.org/10.1016/j.epsl.2022.117641 (2022).
66. Aze, T. *et al.* Extreme warming of tropical waters during the Paleocene–Eocene Thermal Maximum. *Geology* **42**, 739–742, https://doi.org/10.1130/g35637.1 (2014).
67. Azmy, K., Veizer, J., Bassett, M. G. & Copper, P. Oxygen and carbon isotopic composition of Silurian brachiopods: Implications for coeval seawater and glaciations. *Geol. Soc. Am. Bull.* **110**, 1499–1512, https://doi.org/10.1130/0016-7606(1998)110%3C1499:OACICO%3E2.3.CO;2 (1998).
68. Azmy, K. & Jin, J. Geochemistry of Late Ordovician dalmanelloid brachiopods from Laurentia: Testing the effects of paleolatitudinal gradient. *Can. J. Earth Sci.* **56**, 235–244, https://doi.org/10.1139/cjes-2018-0181 (2019).
69. Babila, T. L. *Boron/calcium in planktonic foraminifera: Proxy development and application to the Paleocene-Eocene boundary*. Ph.D. thesis, Rutgers The State University of New Jersey-New Brunswick (2014).
70. Babila, T. L., Rosenthal, Y., Wright, J. D. & Miller, K. G. A continental shelf perspective of ocean acidification and temperature evolution during the Paleocene-Eocene Thermal Maximum. *Geology* **44**, 275–278, https://doi.org/10.1130/g37522.1 (2016).
71. Bachem, P. E., Risebrobakken, B., Schepper, S. D. & McClymont, E. L. Highly variable Pliocene sea surface conditions in the Norwegian Sea. *Clim. Past.* **13**, 1153–1168, https://doi.org/10.5194/cp-13-1153-2017 (2017).
72. Bádenas, B. *et al.* Sedimentary and chemostratigraphic record of climatic cycles in Lower Pliensbachian marl–limestone platform successions of Asturias (North Spain. *Sediment. Geol.* **281**, 119–138, https://doi.org/10.1016/j.sedgeo.2012.08.010 (2012).
73. Badger, M. P. S., Schmidt, D. N., Mackensen, A. & Pancost, R. D. High-resolution alkenone palaeobarometry indicates relatively stable pCO_2 during the Pliocene (3.3–2.8 Ma). *Phil. Trans. R. Soc. A.* **371**, 20130094, https://doi.org/10.1098/rsta.2013.0094 (2013).
74. Bailey, T., Rosenthal, Y., McArthur, J., van de Schootbrugge, B. & Thirlwall, M. Paleoceanographic changes of the Late Pliensbachian–Early Toarcian interval: A possible link to the genesis of an Oceanic Anoxic Event. *Earth Planet. Sci. Lett.* **212**, 307–320, https://doi.org/10.1016/s0012-821x(03)00278-4 (2003).
75. Balinski, A. & Biernat, G. New observations on rhynchonelloid brachiopod *Dzieduszyckia* from the Famennian of Morocco. *Acta Palaeontologica Polonica* **48** (2003).
76. Balter, V., Renaud, S., Girard, C. & Joachimski, M. M. Record of climate-driven morphological changes in 376 Ma Devonian fossils. *Geology* **36**, 907, https://doi.org/10.1130/g24989a.1 (2008).
77. Barham, M., Joachimski, M., Murray, J. & Williams, D. Diagenetic alteration of the structure and $\delta^{18}O$ signature of Palaeozoic fish and conodont apatite: Potential use for corrected isotope signatures in palaeoenvironmental interpretation. *Chem. Geol.* **298-299**, 11–19, https://doi.org/10.1016/j.chemgeo.2011.12.026 (2012).
78. Barnet, J. S. *et al.* Coupled evolution of temperature and carbonate chemistry during the Paleocene–Eocene; new trace element records from the low latitude Indian Ocean. *Earth Planet. Sci. Lett.* **545**, 116414, https://doi.org/10.1016/j.epsl.2020.116414 (2020).
79. Barney, B. B. & Grossman, E. L. Reassessment of ocean paleotemperatures during the Late Ordovician. *Geology* **50**, 572–576, https://doi.org/10.1130/G49422.1 (2022).
80. Barrera, E. & Huber, B. Evolution of Antarctic waters during the Maestrichtian: Foraminifer oxygen and carbon isotope ratios, Leg 113. In *Proceedings of the Ocean Drilling Program, 113 Scientific Reports*, https://doi.org/10.2973/odp.proc.sr.113.137.1990 (Ocean Drilling Program, 1990).
81. Barrera, E. & Huber, B. Paleogene and Early Neogene oceanography of the southern Indian Ocean: Leg 119 foraminifer stable isotope results. In *Proceedings of the Ocean Drilling Program, 119 Scientific Results*, https://doi.org/10.2973/odp.proc.sr.119.167.1991 (Ocean Drilling Program, 1991).
82. Barrera, E. & Keller, G. Productivity across the Cretaceous/Tertiary boundary in high latitudes. *Geological Society of America Bulletin* **106**, 1254–1266, 10.1130/0016-7606(1994)106<1254:patctb>2.3.co;2 (1994).
83. Barrera, E. & Savin, S. M. Evolution of late Campanian-Maastrichtian marine climates and oceans. In *Evolution of the Cretaceous Ocean-Climate System*, https://doi.org/10.1130/0-8137-2332-9.245 (Geological Society of America, 1999).
84. Bartlett, R. *et al.* Abrupt global-ocean anoxia during the Late Ordovician–early Silurian detected using uranium isotopes of marine carbonates. *Proc. Natl Acad. Sci.* **115**, 5896–5901, https://doi.org/10.1073/pnas.1802438115 (2018).
85. Bassett, D., MacLeod, K. G., Miller, J. F. & Ethington, R. L. Oxygen isotopic composition of biogenic phosphate and the temperature of Early Ordovician seawater. *PALAIOS* **22**, 98–103, https://doi.org/10.2110/palo.2005.p05-089r (2007).
86. Belanger, P. & Matthews, R. The foraminiferal isotope record across the Eocene/Oligocene boundary at Deep Sea Drilling Project Site 540. In *Initial Reports of the Deep Sea Drilling Project*, 77, https://doi.org/10.2973/dsdp.proc.77.124.1984 (U.S. Government Printing Office, 1984).

87. Beltran, C. *et al*. Long chain alkenones in the Early Pliocene Sicilian sediments (Trubi Formation — Punta di Maiata section): Implications for the alkenone paleothermometry. *Palaeogeography, Palaeoclimatology, Palaeoecology* **308**, 253–263, https://doi.org/10.1016/j.palaeo.2011.03.017 (2011).
88. Beltran, C., Ohneiser, C., Hageman, K. & Scanlan, E. Evolution of the southwestern Pacific surface waters during the early Pleistocene. *N. ZealJ. Geol. Geophysics* **59**, 514–521, https://doi.org/10.1080/00288306.2016.1195756 (2016).
89. Beltran, C. *et al*. Evolution of the zonal gradients across the equatorial Pacific during the Miocene–Pleistocene. *J. Sediment. Res.* **89**, 242–252, https://doi.org/10.2110/jsr.2019.15 (2019).
90. Bemis, B. E. & Geary, D. H. The usefulness of bivalve stable isotope profiles as environmental indicators: Data from the Eastern Pacific Ocean and the Southern Caribbean Sea. *PALAIOS* **11**, 328, https://doi.org/10.2307/3515243 (1996).
91. Berger, W., Bickert, T., Schmidt, H., Wefer, G. & Yasuda, M. Quaternary oxygen isotope record of pelagic foraminifers: Site 805, Ontong Java Plateau. In *Proceedings of the Ocean Drilling Program, 130 Scientific Results*, https://doi.org/10.2973/odp.proc.sr.130.032.1993 (Ocean Drilling Program, 1993).
92. Bergmann, K. D. *et al*. A paired apatite and calcite clumped isotope thermometry approach to estimating Cambro-Ordovician seawater temperatures and isotopic composition. *Geochim. Cosmochim. Acta* **224**, 18–41, https://doi.org/10.1016/j.gca.2017.11.015 (2018).
93. Bice, K. L., Huber, B. T. & Norris, R. D. Extreme polar warmth during the Cretaceous greenhouse? Paradox of the late Turonian $\delta^{18}O$ record at Deep Sea Drilling Project Site 511. *Paleoceanography* **18**, https://doi.org/10.1029/2002pa000848 (2003).
94. Bice, K. & Norris, R. Data report: Stable isotope ratios of foraminifers from ODP Leg 207 Sites 1257, 1258, and 1260 and a cleaning procedure for foraminifers in organic-rich shales. In *Proceedings of the Ocean Drilling Program, 207 Scientific Results*, https://doi.org/10.2973/odp.proc.sr.207.104.2005 (Ocean Drilling Program, 2005).
95. Bice, K. L. *et al*. A multiple proxy and model study of Cretaceous upper ocean temperatures and atmospheric CO_2 concentrations. *Paleoceanography* **21**, https://doi.org/10.1029/2005pa001203 (2006).
96. Bijl, P. K. *et al*. Transient Middle Eocene atmospheric CO_2 and temperature variations. *Science* **330**, 819–821, https://doi.org/10.1126/science.1193654 (2010).
97. Bijl, P. K. *et al*. Eocene cooling linked to early flow across the Tasmanian Gateway. *Proc. Natl Acad. Sci.* **110**, 9645–9650, https://doi.org/10.1073/pnas.1220872110 (2013).
98. Bijl, P. K. *et al*. Maastrichtian-Rupelian paleoclimates in the southwest Pacific – a critical evaluation of biomarker paleothermometry and dinoflagellate cyst paleoecology at Ocean Drilling Program Site 1172. *Clim. Past*. https://doi.org/10.5194/cp-2021-18 (2021).
99. Biolzi, M. Stable isotopic study of Oligocene-Miocene sediments from DSDP Site 354, Equatorial Atlantic. *Mar. Micropaleontology* **8**, 121–139, https://doi.org/10.1016/0377-8398(83)90008-7 (1983).
100. Birch, H. S., Coxall, H. K. & Pearson, P. N. Evolutionary ecology of Early Paleocene planktonic foraminifera: Size, depth habitat and symbiosis. *Paleobiology* **38**, 374–390, https://doi.org/10.1666/11027.1 (2012).
101. bin Shaari, H., Yamamoto, M. & Irino, T. Enhanced upwelling in the eastern equatorial Pacific at the last five glacial terminations. *Palaeogeography, Palaeoclimatology, Palaeoecology* **386**, 8–15, https://doi.org/10.1016/j.palaeo.2013.03.022 (2013).
102. Birch, H. S., Coxall, H. K., Pearson, P. N., Kroon, D. & Schmidt, D. N. Partial collapse of the marine carbon pump after the Cretaceous-Paleogene boundary. *Geology* **44**, 287–290, https://doi.org/10.1130/g37581.1 (2016).
103. Bodin, S. *et al*. Early Cretaceous (late Berriasian to early Aptian) palaeoceanographic change along the northwestern Tethyan margin (Vocontian Trough, southeastern France): $\delta^{13}C$, $\delta^{18}O$ and Sr-isotope belemnite and whole-rock records. *Cretac. Res.* **30**, 1247–1262, https://doi.org/10.1016/j.cretres.2009.06.006 (2009).
104. Boersma, A., Shackleton, N., Hall, M. & Given, Q. Carbon and oxygen isotope records at DSDP Site 384 (North Atlantic) and some Paleocene paleotemperatures and carbon isotope variations in the Atlantic Ocean. In *Initial Reports of the Deep Sea Drilling Project*, https://doi.org/10.2973/dsdp.proc.43.131.1979 (U.S. Government Printing Office, 1979).
105. Boersma, A. & Shackleton, N. Oxygen- and carbon-isotope variations and planktonic foraminifer depth habitats, Late Cretaceous to Paleocene, central Pacific, Deep Sea Drilling Project Sites 463 and 465. In *Initial Reports of the Deep Sea Drilling Project*, 62, https://doi.org/10.2973/dsdp.proc.62.116.1981 (U.S. Government Printing Office, 1981).
106. Bohaty, S. M., Zachos, J. C. & Delaney, M. L. Foraminiferal Mg/Ca evidence for Southern Ocean cooling across the Eocene–Oligocene transition. *Earth Planet. Sci. Lett.* **317-318**, 251–261, https://doi.org/10.1016/j.epsl.2011.11.037 (2012).
107. Bojar, A.-V., Hiden, H., Fenninger, A. & Neubauer, F. Middle Miocene seasonal temperature changes in the Styrian basin, Austria, as recorded by the isotopic composition of pectinid and brachiopod shells. *Palaeogeography, Palaeoclimatology, Palaeoecology* **203**, 95–105, https://doi.org/10.1016/s0031-0182(03)00662-x (2004).
108. Bonin, A. *et al*. Cool episode and platform demise in the Early Aptian: New insights on the links between climate and carbonate production. *Paleoceanography* **31**, 66–80, https://doi.org/10.1002/2015pa002835 (2016).
109. Bornemann, A. *et al*. Isotopic evidence for glaciation during the Cretaceous supergreenhouse. *Science* **319**, 189–192, https://doi.org/10.1126/science.1148777 (2008).
110. Bornemann, A. *et al*. Persistent environmental change after the Paleocene–Eocene Thermal Maximum in the eastern North Atlantic. *Earth Planet. Sci. Lett.* **394**, 70–81, https://doi.org/10.1016/j.epsl.2014.03.017 (2014).
111. Bornemann, A., Dhaenens, S., Norris, R. D. & Speijer, R. P. The demise of the early Eocene greenhouse – Decoupled deep and surface water cooling in the eastern North Atlantic. *Glob. Planet. Change* **145**, 130–140, https://doi.org/10.1016/j.gloplacha.2016.08.010 (2016).
112. Bralower, T. J. *et al*. Late Paleocene to Eocene paleoceanography of the equatorial Pacific Ocean: Stable isotopes recorded at Ocean Drilling Program Site 865, Allison Guyot. *Paleoceanography* **10**, 841–865, https://doi.org/10.1029/95pa01143 (1995).
113. Brand, U. & Veizer, J. Chemical diagenesis of a multicomponent carbonate system; 2: Stable isotopes. *Journal of Sedimentary Research* **51**, https://doi.org/10.1306/212f7df6-2b24-11d7-8648000102c1865d (1981).
114. Brand, U. Global climatic changes during the Devonian-Mississippian: Stable isotope biogeochemistry of brachiopods. *Glob. Planet. Change* **1**, 311–329, https://doi.org/10.1016/0921-8181(89)90008-8 (1989).
115. Brand, U. Aragonite-calcite transformation based on Pennsylvanian molluscs. *Geological Society of America Bulletin* **101**, 377–390, 10.1130/0016-7606(1989)101<0377:actbop>2.3.co;2 (1989).
116. Brand, U. & Legrand-Blain, M. Paleoecology and biogeochemistry of brachiopods from the Devonian-Carboniferous boundary interval of the Griotte Formation, La Serre, Montagne Noire, France. *Annales de la Société géologique de Belgique* (1992).
117. Brand, U. & Brenckle, P. Chemostratigraphy of the Mid-Carboniferous boundary global stratotype section and point (GSSP), Bird Spring Formation, Arrow Canyon, Nevada, USA. *Palaeogeography, Palaeoclimatology, Palaeoecology* **165**, 321–347, https://doi.org/10.1016/s0031-0182(00)00169-3 (2001).
118. Brand, U. & Bruckschen, P. Correlation of the askyn river section, southern urals, russia, with the mid-carboniferous boundary gssp, bird spring formation, arrow canyon, nevada, usa: implications for global paleoceanography. *Palaeogeography, Palaeoclimatology, Palaeoecology* **184**, 177–193, https://doi.org/10.1016/S0031-0182(02)00257-2 (2002).
119. Brand, U., Logan, A., Hiller, N. & Richardson, J. Geochemistry of modern brachiopods: applications and implications for oceanography and paleoceanography. *Chem. Geol.* **198**, 305–334, https://doi.org/10.1016/s0009-2541(03)00032-9 (2003).
120. Brand, U. Carbon, oxygen and strontium isotopes in Paleozoic carbonate components: an evaluation of original seawater-chemistry proxies. *Chem. Geol.* **204**, 23–44, https://doi.org/10.1016/j.chemgeo.2003.10.013 (2004).

121. Brand, U., Legrand-Blain, M. & Streel, M. Biochemostratigraphy of the Devonian-Carboniferous boundary global stratotype section and point, Griotte Formation, La Serre, Montagne Noire, France. *Palaeogeography, Palaeoclimatology, Palaeoecology* **205**, 337–357, https://doi.org/10.1016/j.palaeo.2003.12.015 (2004).
122. Brand, U. *et al*. The end-Permian mass extinction: A rapid volcanic CO_2 and CH_4-climatic catastrophe. *Chem. Geol.* **322-323**, 121–144, https://doi.org/10.1016/j.chemgeo.2012.06.015 (2012).
123. Brierley, C. M. *et al*. Greatly expanded tropical warm pool and weakened Hadley circulation in the Early Pliocene. *Science* **323**, 1714–1718, https://doi.org/10.1126/science.1167625 (2009).
124. Brigaud, B., Pucéat, E., Pellenard, P., Vincent, B. & Joachimski, M. M. Climatic fluctuations and seasonality during the Late Jurassic (Oxfordian–Early Kimmeridgian) inferred from $\delta^{18}O$ of Paris Basin oyster shells. *Earth Planet. Sci. Lett.* **273**, 58–67, https://doi.org/10.1016/j.epsl.2008.06.015 (2008).
125. Brigaud, B. *et al*. Facies and climate/environmental changes recorded on a carbonate ramp: A sedimentological and geochemical approach on Middle Jurassic carbonates (Paris Basin, France. *Sediment. Geol.* **222**, 181–206, https://doi.org/10.1016/j.sedgeo.2009.09.005 (2009).
126. Brookfield, M. & Hannigan, R. Carbon and oxygen isotope variations in shell beds from the Upper Ordovician (mid-Cincinnatian: Maysvillian to early Richmondian) of Ontario: Evaluation of the Warm Saline Deep Ocean hypothesis, paleoceanographic changes, and Milankovitch orbital cycles in the transition to the Hirnantian glaciation. *Palaeogeography, Palaeoclimatology, Palaeoecology* **577**, 110528, https://doi.org/10.1016/j.palaeo.2021.110528 (2021).
127. Bruckschen, P. & Veizer, J. Oxygen and carbon isotopic composition of Dinantian brachiopods: Paleoenvironmental implications for the Lower Carboniferous of western Europe. *Palaeogeography, Palaeoclimatology, Palaeoecology* **132**, 243–264, https://doi.org/10.1016/s0031-0182(97)00066-7 (1997).
128. Bruckschen, P., Oesmann, S. & Veizer, J. Isotope stratigraphy of the European Carboniferous: proxy signals for ocean chemistry, climate and tectonics. *Chem. Geol.* **161**, 127–163, https://doi.org/10.1016/s0009-2541(99)00084-4 (1999).
129. Bruckschen, P., Veizer, J., Schwark, L. & Leythaeuser, D. Isotope stratigraphy for the transition from the late Palaeozoic greenhouse in the Permo-Carboniferous icehouse–new results. *Terra Nostra* **4**, 7–11 (2001).
130. Buening, N., Carlson, S. J., Spero, H. J. & Lee, D. E. Evidence for the Early Oligocene formation of a proto-Subtropical Convergence from oxygen isotope records of New Zealand Paleogene brachiopods. *Palaeogeography, Palaeoclimatology, Palaeoecology* **138**, 43–68, https://doi.org/10.1016/s0031-0182(97)00113-2 (1998).
131. Buggisch, W., Joachimski, M. M., Sevastopulo, G. & Morrow, J. R. Mississippian $\delta^{13}C_{carb}$ and conodont apatite $\delta^{18}O$ records — Their relation to the Late Palaeozoic Glaciation. *Palaeogeography, Palaeoclimatology, Palaeoecology* **268**, 273–292, https://doi.org/10.1016/j.palaeo.2008.03.043 (2008).
132. Buggisch, W. *et al*. Did intense volcanism trigger the first Late Ordovician icehouse? *Geology* **38**, 327–330, https://doi.org/10.1130/g30577.1 (2010).
133. Bühring, C., Sarnthein, M. & Erlenkeuser, H. Toward a high-resolution stable isotope stratigraphy of the last 1.1 m.y.: Site 1144, South China Sea. In *Proceedings of the Ocean Drilling Program*, https://doi.org/10.2973/odp.proc.sr.184.205.2004 (Ocean Drilling Program, 2004).
134. Buick, D. P. & Ivany, L. C. 100 years in the dark: Extreme longevity of Eocene bivalves from Antarctica. *Geology* **32**, 921, https://doi.org/10.1130/g20796.1 (2004).
135. Burgess, C. E. *et al*. Middle Eocene climate cyclicity in the southern Pacific: Implications for global ice volume. *Geology* **36**, 651, https://doi.org/10.1130/g24762a.1 (2008).
136. Caley, T. *et al*. High-latitude obliquity as a dominant forcing in the Agulhas current system. *Clim. Past.* **7**, 1285–1296, https://doi.org/10.5194/cp-7-1285-2011 (2011).
137. Came, R. E. *et al*. Coupling of surface temperatures and atmosphericCO_2 concentrations during the Palaeozoic era. *Nature* **449**, 198–201, https://doi.org/10.1038/nature06085 (2007).
138. Cannariato, K. G. & Ravelo, A. C. Pliocene-Pleistocene evolution of eastern tropical Pacific surface water circulation and thermocline depth. *Paleoceanography* **12**, 805–820, https://doi.org/10.1029/97pa02514 (1997).
139. Carpentier, C., Martin-Garin, B., Lathuiliere, B. & Ferry, S. Correlation of reefal Oxfordian episodes and climatic implications in the eastern Paris Basin (France). *Terra Nova* **18**, 191–201, https://doi.org/10.1111/j.1365-3121.2006.00679.x (2006).
140. Cartagena-Sierra, A. *et al*. Latitudinal migrations of the subtropical front at the Agulhas Plateau through the Mid-Pleistocene Transition. *Paleoceanogr. Paleoclimatol.* **36**, https://doi.org/10.1029/2020pa004084 (2021).
141. Carter, R., Gammon, P. & Millwood, L. Glacial–interglacial (MIS 1–10) migrations of the Subtropical Front across ODP Site 1119, Canterbury Bight, Southwest Pacific Ocean. *Mar. Geol.* **205**, 29–58, https://doi.org/10.1016/s0025-3227(04)00017-9 (2004).
142. Carter, R. M. & Gammon, P. New Zealand maritime glaciation: Millennial-scale southern climate change since 3.9 Ma. *Science* **304**, 1659–1662, https://doi.org/10.1126/science.1093726 (2004).
143. Castañeda, I. S. *et al*. Millennial-scale sea surface temperature changes in the eastern Mediterranean (Nile River Delta region) over the last 27,000 years. *Paleoceanography* **25**, https://doi.org/10.1029/2009pa001740 (2010).
144. Cavalheiro, L. *et al*. Impact of global cooling on Early Cretaceous high pCO_2 world during the Weissert Event. *Nat. Commun.* **12**, 5411, https://doi.org/10.1038/s41467-021-25706-0 (2021).
145. Channell, J. E. T., Hodell, D. A. & Curtis, J. H. ODP Site 1063 (Bermuda Rise) revisited: Oxygen isotopes, excursions and paleointensity in the Brunhes Chron. *Geochem. Geophys. Geosyst.* **13**, https://doi.org/10.1029/2011gc003897 (2012).
146. Channell, J., Wright, J., Mazaud, A. & Stoner, J. Age through tandem correlation of Quaternary relative paleointensity (RPI) and oxygen isotope data at IODP Site U1306 (Eirik Drift, SW Greenland. *Quaternary Sci. Rev.* **88**, 135–146, https://doi.org/10.1016/j.quascirev.2014.01.022 (2014).
147. Chen, B. *et al*. Permian ice volume and palaeoclimate history: Oxygen isotope proxies revisited. *Gondwana Res.* **24**, 77–89, https://doi.org/10.1016/j.gr.2012.07.007 (2013).
148. Chen, J. *et al*. High-resolution SIMS oxygen isotope analysis on conodont apatite from South China and implications for the end-Permian mass extinction. *Palaeogeography, Palaeoclimatology, Palaeoecology* **448**, 26–38, https://doi.org/10.1016/j.palaeo.2015.11.025 (2016).
149. Chen, B. *et al*. Ice volume and paleoclimate history of the Late Paleozoic Ice Age from conodont apatite oxygen isotopes from Naqing (Guizhou, China. *Palaeogeography, Palaeoclimatology, Palaeoecology* **448**, 151–161, https://doi.org/10.1016/j.palaeo.2016.01.002 (2016).
150. Chen, J. *et al*. Abrupt warming in the latest Permian detected using high-resolution in situ oxygen isotopes of conodont apatite from Abadeh, central Iran. *Palaeogeography, Palaeoclimatology, Palaeoecology* **560**, 109973, https://doi.org/10.1016/j.palaeo.2020.109973 (2020).
151. Chen, B. *et al*. Devonian paleoclimate and its drivers: A reassessment based on a new conodont $\delta^{18}O$ record from South China. *Earth-Sci. Rev.* **222**, 103814, https://doi.org/10.1016/j.earscirev.2021.103814 (2021).
152. Chen, Y. *et al*. Smithian and Spathian (Early Triassic) conodonts from Oman and Croatia and their depth habitat revealed. *Glob. Planet. Change* **196**, 103362, https://doi.org/10.1016/j.gloplacha.2020.103362 (2021).
153. Chen, B. *et al*. Was climatic cooling during the earliest Carboniferous driven by expansion of seed plants? *Earth Planet. Sci. Lett.* **565**, 116953, https://doi.org/10.1016/j.epsl.2021.116953 (2021).
154. Cheng, X., Tian, J. & Wang, P. Data report: Stable isotopes from Site 1143. In *Proceedings of the Ocean Drilling Program*, https://doi.org/10.2973/odp.proc.sr.184.221.2004 (Ocean Drilling Program, 2004).

155. Cheng, X. *et al*. Data report: Stable isotopes from Sites 1147 and 1148. In *Proceedings of the Ocean Drilling Program*, https://doi.org/10.2973/odp.proc.sr.184.223.2004 (Ocean Drilling Program, 2004).
156. Christensen, B. A. *et al*. Indonesian Throughflow drove Australian climate from humid Pliocene to arid Pleistocene. *Geophys. Res. Lett.* **44**, 6914–6925, https://doi.org/10.1002/2017gl072977 (2017).
157. Clemens, S. C., Murray, D. W. & Prell, W. L. Nonstationary phase of the Plio-Pleistocene Asian monsoon. *Science* **274**, 943–948, https://doi.org/10.1126/science.274.5289.943 (1996).
158. Clemens, S. C. *et al*. Remote and local drivers of Pleistocene South Asian summer monsoon precipitation: A test for future predictions. *Sci. Adv*. **7**, https://doi.org/10.1126/sciadv.abg3848 (2021).
159. Coimbra, R. & Olóriz, F. Geochemical evidence for sediment provenance in mudstones and fossil-poor wackestones (Upper Jurassic, Majorca Island). *Terra Nova* **24**, 437–445, https://doi.org/10.1111/j.1365-3121.2012.01082.x (2012).
160. Compston, W. The carbon isotopic compositions of certain marine invertebrates and coals from the Australian Permian. *Geochim. Cosmochim. Acta* **18**, 1–22, https://doi.org/10.1016/0016-7037(60)90013-2 (1960).
161. Corfield, R. M. & Cartlidge, J. E. Oceanographic and climatic implications of the Palaeocene carbon isotope maximum. *Terra Nova* **4**, 443–455, https://doi.org/10.1111/j.1365-3121.1992.tb00579.x (1992).
162. Corfield, R. & Cartlidge, J. Oxygen and carbon isotope stratigraphy of the Middle Miocene, Holes 805B and 806B. In *Proceedings of the Ocean Drilling Program, 130 Scientific Results*, https://doi.org/10.2973/odp.proc.sr.130.026.1993 (Ocean Drilling Program, 1993).
163. Cramwinckel, M. J. *et al*. A warm, stratified, and restricted Labrador Sea across the Middle Eocene and its climatic optimum. *Paleoceanogr. Paleoclimatol*. **35**, https://doi.org/10.1029/2020pa003932 (2020).
164. Cramwinckel, M. J. *et al*. Surface-circulation change in the southwest Pacific Ocean across the Middle Eocene Climatic Optimum: Inferences from dinoflagellate cysts and biomarker paleothermometry. *Clim. Past.* **16**, 1667–1689, https://doi.org/10.5194/cp-16-1667-2020 (2020).
165. Crivellari, S. *et al*. Thermal response of the western tropical Atlantic to slowdown of the Atlantic Meridional Overturning Circulation. *Earth Planet. Sci. Lett*. **519**, 120–129, https://doi.org/10.1016/j.epsl.2019.05.006 (2019).
166. Crouch, E. *et al*. Climatic and environmental changes across the early Eocene climatic optimum at mid-Waipara River, Canterbury Basin, New Zealand. *Earth-Sci. Rev.* **200**, 102961, https://doi.org/10.1016/j.earscirev.2019.102961 (2020).
167. Dauner, A. L. L. *et al*. Multi-proxy reconstruction of sea surface and subsurface temperatures in the western South Atlantic over the last:75 kyr. *Quaternary Sci. Rev.* **215**, 22–34, https://doi.org/10.1016/j.quascirev.2019.04.020 (2019).
168. Davtian, N., Bard, E., Darfeuil, S., Ménot, G. & Rostek, F. The novel hydroxylated tetraether index RI-OH' as a sea surface temperature proxy for the 160-45 ka BP period off the Iberian Margin. *Paleoceanogr. Paleoclimatol*. **36**, https://doi.org/10.1029/2020pa004077 (2021).
169. de Bar, M. W., Rampen, S. W., Hopmans, E. C., Sinninghe Damsté, J. S. & Schouten, S. Constraining the applicability of organic paleotemperature proxies for the last 90 Myrs. *Org. Geochem.* **128**, 122–136, https://doi.org/10.1016/j.orggeochem.2018.12.005 (2019).
170. de Garidel-Thoron, T., Rosenthal, Y., Bassinot, F. & Beaufort, L. Stable sea surface temperatures in the western Pacific warm pool over the past 1.75 million years. *Nature* **433**, 294–298, https://doi.org/10.1038/nature03189 (2005).
171. Dekens, P. S., Ravelo, A. C. & McCarthy, M. D. Warm upwelling regions in the Pliocene warm period. *Paleoceanography* **22**, https://doi.org/10.1029/2006pa001394 (2007).
172. Delaney, M. L., Popp, B. N., Lepzelter, C. G. & Anderson, T. F. Lithium-to-calcium ratios in Modern, Cenozoic, and Paleozoic articulate brachiopod shells. *Paleoceanography* **4**, 681–691, https://doi.org/10.1029/pa004i006p00681 (1989).
173. Dera, G. *et al*. Water mass exchange and variations in seawater temperature in the NW Tethys during the Early Jurassic: Evidence from neodymium and oxygen isotopes of fish teeth and belemnites. *Earth Planet. Sci. Lett.* **286**, 198–207, https://doi.org/10.1016/j.epsl.2009.06.027 (2009).
174. Dera, G. *et al*. Climatic ups and downs in a disturbed Jurassic world. *Geology* **39**, 215–218, https://doi.org/10.1130/g31579.1 (2011).
175. De Schepper, S. *et al*. Northern hemisphere glaciation during the globally warm early Late Pliocene. *PLoS ONE* **8**, https://doi.org/10.1371/journal.pone.0081508 (2013).
176. De Vleeschouwer, D. *et al*. The amplifying effect of Indonesian Throughflow heat transport on Late Pliocene Southern Hemisphere climate cooling. *Earth Planet. Sci. Lett.* **500**, 15–27, https://doi.org/10.1016/j.epsl.2018.07.035 (2018).
177. De Vleeschouwer, D., Petrick, B. F. & Martnez-Garca, A. Stepwise weakening of the Pliocene Leeuwin Current. *Geophys. Res. Lett.* **46**, 8310–8319, https://doi.org/10.1029/2019gl083670 (2019).
178. DHondt, S. & Zachos, J. C. On stable isotopic variation and earliest Paleocene planktonic foraminifera. *Paleoceanography* **8**, 527–547, https://doi.org/10.1029/93pa00952 (1993).
179. DHondt, S. & Lindinger, M. A stable isotopic record of the Maastrichtian ocean-climate system: South Atlantic DSDP Site 528. *Palaeogeography, Palaeoclimatology, Palaeoecology* **112**, 363–378, https://doi.org/10.1016/0031-0182(94)90081-7 (1994).
180. Ditchfield, P., Marshall, J. & Pirrie, D. High latitude palaeotemperature variation: New data from the Thithonian to Eocene of James Ross Island, Antarctica. *Palaeogeography, Palaeoclimatology, Palaeoecology* **107**, 79–101, https://doi.org/10.1016/0031-0182(94)90166-x (1994).
181. Ditchfield, P. W. High northern palaeolatitude Jurassic-Cretaceous palaeotemperature variation: New data from Kong Karls Land, Svalbard. *Palaeogeography, Palaeoclimatology, Palaeoecology* **130**, 163–175, https://doi.org/10.1016/s0031-0182(96)00054-5 (1997).
182. Dorman, F. H. & Gill, E. D. Oxygen isotope paleotemperature determinations of Australian Cainozoic fossils. *Science* **130**, 1576–1576, https://doi.org/10.1126/science.130.3388.1576 (1959).
183. Douglas, R. G. & Savin, S. M. Oxygen isotopic evidence for the depth stratification of Tertiary and Cretaceous planktic foraminifera. *Mar. Micropaleontology* **3**, 175–196, https://doi.org/10.1016/0377-8398(78)90004-x (1978).
184. Douglas, P. M. J. *et al*. Pronounced zonal heterogeneity in Eocene southern high-latitude sea surface temperatures. *Proc. Natl Acad. Sci.* **111**, 6582–6587, https://doi.org/10.1073/pnas.1321441111 (2014).
185. Dowsett, H. J., Foley, K. M., Robinson, M. M. & Herbert, T. D. PRISM late Pliocene (Piacenzian) alkenone-derived SST data. *US Geological Survey data release* https://doi.org/10.5066/F7959G1S (2017).
186. Droxler, A., Bruce, C., Sager, W. & Watkins, D. Pliocene-Pleistocene variations in aragonite content and planktonic oxygen-isotope record in Bahamian periplatform ooze, Hole 633A. In *Proceedings of the Ocean Drilling Program, 101 Scientific Results*, https://doi.org/10.2973/odp.proc.sr.101.134.1988 (Ocean Drilling Program, 1988).
187. Droxler, A., Haddad, G., Mucciarone, D. & Cullen, J. Pliocene-Pleistocene aragonite cyclic variations in Holes 714A and 716B (the Maldives) compared with Hole 633A (the Bahamas): Records of climate-induced $CaCO_3$ preservation at intermediate water depths. In *Proceedings of the Ocean Drilling Program, 115 Scientific Results*, https://doi.org/10.2973/odp.proc.sr.115.179.1990 (Ocean Drilling Program, 1990).
188. Drury, A. J. *et al*. Deciphering the state of the Late Miocene to Early Pliocene equatorial Pacific. *Paleoceanogr. Paleoclimatol.* **33**, 246–263, https://doi.org/10.1002/2017pa003245 (2018).
189. Dumitrescu, M., Brassell, S. C., Schouten, S., Hopmans, E. C. & Sinninghe Damsté, J. S. Instability in tropical Pacific sea-surface temperatures during the early Aptian. *Geology* **34**, 833, https://doi.org/10.1130/g22882.1 (2006).
190. Dupont, L., Donner, B., Schneider, R. & Wefer, G. Mid-Pleistocene environmental change in tropical Africa began as early as 1.05 Ma. *Geology* **29**, 195, 10.1130/0091-7613(2001)029<0195:mpecit>2.0.co;2 (2001).

191. Dutton, A., Lohmann, K. & Leckie, R. Data report: Stable isotope and Mg/Ca of Paleocene and Eocene foraminifers, ODP Site 1209, Shatsky Rise. In *Proceedings of the Ocean Drilling Program, 198 Scientific Results*, https://doi.org/10.2973/odp.proc.sr.198.119.2005 (Ocean Drilling Program, 2005).
192. Dutton, A., Huber, B. T., Lohmann, K. C. & Zinsmeister, W. J. High-resolution stable isotope profiles of a Dimitobelid belemnite: Implications for paleodepth habitat and late Maastrichtian climate seasonality. *PALAIOS* **22**, 642–650, https://doi.org/10.2110/palo.2005.p05-064r (2007).
193. Dyez, K. A. & Ravelo, A. C. Dynamical changes in the tropical Pacific warm pool and zonal SST gradient during the Pleistocene. *Geophys. Res. Lett.* **41**, 7626–7633, https://doi.org/10.1002/2014gl061639 (2014).
194. Edgar, K. M., Wilson, P. A., Sexton, P. F. & Suganuma, Y. No extreme bipolar glaciation during the main Eocene calcite compensation shift. *Nature* **448**, 908–911, https://doi.org/10.1038/nature06053 (2007).
195. Edgar, K. M. *et al.* Symbiont bleaching in planktic foraminifera during the Middle Eocene Climatic Optimum. *Geology* **41**, 15–18, https://doi.org/10.1130/g33388.1 (2012).
196. Edwards, C. T., Jones, C. M., Quinton, P. C. & Fike, D. A. Oxygen isotope (δ^{18} O) trends measured from Ordovician conodont apatite using secondary ion mass spectrometry (SIMS): Implications for paleo-thermometry studies. *Geological Society of America Bulletin* https://doi.org/10.1130/b35891.1 (2021).
197. Edward, O. *et al.* A Baltic Perspective on the Early to Early Late Ordovician δ13C and δ18O Records and Its Paleoenvironmental Significance. *Paleoceanogr. Paleoclimatol.* **37**, e2021PA004309, https://doi.org/10.1029/2021PA004309 (2022).
198. Elling, F. J. *et al.* Archaeal lipid biomarker constraints on the Paleocene-Eocene carbon isotope excursion. *Nature Communications* **10**, https://doi.org/10.1038/s41467-019-12553-3 (2019).
199. Elorza, J., Garcia-Garmilla, F. & Jagt, J. Diagenesis-related differences in isotopic and elemental composition of Late Campanian and Early Maastrichtian inoceramids and belemnites from NE Belgium: Palaeoenvironmental implications. *Geologie en. Mijnb.* **75**, 349–360 (1996).
200. Elrick, M. *et al.* Stratigraphic and oxygen isotope evidence for My-scale glaciation driving eustasy in the Early–Middle Devonian greenhouse world. *Palaeogeography, Palaeoclimatology, Palaeoecology* **276**, 170–181, https://doi.org/10.1016/j.palaeo.2009.03.008 (2009).
201. Elrick, M. & Scott, L. A. Carbon and oxygen isotope evidence for high-frequency (10^4–10^5 yr) and My-scale glacio-eustasy in Middle Pennsylvanian cyclic carbonates (Gray Mesa Formation), central New Mexico. *Palaeogeography, Palaeoclimatology, Palaeoecology* **285**, 307–320, https://doi.org/10.1016/j.palaeo.2009.11.023 (2010).
202. Elrick, M. *et al.* Orbital-scale climate change and glacioeustasy during the early Late Ordovician (pre-Hirnantian) determined from δ^{18}O values in marine apatite. *Geology* **41**, 775–778, https://doi.org/10.1130/g34363.1 (2013).
203. Elrick, M. & Witzke, B. Orbital-scale glacio-eustasy in the Middle Devonian detected using oxygen isotopes of conodont apatite: Implications for long-term greenhouse–icehouse climatic transitions. *Palaeogeography, Palaeoclimatology, Palaeoecology* **445**, 50–59, https://doi.org/10.1016/j.palaeo.2015.12.019 (2016).
204. Erbacher, J., Huber, B. T., Norris, R. D. & Markey, M. Increased thermohaline stratification as a possible cause for an ocean anoxic event in the Cretaceous period. *Nature* **409**, 325–327, https://doi.org/10.1038/35053041 (2001).
205. Erbacher, J., Friedrich, O., Wilson, P. A., Lehmann, J. & Weiss, W. Short-term warming events during the boreal Albian (mid-Cretaceous). *Geology* **39**, 223–226, https://doi.org/10.1130/g31606.1 (2011).
206. Esmeray-Senlet, S. *et al.* Evidence for reduced export productivity following the Cretaceous/Paleogene mass extinction. *Paleoceanography* **30**, 718–738, https://doi.org/10.1002/2014pa002724 (2015).
207. Etourneau, J., Martinez, P., Blanz, T. & Schneider, R. Pliocene–Pleistocene variability of upwelling activity, productivity, and nutrient cycling in the Benguela region. *Geology* **37**, 871–874, https://doi.org/10.1130/g25733a.1 (2009).
208. Etourneau, J., Schneider, R., Blanz, T. & Martinez, P. Intensification of the Walker and Hadley atmospheric circulations during the Pliocene–Pleistocene climate transition. *Earth Planet. Sci. Lett.* **297**, 103–110, https://doi.org/10.1016/j.epsl.2010.06.010 (2010).
209. Evangelinos, D. *et al.* Late Oligocene-Miocene proto-Antarctic Circumpolar Current dynamics off the Wilkes Land margin, East Antarctica. *Glob. Planet. Change* **191**, 103221, https://doi.org/10.1016/j.gloplacha.2020.103221 (2020).
210. Falzoni, F., Petrizzo, M. R., MacLeod, K. G. & Huber, B. T. Santonian–Campanian planktonic foraminifera from Tanzania, Shatsky Rise and Exmouth Plateau: Species depth ecology and paleoceanographic inferences. *Mar. Micropaleontology* **103**, 15–29, https://doi.org/10.1016/j.marmicro.2013.07.003 (2013).
211. Farrell, J. & Janecek, T. Late Neogene paleoceanography and paleoclimatology of the northeast Indian Ocean (Site 758). In *Proceedings of the Ocean Drilling Program, 121 Scientific Results*, https://doi.org/10.2973/odp.proc.sr.121.124.1991 (Ocean Drilling Program, 1991).
212. Fassell, M. L. & Bralower, T. J. Warm, equable mid-Cretaceous: Stable isotope evidence. In *Evolution of the Cretaceous Ocean-Climate System*, https://doi.org/10.1130/0-8137-2332-9.121 (Geological Society of America, 1999).
213. Feakins, S. J. *et al.* Miocene C_4 grassland expansion as recorded by the Indus Fan. *Paleoceanogr. Paleoclimatol.* **35**, https://doi.org/10.1029/2020pa003856 (2020).
214. Fedorov, A. V., Burls, N. J., Lawrence, K. T. & Peterson, L. C. Tightly linked zonal and meridional sea surface temperature gradients over the past five million years. *Nat. Geosci.* **8**, 975–980, https://doi.org/10.1038/ngeo2577 (2015).
215. Finnegan, S. *et al.* The magnitude and duration of Late Ordovician–Early Silurian glaciation. *Science* **331**, 903–906, https://doi.org/10.1126/science.1200803 (2011).
216. Flower, B. P. & Kennett, J. P. Middle Miocene ocean-climate transition: High-resolution oxygen and carbon isotopic records from Deep Sea Drilling Project Site 588A, southwest Pacific. *Paleoceanography* **8**, 811–843, https://doi.org/10.1029/93pa02196 (1993).
217. Forster, A., Schouten, S., Baas, M. & Sinninghe Damsté, J. S. Mid-Cretaceous (Albian–Santonian) sea surface temperature record of the tropical Atlantic Ocean. *Geology* **35**, 919, https://doi.org/10.1130/g23874a.1 (2007).
218. Forster, A., Schouten, S., Moriya, K., Wilson, P. A. & Sinninghe Damsté, J. S. Tropical warming and intermittent cooling during the Cenomanian/Turonian Oceanic Anoxic Event 2: Sea surface temperature records from the equatorial Atlantic. *Paleoceanography* **22**, https://doi.org/10.1029/2006pa001349 (2007).
219. Foster, G. L., Lear, C. H. & Rae, J. W. The evolution of pCO_2, ice volume and climate during the middle Miocene. *Earth Planet. Sci. Lett.* **341-344**, 243–254, https://doi.org/10.1016/j.epsl.2012.06.007 (2012).
220. Fox, L. R. *Mid Miocene orbital climate variability and biotic response in the Pacific Ocean*. Ph.D. thesis, University of Leeds (2014).
221. Főzy, I., Janssen, N. & Price, G. High-resolution ammonite, belemnite and stable isotope record from the most complete Upper Jurassic section of the Bakony Mts (Transdanubian Range, Hungary. *Geologica Carpath.* **62**, 413–433, https://doi.org/10.2478/v10096-011-0030-y (2011).
222. Frank, T. D. & Arthur, M. A. Tectonic forcings of Maastrichtian ocean-climate evolution. *Paleoceanography* **14**, 103–117, https://doi.org/10.1029/1998pa900017 (1999).
223. Frank, T. D., Shultis, A. I. & Fielding, C. R. Acme and demise of the late Palaeozoic ice age: A view from the southeastern margin of Gondwana. *Palaeogeography, Palaeoclimatology, Palaeoecology* **418**, 176–192, https://doi.org/10.1016/j.palaeo.2014.11.016 (2015).
224. Franz, S.-O. *Pliozäne Zeitreihen zur Rekonstruktion der Tiefenwasserzirkulation und der siliziklastischen Amazonasfracht im äquatorialen Westatlantik (Ceara-Schwelle, ODP Leg 154)*. Ph.D. thesis, Christian-Albrechts-Universität (1999).

225. Friedrich, O., Herrle, J. O., Kößler, P. & Hemleben, C. Early Maastrichtian stable isotopes: Changing deep water sources in the North Atlantic. *Palaeogeography, Palaeoclimatology, Palaeoecology* **211**, 171–184, https://doi.org/10.1016/j.palaeo.2004.05.004 (2004).
226. Friedrich, O., Erbacher, J., Moriya, K., Wilson, P. A. & Kuhnert, H. Warm saline intermediate waters in the Cretaceous tropical Atlantic Ocean. *Nat. Geosci.* **1**, 453–457, https://doi.org/10.1038/ngeo217 (2008).
227. Friedrich, O. *et al*. Early Maastrichtian carbon cycle perturbation and cooling event: Implications from the South Atlantic Ocean. *Paleoceanography* **24**, https://doi.org/10.1029/2008pa001654 (2009).
228. Frieling, J. *et al*. Paleocene–Eocene warming and biotic response in the epicontinental West Siberian Sea. *Geology* **42**, 767–770, https://doi.org/10.1130/g35724.1 (2014).
229. Frieling, J. *et al*. Extreme warmth and heat-stressed plankton in the tropics during the Paleocene-Eocene Thermal Maximum. *Sci. Adv.* **3**, https://doi.org/10.1126/sciadv.1600891 (2017).
230. Frieling, J. *et al*. Tropical Atlantic climate and ecosystem regime shifts during the Paleocene–Eocene Thermal Maximum. *Clim. Past.* **14**, 39–55, https://doi.org/10.5194/cp-14-39-2018 (2018).
231. Frýda, J. *et al*. The Mid-Ludfordian (late Silurian) Glaciation: A link with global changes in ocean chemistry and ecosystem overturns. *Earth-Sci. Rev.* **220**, 103652, https://doi.org/10.1016/j.earscirev.2021.103652 (2021).
232. Fürsich, F. *et al*. Palaeoclimate reconstructions of the Middle Jurassic of Kachchh (western India): An integrated approach based on palaeoecological, oxygen isotopic, and clay mineralogical data. *Palaeogeography, Palaeoclimatology, Palaeoecology* **217**, 289–309, https://doi.org/10.1016/j.palaeo.2004.11.026 (2005).
233. Garbelli, C. *et al*. Neotethys seawater chemistry and temperature at the dawn of the end Permian mass extinction. *Gondwana Res.* **35**, 272–285, https://doi.org/10.1016/j.gr.2015.05.012 (2016).
234. Garbelli, C. *et al*. Timing of Early and Middle Permian deglaciation of the southern hemisphere: Brachiopod-based $^{87}Sr/^{86}Sr$ calibration. *Earth Planet. Sci. Lett.* **516**, 122–135, https://doi.org/10.1016/j.epsl.2019.03.039 (2019).
235. Gasperi, J. & Kennett, J. Miocene planktonic foraminifers at DSDP Site 289: Depth stratification using isotopic differences. In *Proceedings of the Ocean Drilling Program, 130 Scientific Results*, https://doi.org/10.2973/odp.proc.sr.130.061.1993 (Ocean Drilling Program, 1993).
236. Geary, D. H., Brieske, T. A. & Bemis, B. E. The influence and interaction of temperature, salinity, and upwelling on the stable isotopic profiles of strombid gastropod shells. *PALAIOS* **7**, 77, https://doi.org/10.2307/3514797 (1992).
237. Gillikin, D. P. *et al*. Strong biological controls on Sr/Ca ratios in aragonitic marine bivalve shells. *Geochem. Geophys. Geosyst.* **6**, https://doi.org/10.1029/2004gc000874 (2005).
238. Girard, C. *et al*. Paleogeographic differences in temperature, water depth and conodont biofacies during the Late Devonian. *Palaeogeography, Palaeoclimatology, Palaeoecology* **549**, 108852, https://doi.org/10.1016/j.palaeo.2018.06.046 (2020).
239. Gómez, J., Goy, A. & Canales, M. Seawater temperature and carbon isotope variations in belemnites linked to mass extinction during the Toarcian (Early Jurassic) in Central and Northern Spain. Comparison with other European sections. *Palaeogeography, Palaeoclimatology, Palaeoecology* **258**, 28–58, https://doi.org/10.1016/j.palaeo.2007.11.005 (2008).
240. Gómez, J. J., Canales, M. L., Ureta, S. & Goy, A. Palaeoclimatic and biotic changes during the Aalenian (Middle Jurassic) at the southern Laurasian Seaway (Basque–Cantabrian Basin, northern Spain. *Palaeogeography, Palaeoclimatology, Palaeoecology* **275**, 14–27, https://doi.org/10.1016/j.palaeo.2009.01.009 (2009).
241. Gómez, J. J. & Goy, A. Warming-driven mass extinction in the Early Toarcian (Early Jurassic) of northern and central Spain. Correlation with other time-equivalent European sections. *Palaeogeography, Palaeoclimatology, Palaeoecology* **306**, 176–195, https://doi.org/10.1016/j.palaeo.2011.04.018 (2011).
242. Gómez-Alday, J. J., López, G. & Elorza, J. Evidence of climatic cooling at the Early/Late Maastrichtian boundary from inoceramid distribution and isotopes: Sopelana sections, Basque Country, Spain. *Cretac. Res.* **25**, 649–668, https://doi.org/10.1016/j.cretres.2004.06.009 (2004).
243. Gómez Dacal, A. R. *et al*. First record of the Valanginian positive carbon isotope anomaly in the Mendoza shelf, Neuquén Basin, Argentina: palaeoclimatic implications. *Andean Geol.* **45**, 111, https://doi.org/10.5027/andgeov45n2-3059 (2018).
244. Goodwin, D. H., Flessa, K. W., Schone, B. R. & Dettman, D. L. Cross-calibration of daily growth increments, stable isotope variation, and temperature in the Gulf of California bivalve mollusk *Chione cortezi*: Implications for paleoenvironmental analysis. *PALAIOS* **16**, 387–398, 10.1669/0883-1351(2001)016<0387:ccodgi>2.0.co;2 (2001).
245. Goudemand, N. *et al*. Dynamic interplay between climate and marine biodiversity upheavals during the early Triassic Smithian-Spathian biotic crisis. *Earth-Sci. Rev.* **195**, 169–178, https://doi.org/10.1016/j.earscirev.2019.01.013 (2019).
246. Greenop, R. *et al*. Orbital forcing, ice volume, and CO_2 across the Oligocene-Miocene transition. *Paleoceanogr. Paleoclimatol.* **34**, 316–328, https://doi.org/10.1029/2018pa003420 (2019).
247. Gröcke, D. R., Price, G. D., Ruffell, A. H., Mutterlose, J. & Baraboshkin, E. Isotopic evidence for Late Jurassic–Early Cretaceous climate change. *Palaeogeography, Palaeoclimatology, Palaeoecology* **202**, 97–118, https://doi.org/10.1016/s0031-0182(03)00631-x (2003).
248. Groeneveld, J. *Effect of the Pliocene closure of the Panamanian Gateway on Caribbean and east Pacific sea surface temperatures and salinities by applying combined Mg/Ca and $\delta^{18}O$ measurements (5.6-2.2 Ma)*. Ph.D. thesis, Christian-Albrechts-Universität Kiel (2005).
249. Groeneveld, J. *et al*. Pliocene mixed-layer oceanography for Site 1241, using combined Mg/Ca and $\delta^{18}O$ analyses of Globigerinoides sacculifer. In *Proceedings of the Ocean Drilling Program, 202 Scientific Results*, https://doi.org/10.2973/odp.proc.sr.202.209.2006 (Ocean Drilling Program, 2006).
250. Grossman, E. L., Zhang, C. & Yancey, T. E. Stable-isotope stratigraphy of brachiopods from Pennsylvanian shales in Texas. *Geological Society of America Bulletin* **103**, 953–965, 10.1130/0016-7606(1991)103<0953:sisobf>2.3.co;2 (1991).
251. Grossman, E. L., Mii, H.-S. & Yancey, T. E. Stable isotopes in Late Pennsylvanian brachiopods from the United States: Implications for Carboniferous paleoceanography. *Geological Society of America Bulletin* **105**, 1284–1296, 10.1130/0016-7606(1993)105<1284:siilpb>2.3.co;2 (1993).
252. Grossman, E. L. *et al*. Glaciation, aridification, and carbon sequestration in the Permo-Carboniferous: The isotopic record from low latitudes. *Palaeogeography, Palaeoclimatology, Palaeoecology* **268**, 222–233, https://doi.org/10.1016/j.palaeo.2008.03.053 (2008).
253. Grunert, P., Tzanova, A., Harzhauser, M. & Piller, W. E. Mid-Burdigalian Paratethyan alkenone record reveals link between orbital forcing, Antarctic ice-sheet dynamics and European climate at the verge to Miocene Climate Optimum. *Glob. Planet. Change* **123**, 36–43, https://doi.org/10.1016/j.gloplacha.2014.10.011 (2014).
254. Guitián, J. *et al*. Midlatitude temperature variations in the Oligocene to Early Miocene. *Paleoceanogr. Paleoclimatol.* **34**, 1328–1343, https://doi.org/10.1029/2019pa003638 (2019).
255. Gussone, N. *et al*. Reconstruction of Caribbean Sea surface temperature and salinity fluctuations in response to the Pliocene closure of the Central American Gateway and radiative forcing, using $\delta^{44/40}Ca$, $\delta^{18}O$ and Mg/Ca ratios. *Earth Planet. Sci. Lett.* **227**, 201–214, https://doi.org/10.1016/j.epsl.2004.09.004 (2004).
256. Gustafsson, M., Holbourn, A. & Kuhnt, W. Changes in Northeast Atlantic temperature and carbon flux during the Cenomanian/Turonian paleoceanographic event: The Goban Spur stable isotope record. *Palaeogeography, Palaeoclimatology, Palaeoecology* **201**, 51–66, https://doi.org/10.1016/s0031-0182(03)00509-1 (2003).
257. Gutjahr, M. *et al*. Very large release of mostly volcanic carbon during the Paleocene–Eocene Thermal Maximum. *Nature* **548**, 573–577, https://doi.org/10.1038/nature23646 (2017).

258. Haggerty, J. Petrology, and carbon and oxygen stable isotopic composition of macrofossils and sediments from the Blake-Bahama Formation, Deep Sea Drilling Project Site 603, western North Atlantic lower continental rise. In *Initial Reports of the Deep Sea Drilling Project*, https://doi.org/10.2973/dsdp.proc.93.140.1987 (U.S. Government Printing Office, 1987).
259. Harazim, D. *et al*. Spatial variability of watermass conditions within the European Epicontinental Seaway during the Early Jurassic (Pliensbachian-Toarcian). *Sedimentology* **60**, 359–390, https://doi.org/10.1111/j.1365-3091.2012.01344.x (2012).
260. Harning, D. J. *et al*. Sea ice control on winter subsurface temperatures of the North Iceland Shelf during the Little Ice Age: A TEX_{86} calibration case study. *Paleoceanogr. Paleoclimatol.* **34**, 1006–1021, https://doi.org/10.1029/2018pa003523 (2019).
261. Harper, D. T. *et al*. Subtropical sea-surface warming and increased salinity during Eocene Thermal Maximum 2. *Geology* **46**, 187–190, https://doi.org/10.1130/g39658.1 (2017).
262. Harper, D. T. *et al*. The magnitude of surface ocean acidification and carbon release during Eocene Thermal Maximum 2 (ETM-2) and the Paleocene-Eocene Thermal Maximum (PETM). *Paleoceanogr. Paleoclimatol.* **35**, https://doi.org/10.1029/2019pa003699 (2020).
263. Hartman, J. D. *et al*. Paleoceanography and ice sheet variability offshore Wilkes Land, Antarctica – Part 3: Insights from Oligocene–Miocene TEX_{86}-based sea surface temperature reconstructions. *Clim. Past.* **14**, 1275–1297, https://doi.org/10.5194/cp-14-1275-2018 (2018).
264. Hasenfratz, A. P. *et al*. The residence time of Southern Ocean surface waters and the 100,000-year ice age cycle. *Science* **363**, 1080–1084, https://doi.org/10.1126/science.aat7067 (2019).
265. Haug, G. H., Tiedemann, R., Zahn, R. & Ravelo, A. C. Role of Panama uplift on oceanic freshwater balance. *Geology* **29**, 207, 10.1130/0091-7613(2001)029<0207:ropuoo>2.0.co;2 (2001).
266. Henehan, M. J. *et al*. Rapid ocean acidification and protracted Earth system recovery followed the end-Cretaceous Chicxulub impact. *Proc. Natl Acad. Sci.* **116**, 22500–22504, https://doi.org/10.1073/pnas.1905989116 (2019).
267. Henehan, M. J. *et al*. Revisiting the Middle Eocene Climatic Optimum "carbon cycle conundrum" with new estimates of atmospheric pCO_2 from boron isotopes. *Paleoceanogr. Paleoclimatol.* **35**, https://doi.org/10.1029/2019pa003713 (2020).
268. Herbert, T. & Schuffert, J. Alkenone unsaturation estimates of late Miocene through late Pliocene sea-surface temperatures at Site 958. In *Proceedings of the Ocean Drilling Program, 159T Scientific Results*, https://doi.org/10.2973/odp.proc.sr.159t.063.1998 (Ocean Drilling Program, 1998).
269. Herbert, T. D., Peterson, L. C., Lawrence, K. T. & Liu, Z. Tropical ocean temperatures over the past 3.5 million years. *Science* **328**, 1530–1534, https://doi.org/10.1126/science.1185435 (2010).
270. Herbert, T. D. *et al*. Late Miocene global cooling and the rise of modern ecosystems. *Nat. Geosci.* **9**, 843–847, https://doi.org/10.1038/ngeo2813 (2016).
271. Herbert, T. D., Rose, R., Dybkjær, K., Rasmussen, E. S. & Śliwińska, K. K. Bihemispheric warming in the Miocene Climatic Optimum as seen from the Danish North Sea. *Paleoceanogr. Paleoclimatol.* **35**, https://doi.org/10.1029/2020pa003935 (2020).
272. Herrmann, A. D., MacLeod, K. G. & Leslie, S. A. Did a volcanic mega-eruption cause global cooling during the Late Ordovician? *PALAIOS* **25**, 831–836, https://doi.org/10.2110/palo.2010.p10-069r (2010).
273. Herrmann, A. D., Barrick, J., Algeo, T. J. & Peng, Y. Conodont biofacies and watermass structure of the Middle Pennsylvanian North American Midcontinent Sea. *Palaeogeography, Palaeoclimatology, Palaeoecology* **531**, 109235, https://doi.org/10.1016/j.palaeo.2019.109235 (2019).
274. Hesselbo, S. P. *et al*. Massive dissociation of gas hydrate during a Jurassic oceanic anoxic event. *Nature* **406**, 392–395, https://doi.org/10.1038/35019044 (2000).
275. Hines, B. R. *et al*. Reduction of oceanic temperature gradients in the early Eocene Southwest Pacific Ocean. *Palaeogeography, Palaeoclimatology, Palaeoecology* **475**, 41–54, https://doi.org/10.1016/j.palaeo.2017.02.037 (2017).
276. Ho, S. L. *et al*. Sea surface temperature variability in the Pacific sector of the Southern Ocean over the past 700 kyr. *Paleoceanography* **27**, https://doi.org/10.1029/2012pa002317 (2012).
277. Hodell, D. *et al*. Data report: Oxygen isotope stratigraphy of ODP Leg 177 Sites 1088, 1089, 1090, 1093, and 1094. In *Proceedings of the Ocean Drilling Program, 177 Scientific Results*, https://doi.org/10.2973/odp.proc.sr.177.120.2003 (Ocean Drilling Program, 2003).
278. Hodell, D. A., Venz, K. A., Charles, C. D. & Ninnemann, U. S. Pleistocene vertical carbon isotope and carbonate gradients in the South Atlantic sector of the Southern Ocean. *Geochem. Geophys. Geosyst.* **4**, 1–19, https://doi.org/10.1029/2002gc000367 (2003).
279. Hofmann, P., Stüsser, I., Wagner, T., Schouten, S. & Sinninghe Damsté, J. S. Climate–ocean coupling off North-West Africa during the Lower Albian: The Oceanic Anoxic Event 1b. *Palaeogeography, Palaeoclimatology, Palaeoecology* **262**, 157–165, https://doi.org/10.1016/j.palaeo.2008.02.014 (2008).
280. Holbourn, A. *et al*. Does Antarctic glaciation force migration of the tropical rain belt? *Geology* **38**, 783–786, https://doi.org/10.1130/g31043.1 (2010).
281. Holbourn, A. E. *et al*. Late Miocene climate cooling and intensification of southeast Asian winter monsoon. *Nature Communications* **9**, https://doi.org/10.1038/s41467-018-03950-1 (2018).
282. Holbourn, A., Kuhnt, W., Clemens, S. C. & Heslop, D. A:12 Myr Miocene record of East Asian Monsoon variability from the South China Sea. *Paleoceanogr. Paleoclimatol.* **36** (2021).
283. Hollis, C. J. *et al*. Tropical sea temperatures in the high-latitude South Pacific during the Eocene. *Geology* **37**, 99–102, https://doi.org/10.1130/g25200a.1 (2009).
284. Hollis, C. J. *et al*. Early Paleogene temperature history of the Southwest Pacific Ocean: Reconciling proxies and models. *Earth Planet. Sci. Lett.* **349**, 53–66 (2012).
285. Hollis, C. J. *et al*. The Paleocene–Eocene Thermal Maximum at DSDP Site 277, Campbell Plateau, southern Pacific Ocean. *Clim. Past.* **11**, 1009–1025, https://doi.org/10.5194/cp-11-1009-2015 (2015).
286. Hornung, T., Brandner, R., Krystyn, L., Joachimski, M. M. & Keim, L. Multistratigraphic constraints on the NW Tethyan "Carnian crisis". *Glob. Triassic* **41**, 59–67 (2007).
287. Houben, A. J. P., Bijl, P. K., Sluijs, A., Schouten, S. & Brinkhuis, H. Late Eocene Southern Ocean cooling and invigoration of circulation preconditioned Antarctica for full-scale glaciation. *Geochem. Geophys. Geosyst.* https://doi.org/10.1029/2019gc008182 (2019).
288. Huang, C., Joachimski, M. M. & Gong, Y. Did climate changes trigger the Late Devonian Kellwasser Crisis? Evidence from a high-resolution conodont $\delta^{18}O_{PO4}$ record from South China. *Earth Planet. Sci. Lett.* **495**, 174–184, https://doi.org/10.1016/j.epsl.2018.05.016 (2018).
289. Huber, B. T., Hodell, D. A. & Hamilton, C. P. Middle–Late Cretaceous climate of the southern high latitudes: Stable isotopic evidence for minimal equator-to-pole thermal gradients. *Geological Society of America Bulletin* **107**, 1164–1191, 10.1130/0016-7606(1995)107<1164:mlccot>2.3.co;2 (1995).
290. Huber, B. T., Leckie, R. M., Norris, R. D., Bralower, T. J. & CoBabe, E. Foraminiferal assemblage and stable isotopic change across the Cenomanian-Turonian boundary in the subtropical North Atlantic. *J. Foraminifer. Res.* **29**, 392–417 (1999).
291. Huber, R., Meggers, H., Baumann, K.-H., Raymo, M. E. & Henrich, R. Shell size variation of the planktonic foraminifer *Neogloboquadrina pachyderma* sin. in the Norwegian–Greenland Sea during the last 1.3 Myrs: Implications for paleoceanographic reconstructions. *Palaeogeography, Palaeoclimatology, Palaeoecology* **160**, 193–212, https://doi.org/10.1016/s0031-0182(00)00066-3 (2000).

292. Huber, B. T., Norris, R. D. & MacLeod, K. G. Deep-sea paleotemperature record of extreme warmth during the Cretaceous. *Geology* **30**, 123, 10.1130/0091-7613(2002)030<0123:dsproe>2.0.co;2 (2002).
293. Huber, B. T., MacLeod, K. G., Gröcke, D. R. & Kucera, M. Paleotemperature and paleosalinity inferences and chemostratigraphy across the Aptian/Albian boundary in the subtropical North Atlantic. *Paleoceanography* **26**, https://doi.org/10.1029/2011pa002178 (2011).
294. Huber, B. T., MacLeod, K. G., Watkins, D. K. & Coffin, M. F. The rise and fall of the Cretaceous Hot Greenhouse climate. *Glob. Planet. Change* **167**, 1–23, https://doi.org/10.1016/j.gloplacha.2018.04.004 (2018).
295. Huguet, C., Kim, J.-H., Sinninghe Damsté, J. S. & Schouten, S. Reconstruction of sea surface temperature variations in the Arabian Sea over the last 23 kyr using organic proxies (TEX_{86} and $U^{K'}_{37}$). *Paleoceanography* **21**, https://doi.org/10.1029/2005pa001215 (2006).
296. Huguet, C., Martrat, B., Grimalt, J. O., Sinninghe Damsté, J. S. & Schouten, S. Coherent millennial-scale patterns in $U^{K'}_{37}$ and TEX^{H}_{86} temperature records during the penultimate interglacial-to-glacial cycle in the western Mediterranean. *Paleoceanography* **26**, https://doi.org/10.1029/2010pa002048 (2011).
297. Hull, P. M. *et al*. On impact and volcanism across the Cretaceous-Paleogene boundary. *Science* **367**, 266–272, https://doi.org/10.1126/science.aay5055 (2020).
298. Immenhauser, A. *et al*. Origin and significance of isotope shifts in Pennsylvanian carbonates (Asturias, NW Spain). *J. Sediment. Res.* **72**, 82–94, https://doi.org/10.1306/051701720082 (2002).
299. Inglis, G. N. *et al*. Descent toward the Icehouse: Eocene sea surface cooling inferred from GDGT distributions. *Paleoceanography* **30**, 1000–1020, https://doi.org/10.1002/2014PA002723 (2015).
300. Inglis, G. N., Carmichael, M. J., Farnsworth, A., Lunt, D. J. & Pancost, R. D. A long-term, high-latitude record of Eocene hydrological change in the Greenland region. *Palaeogeography, Palaeoclimatology, Palaeoecology* **537**, 109378, https://doi.org/10.1016/j.palaeo.2019.109378 (2020).
301. Isaza-Londoño, C., MacLeod, K. G. & Huber, B. T. Maastrichtian North Atlantic warming, increasing stratification, and foraminiferal paleobiology at three timescales. *Paleoceanography* **21**, https://doi.org/10.1029/2004pa001130 (2006).
302. Jansen, E. & Sejrup, H. Stable isotope stratigraphy and amino-acid empimerization for the last 2.4 m.y. at Site 610, Holes 610 and 610A. In *Initial Reports of the Deep Sea Drilling Project*, https://doi.org/10.2973/dsdp.proc.94.123.1987 (U.S. Government Printing Office, 1987).
303. Jenkyns, H. C., Jones, C. E., Gröcke, D. R., Hesselbo, S. P. & Parkinson, D. N. Chemostratigraphy of the Jurassic System: applications, limitations and implications for palaeoceanography. *J. Geol. Soc.* **159**, 351–378, https://doi.org/10.1144/0016-764901-130 (2002).
304. Jenkyns, H. C., Forster, A., Schouten, S. & Sinninghe Damsté, J. S. High temperatures in the Late Cretaceous Arctic Ocean. *Nature* **432**, 888–892, https://doi.org/10.1038/nature03143 (2004).
305. Jenkyns, H. C., Schouten-Huibers, L., Schouten, S. & Sinninghe Damsté, J. S. Warm Middle Jurassic–Early Cretaceous high-latitude sea-surface temperatures from the Southern Ocean. *Clim. Past.* **8**, 215–226, https://doi.org/10.5194/cp-8-215-2012 (2012).
306. Jia, G., Chen, F. & Peng, P. Sea surface temperature differences between the western equatorial Pacific and northern South China Sea since the Pliocene and their paleoclimatic implications. *Geophys. Res. Lett*. **35**, https://doi.org/10.1029/2008gl034792 (2008).
307. Jian, Z. *et al*. Foraminiferal responses to major Pleistocene paleoceanographic changes in the southern South China Sea. *Paleoceanography* **15**, 229–243, https://doi.org/10.1029/1999pa000431 (2000).
308. Jin, J., Zhan, R. & Wu, R. Equatorial cold-water tongue in the Late Ordovician. *Geology* **46**, 759–762, https://doi.org/10.1130/g45302.1 (2018).
309. Jin, X., Shi, Z., Rigo, M., Franceschi, M. & Preto, N. Carbonate platform crisis in the Carnian (Late Triassic) of Hanwang (Sichuan Basin, South China): Insights from conodonts and stable isotope data. *J. Asian Earth Sci.* **164**, 104–124, https://doi.org/10.1016/j.jseaes.2018.06.021 (2018).
310. Joachimski, M. M., van Geldern, R., Breisig, S., Buggisch, W. & Day, J. Oxygen isotope evolution of biogenic calcite and apatite during the Middle and Late Devonian. *Int. J. Earth Sci.* **93**, 542–553, https://doi.org/10.1007/s00531-004-0405-8 (2004).
311. Joachimski, M. M., von Bitter, P. H. & Buggisch, W. Constraints on Pennsylvanian glacioeustatic sea-level changes using oxygen isotopes of conodont apatite. *Geology* **34**, 277, https://doi.org/10.1130/g22198.1 (2006).
312. Joachimski, M. *et al*. Devonian climate and reef evolution: Insights from oxygen isotopes in apatite. *Earth Planet. Sci. Lett.* **284**, 599–609, https://doi.org/10.1016/j.epsl.2009.05.028 (2009).
313. Joachimski, M. M. *et al*. Climate warming in the latest Permian and the Permian-Triassic mass extinction. *Geology* **40**, 195–198, https://doi.org/10.1130/g32707.1 (2012).
314. Joachimski, M. M. & Lambert, L. L. Salinity contrast in the US Midcontinent Sea during Pennsylvanian glacio-eustatic highstands: Evidence from conodont apatite $\delta^{18}O$. Palaeogeography, Palaeoclimatology, Palaeo. *ecology* **433**, 71–80, https://doi.org/10.1016/j.palaeo.2015.05.014 (2015).
315. Joachimski, M., Alekseev, A., Grigoryan, A. & Gatovsky, Y. Siberian Trap volcanism, global warming and the Permian-Triassic mass extinction: New insights from Armenian Permian-Triassic sections. *Geol. Soc. Am. Bull.* **132**, 427–443, https://doi.org/10.1130/b35108.1 (2019).
316. John, C. M. *et al*. North American continental margin records of the Paleocene-Eocene Thermal Maximum: Implications for global carbon and hydrological cycling. *Paleoceanography* **23**, https://doi.org/10.1029/2007pa001465 (2008).
317. Jones, C. E. *Strontium isotopes in Jurassic and early Cretaceous seawater*. Ph.D. thesis, University of Oxford (1992).
318. Jones, D. S., Williams, D. F. & Arthur, M. A. Growth history and ecology of the Atlantic surf clam, *Spisula solidissima* (Dillwyn), as revealed by stable isotopes and annual shell increments. *J. Exp. Mar. Biol. Ecol.* **73**, 225–242, https://doi.org/10.1016/0022-0981(83)90049-7 (1983).
319. Jones, D. S. & Allmon, W. D. Records of upwelling, seasonality and growth in stable-isotope profiles of Pliocene mollusk shells from Florida. *Lethaia* **28**, 61–74, https://doi.org/10.1111/j.1502-3931.1995.tb01593.x (1995).
320. Jones, D. S. & Quitmyer, I. R. Marking time with bivalve shells: Oxygen isotopes and season of annual increment formation. *PALAIOS* **11**, 340, https://doi.org/10.2307/3515244 (1996).
321. Jung, C., Voigt, S., Friedrich, O., Koch, M. C. & Frank, M. Campanian-Maastrichtian ocean circulation in the tropical Pacific. *Paleoceanography* **28**, 562–573, https://doi.org/10.1002/palo.20051 (2013).
322. Kaiser, S. I., Steuber, T., Becker, R. T. & Joachimski, M. M. Geochemical evidence for major environmental change at the Devonian–Carboniferous boundary in the Carnic Alps and the Rhenish Massif. *Palaeogeography, Palaeoclimatology, Palaeoecology* **240**, 146–160, https://doi.org/10.1016/j.palaeo.2006.03.048 (2006).
323. Karas, C. *et al*. Mid-Pliocene climate change amplified by a switch in Indonesian subsurface throughflow. *Nat. Geosci.* **2**, 434–438, https://doi.org/10.1038/ngeo520 (2009).
324. Karas, C., Nürnberg, D., Tiedemann, R. & Garbe-Schönberg, D. Pliocene climate change of the Southwest Pacific and the impact of ocean gateways. *Earth Planet. Sci. Lett.* **301**, 117–124, https://doi.org/10.1016/j.epsl.2010.10.028 (2011).
325. Karas, C., Nürnberg, D., Tiedemann, R. & Garbe-Schönberg, D. Pliocene Indonesian Throughflow and Leeuwin Current dynamics: Implications for Indian Ocean polar heat flux. *Paleoceanography* **26**, https://doi.org/10.1029/2010pa001949 (2011).
326. Karas, C. *et al*. Did North Atlantic cooling and freshening from 3.65–3.5 Ma precondition Northern Hemisphere ice sheet growth? *Glob. Planet. Change* **185**, 103085, https://doi.org/10.1016/j.gloplacha.2019.103085 (2020).

327. Kearsey, T., Twitchett, R. J., Price, G. D. & Grimes, S. T. Isotope excursions and palaeotemperature estimates from the Permian/Triassic boundary in the Southern Alps (Italy. *Palaeogeography, Palaeoclimatology, Palaeoecology* **279**, 29–40, https://doi.org/10.1016/j.palaeo.2009.04.015 (2009).
328. Keating-Bitonti, C. R., Ivany, L. C., Affek, H. P., Douglas, P. & Samson, S. D. Warm, not super-hot, temperatures in the early Eocene subtropics. *Geology* **39**, 771–774, https://doi.org/10.1130/g32054.1 (2011).
329. Keigwin, L. D. Late Cenozoic stable isotope stratigraphy and paleoceanography of DSDP sites from the east equatorial and central north Pacific Ocean. *Earth Planet. Sci. Lett.* **45**, 361–382, https://doi.org/10.1016/0012-821x(79)90137-7 (1979).
330. Keigwin, L. D. Palaeoceanographic change in the Pacific at the Eocene–Oligocene boundary. *Nature* **287**, 722–725, https://doi.org/10.1038/287722a0 (1980).
331. Keigwin, L. D. & Corliss, B. H. Stable isotopes in late middle Eocene to Oligocene foraminifera. *Geological Society of America Bulletin* **97**, 335, 10.1130/0016-7606(1986)97<335:siilme>2.0.co;2 (1986).
332. Kelly, D. C., Bralower, T. J., Zachos, J. C., Silva, I. P. & Thomas, E. Rapid diversification of planktonic foraminifera in the tropical Pacific (ODP Site 865) during the late Paleocene thermal maximum. *Geology* **24**, 423, 10.1130/0091-7613(1996)024<0423:rdopfi>2.3.co;2 (1996).
333. Kelly, D. C., Zachos, J. C., Bralower, T. J. & Schellenberg, S. A. Enhanced terrestrial weathering/runoff and surface ocean carbonate production during the recovery stages of the Paleocene-Eocene Thermal Maximum. *Paleoceanography* **20**, https://doi.org/10.1029/2005pa001163 (2005).
334. Kennett, J. Miocene to Early Pliocene oxygen and carbon isotope stratigraphy in the Southwest Pacific, Deep Sea Drilling Project Leg 90. In *Initial Reports of the Deep Sea Drilling Project*, 90, https://doi.org/10.2973/dsdp.proc.90.142.1986 (U.S. Government Printing Office, 1986).
335. Kennett, J. P. & Stott, L. D. Abrupt deep-sea warming, palaeoceanographic changes and benthic extinctions at the end of the Palaeocene. *Nature* **353**, 225–229, https://doi.org/10.1038/353225a0 (1991).
336. Khelifi, N. *et al.* A major and long-term Pliocene intensification of the Mediterranean outflow, 3.5-3.3 Ma ago. *Geology* **37**, 811–814, https://doi.org/10.1130/g30058a.1 (2009).
337. Khélifi, N. *Variations in Mediterranean Outflow Water and its salt discharge versus Pliocene changes in North Atlantic thermohaline circulation prior and during the onset of major Northern Hemisphere Glaciation, 3.7-2.6 Ma*. Ph.D. thesis, Christian-Albrechts-Universität Kiel (2010).
338. Khélifi, N., Sarnthein, M., Frank, M., Andersen, N. & Garbe-Schönberg, D. Late Pliocene variations of the Mediterranean outflow. *Mar. Geol.* **357**, 182–194, https://doi.org/10.1016/j.margeo.2014.07.006 (2014).
339. Kim, J.-H. *et al.* Pronounced subsurface cooling of North Atlantic waters off Northwest Africa during Dansgaard–Oeschger interstadials. *Earth Planet. Sci. Lett.* **339-340**, 95–102, https://doi.org/10.1016/j.epsl.2012.05.018 (2012).
340. Kim, J.-H. *et al.* Influence of deep-water derived isoprenoid tetraether lipids on the TEX_{86}^{H} paleothermometer in the Mediterranean Sea. *Geochim. Cosmochim. Acta* **150**, 125–141, https://doi.org/10.1016/j.gca.2014.11.017 (2015).
341. Kleiven, H. & Jansen, E. Data report: Early-mid-Pleistocene oxygen isotope stratigraphy from the Atlantic sector of the Southern Ocean: ODP Leg 177 Sites 1094 and 1091. In *Proceedings of the Ocean Drilling Program, 177 Scientific Results*, https://doi.org/10.2973/odp.proc.sr.177.114.2003 (Ocean Drilling Program, 2003).
342. Kobashi, T., Grossman, E. L., Yancey, T. E. & Dockery, D. T. Reevaluation of conflicting Eocene tropical temperature estimates: Molluskan oxygen isotope evidence for warm low latitudes. *Geology* **29**, 983, 10.1130/0091-7613(2001)029<0983:rocett>2.0.co;2 (2001).
343. Kobashi, T., Grossman, E. L., Dockery, D. T. & Ivany, L. C. Water mass stability reconstructions from greenhouse (Eocene) to icehouse (Oligocene) for the northern Gulf Coast continental shelf (USA). *Paleoceanography* **19**, https://doi.org/10.1029/2003pa000934 (2004).
344. Korte, C. *et al.* Carbon, sulfur, oxygen and strontium isotope records, organic geochemistry and biostratigraphy across the Permian/Triassic boundary in Abadeh, Iran. *Int. J. Earth Sci.* https://doi.org/10.1007/s00531-004-0406-7 (2004).
345. Korte, C., Jasper, T., Kozur, H. W. & Veizer, J. $\delta^{18}O$ and $\delta^{13}C$ of Permian brachiopods: A record of seawater evolution and continental glaciation. *Palaeogeography, Palaeoclimatology, Palaeoecology* **224**, 333–351, https://doi.org/10.1016/j.palaeo.2005.03.015 (2005).
346. Korte, C., Kozur, H. W. & Veizer, J. $\delta^{13}C$ and $\delta^{18}O$ values of Triassic brachiopods and carbonate rocks as proxies for coeval seawater and palaeotemperature. *Palaeogeography, Palaeoclimatology, Palaeoecology* **226**, 287–306, https://doi.org/10.1016/j.palaeo.2005.05.018 (2005).
347. Korte, C., Hesselbo, S. P., Jenkyns, H. C., Rickaby, R. E. & Spötl, C. Palaeoenvironmental significance of carbon- and oxygen-isotope stratigraphy of marine Triassic–Jurassic boundary sections in SW Britain. *J. Geol. Soc.* **166**, 431–445, https://doi.org/10.1144/0016-76492007-177 (2009).
348. Korte, C. & Hesselbo, S. P. Shallow marine carbon and oxygen isotope and elemental records indicate icehouse-greenhouse cycles during the Early Jurassic. *Paleoceanography* **26**, https://doi.org/10.1029/2011pa002160 (2011).
349. Korte, C. *et al.* Brachiopod biogeochemistry and isotope stratigraphy from the Rhaetian Eiberg section in Austria: potentials and limitations. *Neues Jahrb. für Geologie und Paläontologie-Abhandlungen* **284**, 117–138, https://doi.org/10.1127/njgpa/2017/0651 (2017).
350. Kozdon, R., Kelly, D. C., Kita, N. T., Fournelle, J. H. & Valley, J. W. Planktonic foraminiferal oxygen isotope analysis by ion microprobe technique suggests warm tropical sea surface temperatures during the Early Paleogene. *Paleoceanography* **26**, https://doi.org/10.1029/2010pa002056 (2011).
351. Kozdon, R. *et al.* Enhanced poleward flux of atmospheric moisture to the Weddell Sea Region (ODP Site 690) during the Paleocene-Eocene Thermal Maximum. *Paleoceanogr. Paleoclimatol.* **35**, https://doi.org/10.1029/2019pa003811 (2020).
352. Kroon, D., Reijmer, J. & Rendle, R. Mid- to late-Quaternary variations in the oxygen isotope signature of *Globigerinoides ruber* at Site 1006 in the western subtropical Atlantic. In *Proceedings of the Ocean Drilling Program*, https://doi.org/10.2973/odp.proc.sr.166.104.2000 (Ocean Drilling Program, 2000).
353. LaRiviere, J. P. *et al.* Late Miocene decoupling of oceanic warmth and atmospheric carbon dioxide forcing. *Nature* **486**, 97–100, https://doi.org/10.1038/nature11200 (2012).
354. Latal, C., Piller, W. E. & Harzhauser, M. Small-scaled environmental changes: indications from stable isotopes of gastropods Early Miocene, Korneuburg Basin, Austria. *Int. J. Earth Sci.* **95**, 95–106, https://doi.org/10.1007/s00531-005-0510-3 (2005).
355. Latal, C., Piller, W. E. & Harzhauser, M. Shifts in oxygen and carbon isotope signals in marine molluscs from the Central Paratethys (Europe) around the Lower/Middle Miocene transition. *Palaeogeography, Palaeoclimatology, Palaeoecology* **231**, 347–360, https://doi.org/10.1016/j.palaeo.2005.08.008 (2006).
356. Lathuilière, B. *et al.* Climats Kimméridgiens du site de Bure (Nord-Est de la France). *Trav. et. Doc. des. Laboratoires de. Géologie de Lyon.* **156**, 142–143 (2002).
357. Lattaud, J. *et al.* A comparison of late Quaternary organic proxy-based paleotemperature records of the central Sea of Okhotsk. *Paleoceanogr. Paleoclimatol.* **33**, 732–744, https://doi.org/10.1029/2018pa003388 (2018).
358. Lavoie, D. Early Devonian marine isotopic signatures: Brachiopods from the Upper Gaspe Limestones, Gaspe Peninsula, Quebec, Canada. *Journal of Sedimentary Research* **63**, https://doi.org/10.1306/d4267b90-2b26-11d7-8648000102c1865d (1993).
359. Lawrence, K., Sosdian, S., White, H. & Rosenthal, Y. North Atlantic climate evolution through the Plio-Pleistocene climate transitions. *Earth Planet. Sci. Lett.* **300**, 329–342, https://doi.org/10.1016/j.epsl.2010.10.013 (2010).

360. Lawrence, K. T. & Woodard, S. C. Past sea surface temperatures as measured by different proxies-A cautionary tale from the late Pliocene. *Paleoceanography* **32**, 318–324, https://doi.org/10.1002/2017pa003101 (2017).
361. Lawrence, K. T. *et al*. Comparison of late Neogene $U^{K'}_{37}$ and TEX_{86} paleotemperature records from the eastern equatorial Pacific at orbital resolution. *Paleoceanogr. Paleoclimatol.* **35**, https://doi.org/10.1029/2020pa003858 (2020).
362. Lea, D. W., Pak, D. K. & Spero, H. J. Climate impact of Late Quaternary equatorial Pacific sea surface temperature variations. *Science* **289**, 1719–1724, https://doi.org/10.1126/science.289.5485.1719 (2000).
363. Lea, D. W. *et al*. Paleoclimate history of Galápagos surface waters over the last 135,000 yr. *Quaternary Sci. Rev.* **25**, 1152–1167, https://doi.org/10.1016/j.quascirev.2005.11.010 (2006).
364. Lear, C. H., Bailey, T. R., Pearson, P. N., Coxall, H. K. & Rosenthal, Y. Cooling and ice growth across the Eocene-Oligocene transition. *Geology* **36**, 251, https://doi.org/10.1130/g24584a.1 (2008).
365. Leckie, R. M., Bralower, T. J. & Cashman, R. Oceanic anoxic events and plankton evolution: Biotic response to tectonic forcing during the mid-Cretaceous. *Paleoceanography* **17**, 13-1–13-29, https://doi.org/10.1029/2001pa000623 (2002).
366. Lécuyer, C., Amiot, R., Touzeau, A. & Trotter, J. Calibration of the phosphate $\delta^{18}O$ thermometer with carbonate–water oxygen isotope fractionation equations. *Chem. Geol.* **347**, 217–226, https://doi.org/10.1016/j.chemgeo.2013.03.008 (2013).
367. Lehnert, O., Männik, P., Joachimski, M. M., Calner, M. & Frýda, J. Palaeoclimate perturbations before the Sheinwoodian glaciation: A trigger for extinctions during the 'Ireviken Event'. *Palaeogeography, Palaeoclimatology, Palaeoecology* **296**, 320–331, https://doi.org/10.1016/j.palaeo.2010.01.009 (2010).
368. Le Houedec, S., Girard, C. & Balter, V. Conodont Sr/Ca and $\delta^{18}O$ record seawater changes at the Frasnian–Famennian boundary. *Palaeogeography, Palaeoclimatology, Palaeoecology* **376**, 114–121, https://doi.org/10.1016/j.palaeo.2013.02.025 (2013).
369. Lengger, S. K., Hopmans, E. C., Sinninghe Damsté, J. S. & Schouten, S. Fossilization and degradation of archaeal intact polar tetraether lipids in deeply buried marine sediments (Peru Margin). *Geobiology* **12**, 212–220, https://doi.org/10.1111/gbi.12081 (2014).
370. Leutert, T. J., Auderset, A., Martnez-Garca, A., Modestou, S. & Meckler, A. N. Coupled Southern Ocean cooling and Antarctic ice sheet expansion during the middle Miocene. *Nat. Geosci.* **13**, 634–639, https://doi.org/10.1038/s41561-020-0623-0 (2020).
371. Levy, R. *et al*. Antarctic ice sheet sensitivity to atmosphericCO_2 variations in the early to mid-Miocene. *Proc. Natl Acad. Sci.* **113**, 3453–3458, https://doi.org/10.1073/pnas.1516030113 (2016).
372. Li, L. & Keller, G. Maastrichtian climate, productivity and faunal turnovers in planktic foraminifera in South Atlantic DSDP sites 525A and 21. *Mar. Micropaleontology* **33**, 55–86, https://doi.org/10.1016/s0377-8398(97)00027-3 (1998).
373. Li, L. & Keller, G. Variability in Late Cretaceous climate and deep waters: evidence from stable isotopes. *Mar. Geol.* **161**, 171–190, https://doi.org/10.1016/s0025-3227(99)00078-x (1999).
374. Li, Q. *et al*. Late Miocene development of the western Pacific warm pool: Planktonic foraminifer and oxygen isotopic evidence. *Palaeogeography, Palaeoclimatology, Palaeoecology* **237**, 465–482, https://doi.org/10.1016/j.palaeo.2005.12.019 (2006).
375. Li, L. *et al*. A 4-Ma record of thermal evolution in the tropical western Pacific and its implications on climate change. *Earth Planet. Sci. Lett.* **309**, 10–20, https://doi.org/10.1016/j.epsl.2011.04.016 (2011).
376. Li, Q., McArthur, J. & Atkinson, T. Lower Jurassic belemnites as indicators of palaeo-temperature. *Palaeogeography, Palaeoclimatology, Palaeoecology* **315-316**, 38–45, https://doi.org/10.1016/j.palaeo.2011.11.006 (2012).
377. Li, D., Zhao, M. & Tian, J. Low-high latitude interaction forcing on the evolution of the 400 kyr cycle in East Asian winter monsoon records during the last 2.8 Myr. *Quaternary Sci. Rev.* **172**, 72–82, https://doi.org/10.1016/j.quascirev.2017.08.005 (2017).
378. Li, Q. *et al*. New insights into Kuroshio Current evolution since the last deglaciation based on paired organic paleothermometers from the Middle Okinawa Trough. *Paleoceanogr. Paleoclimatol.* **35**, https://doi.org/10.1029/2020pa004140 (2020).
379. Liu, K., Jiang, M., Zhang, L. & Chen, D. A new high-resolution palaeotemperature record during the Middle-Late Ordovician transition derived from conodont δ18O palaeothermometry. *Journal of the Geological Society* **179**, https://doi.org/10.1144/jgs2021-148 (2022).
380. Liddy, H. M., Feakins, S. J. & Tierney, J. E. Cooling and drying in northeast Africa across the Pliocene. *Earth Planet. Sci. Lett.* **449**, 430–438, https://doi.org/10.1016/j.epsl.2016.05.005 (2016).
381. Linnert, C. *et al*. Evidence for global cooling in the Late Cretaceous. *Nature Communications* **5**, https://doi.org/10.1038/ncomms5194 (2014).
382. Littler, K., Robinson, S. A., Bown, P. R., Nederbragt, A. J. & Pancost, R. D. High sea-surface temperatures during the Early Cretaceous Epoch. *Nat. Geosci.* **4**, 169–172, https://doi.org/10.1038/ngeo1081 (2011).
383. Liu, Z., Cleaveland, L. C. & Herbert, T. D. Early onset and origin of 100-kyr cycles in Pleistocene tropical SST records. *Earth Planet. Sci. Lett.* **265**, 703–715, https://doi.org/10.1016/j.epsl.2007.11.016 (2008).
384. Liu, Z. *et al*. Global cooling during the Eocene-Oligocene climate transition. *Science* **323**, 1187–1190, https://doi.org/10.1126/science.1166368 (2009).
385. Liu, Z. *et al*. Transient temperature asymmetry between hemispheres in the palaeogene Atlantic Ocean. *Nat. Geosci.* **11**, 656–660, https://doi.org/10.1038/s41561-018-0182-9 (2018).
386. Liu, J. *et al*. Eastern equatorial Pacific cold tongue evolution since the late Miocene linked to extratropical climate. *Sci. Adv*. **5**, https://doi.org/10.1126/sciadv.aau6060 (2019).
387. Longinelli, A., Iacumin, P. & Ramigni, M. $\delta^{18}O$ of carbonate, quartz and phosphate from belemnite guards: Implications for the isotopic record of old fossils and the isotopic composition of ancient seawater. *Earth Planet. Sci. Lett.* **203**, 445–459, https://doi.org/10.1016/s0012-821x(02)00854-3 (2002).
388. Longinelli, A., Wierzbowski, H. & Matteo, A. D. $\delta^{18}O$ (PO_4^{3-}) and $\delta^{18}O$ (CO_3^{2-}) from belemnite guards from Eastern Europe: Implications for palaeoceanographic reconstructions and for the preservation of pristine isotopic values. *Earth Planet. Sci. Lett.* **209**, 337–350, https://doi.org/10.1016/s0012-821x(03)00095-5 (2003).
389. Lopes dos Santos, R. A. *et al*. Glacial–interglacial variability in Atlantic meridional overturning circulation and thermocline adjustments in the tropical North Atlantic. *Earth Planet. Sci. Lett.* **300**, 407–414, https://doi.org/10.1016/j.epsl.2010.10.030 (2010).
390. Lopes dos Santos, R. A., Wilkins, D., Deckker, P. D. & Schouten, S. Late Quaternary productivity changes from offshore southeastern Australia: A biomarker approach. *Palaeogeography, Palaeoclimatology, Palaeoecology* **363-364**, 48–56, https://doi.org/10.1016/j.palaeo.2012.08.013 (2012).
391. Lopes dos Santos, R. A. *et al*. Comparison of organic ($U^{K'}_{37}$, TEX^{H}_{86}, LDI) and faunal proxies (foraminiferal assemblages) for reconstruction of late Quaternary sea surface temperature variability from offshore southeastern Australia. *Paleoceanography* **28**, 377–387, https://doi.org/10.1002/palo.20035 (2013).
392. Lowenstam, H. A. Mineralogy, O^{18}/O^{16} ratios, and strontium and magnesium contents of recent and fossil brachiopods and their bearing on the history of the oceans. *J. Geol.* **69**, 241–260, https://doi.org/10.1086/626740 (1961).
393. Lu, G. & Keller, G. The Paleocene-Eocene transition in the Antarctic Indian Ocean: Inference from planktic foraminifera. *Mar. Micropaleontology* **21**, 101–142, https://doi.org/10.1016/0377-8398(93)90012-m (1993).
394. Lu, G., Keller, G., Adatte, T., Ortiz, N. & Molina, E. Long-term (10^5) or short-term (10^3) $\delta^{13}C$ excursion near the Paleocene-Eocene transition: Evidence from the Tethys. *Terra Nova* **8**, 347–355, https://doi.org/10.1111/j.1365-3121.1996.tb00567.x (1996).
395. Lu, G. & Keller, G. Separating ecological assemblages using stable isotope signals: Late Paleocene to early Eocene planktic foraminifera, DSDP Site 577. *J. Foraminifer. Res.* **26**, 103–112, https://doi.org/10.2113/gsjfr.26.2.103 (1996).

396. Mackensen, A. & Ehrmann, W. Middle Eocene through Early Oligocene climate history and paleoceanography in the Southern Ocean: Stable oxygen and carbon isotopes from ODP Sites on Maud Rise and Kerguelen Plateau. *Mar. Geol.* **108**, 1–27, https://doi.org/10.1016/0025-3227(92)90210-9 (1992).
397. MacLeod, K. G., Huber, B. T., Pletsch, T., Röhl, U. & Kucera, M. Maastrichtian foraminiferal and paleoceanographic changes on Milankovitch timescales. *Paleoceanography* **16**, 133–154, https://doi.org/10.1029/2000pa000514 (2001).
398. MacLeod, K. G. & Huber, B. T. The Maastrichtian record at Blake Nose (western North Atlantic) and implications for global palaeoceanographic and biotic changes. *Geol. Society, London, Spec. Publ.* **183**, 111–130, https://doi.org/10.1144/gsl.sp.2001.183.01.06 (2001).
399. MacLeod, K. G., Huber, B. T. & Isaza-Londoño, C. North Atlantic warming during global cooling at the end of the Cretaceous. *Geology* **33**, 437, https://doi.org/10.1130/g21466.1 (2005).
400. MacLeod, K. G., Huber, B. T., Berrocoso, Á. J. & Wendler, I. A stable and hot Turonian without glacial $\delta^{18}O$ excursions is indicated by exquisitely preserved Tanzanian foraminifera. *Geology* **41**, 1083–1086, https://doi.org/10.1130/g34510.1 (2013).
401. Majewski, W. Mid-Miocene invasion of ecological niches by planktonic foraminifera of the Kerguelen Plateau, Antarctica. *Mar. Micropaleontology* **46**, 59–81, https://doi.org/10.1016/s0377-8398(02)00051-8 (2002).
402. Majewski, W. & Bohaty, S. M. Surface-water cooling and salinity decrease during the Middle Miocene climate transition at Southern Ocean ODP Site 747 (Kerguelen Plateau. *Mar. Micropaleontology* **74**, 1–14, https://doi.org/10.1016/j.marmicro.2009.10.002 (2010).
403. Makarova, M. *et al.* Hydrographic and ecologic implications of foraminiferal stable isotopic response across the U.S. mid-Atlantic continental shelf during the Paleocene-Eocene Thermal Maximum. *Paleoceanography* **32**, 56–73, https://doi.org/10.1002/2016pa002985 (2017).
404. Malchus, N. & Steuber, T. Stable isotope records (O, C) of Jurassic aragonitic shells from England and NW Poland: palaeoecologic and environmental implications. *Geobios* **35**, 29–39, https://doi.org/10.1016/s0016-6995(02)00007-4 (2002).
405. Männik, P., Lehnert, O., Nõlvak, J. & Joachimski, M. M. Climate changes in the pre-Hirnantian Late Ordovician based on $\delta^{18}O_{phos}$ studies from Estonia. *Palaeogeography, Palaeoclimatology, Palaeoecology* **569**, 110347, https://doi.org/10.1016/j.palaeo.2021.110347 (2021).
406. Martnez-Garcia, A., Rosell-Melé, A., McClymont, E. L., Gersonde, R. & Haug, G. H. Subpolar link to the emergence of the modern equatorial Pacific cold tongue. *Science* **328**, 1550–1553, https://doi.org/10.1126/science.1184480 (2010).
407. Matsui, H. *et al.* Vertical thermal gradient history in the eastern equatorial Pacific during the early to middle Miocene: Implications for the equatorial thermocline development. *Paleoceanography* **32**, 729–743, https://doi.org/10.1002/2016pa003058 (2017).
408. Mazzullo, S. J., Boardman, D. R., Grossman, E. L. & Dimmick-Wells, K. Oxygen-carbon isotope stratigraphy of upper Carboniferous to lower Permian marine deposits in Midcontinent USA (Kansas and NE Oklahoma): Implications for sea water chemistry and depositional cyclicity. *Carbonates Evaporites* **22**, 55–72, https://doi.org/10.1007/bf03175846 (2007).
409. McAnena, A. *et al.* Atlantic cooling associated with a marine biotic crisis during the mid-Cretaceous period. *Nat. Geosci.* **6**, 558–561, https://doi.org/10.1038/ngeo1850 (2013).
410. McArthur, J., Donovan, D., Thirlwall, M., Fouke, B. & Mattey, D. Strontium isotope profile of the early Toarcian (Jurassic) oceanic anoxic event, the duration of ammonite biozones, and belemnite palaeotemperatures. *Earth Planet. Sci. Lett.* **179**, 269–285, https://doi.org/10.1016/s0012-821x(00)00111-4 (2000).
411. McArthur, J. *et al.* Belemnites of Valanginian, Hauterivian and Barremian age: Sr-isotope stratigraphy, composition ($^{87}Sr/^{86}Sr$, $\delta^{13}C$, $\delta^{18}O$, Na, Sr, Mg), and palaeo-oceanography. *Palaeogeography, Palaeoclimatology, Palaeoecology* **202**, 253–272, https://doi.org/10.1016/s0031-0182(03)00638-2 (2004).
412. McArthur, J. *et al.* Palaeotemperatures, polar ice-volume, and isotope stratigraphy (Mg/Ca, $\delta^{18}O$, $\delta^{13}C$, $^{87}Sr/^{86}Sr$): The Early Cretaceous (Berriasian, Valanginian, Hauterivian). *Palaeogeography, Palaeoclimatology, Palaeoecology* **248**, 391–430, https://doi.org/10.1016/j.palaeo.2006.12.015 (2007).
413. McClymont, E. L. & Rosell-Melé, A. Links between the onset of modern Walker circulation and the mid-Pleistocene climate transition. *Geology* **33**, 389, https://doi.org/10.1130/g21292.1 (2005).
414. McClymont, E. L., Rosell-Melé, A., Haug, G. H. & Lloyd, J. M. Expansion of subarctic water masses in the North Atlantic and Pacific oceans and implications for mid-Pleistocene ice sheet growth. *Paleoceanography* **23**, https://doi.org/10.1029/2008pa001622 (2008).
415. McClymont, E. L. *et al.* Sea-surface temperature records of Termination 1 in the Gulf of California: Challenges for seasonal and interannual analogues of tropical Pacific climate change. *Paleoceanography* **27**, https://doi.org/10.1029/2011pa002226 (2012).
416. McClymont, E. L. *et al.* Pliocene-Pleistocene evolution of sea surface and intermediate water temperatures from the southwest Pacific. *Paleoceanography* **31**, 895–913, https://doi.org/10.1002/2016pa002954 (2016).
417. McKenzie, J. *et al.* Paleoceanographic implications of stable isotope data from Upper Miocene-Lower Pliocene sediments from the Southeast Atlantic (Deep Sea Drilling Project Site 519). In *Initial Reports of the Deep Sea Drilling Project*, https://doi.org/10.2973/dsdp.proc.73.132.1984 (U.S. Government Printing Office, 1984).
418. Medina-Elizalde, M. & Lea, D. W. The mid-Pleistocene transition in the tropical Pacific. *Science* **310**, 1009–1012, https://doi.org/10.1126/science.1115933 (2005).
419. Metodiev, L. & Koleva-Rekalova, E. Stable isotope records ($\delta^{18}O$ and $\delta^{13}C$) of Lower-Middle Jurassic belemnites from the Western Balkan mountains (Bulgaria): Palaeoenvironmental application. *Appl. Geochem.* **23**, 2845–2856, https://doi.org/10.1016/j.apgeochem.2008.04.010 (2008).
420. Mette, W., Elsler, A. & Korte, C. Palaeoenvironmental changes in the Late Triassic (Rhaetian) of the Northern Calcareous Alps: Clues from stable isotopes and microfossils. *Palaeogeography, Palaeoclimatology, Palaeoecology* **350-352**, 62–72, https://doi.org/10.1016/j.palaeo.2012.06.013 (2012).
421. Mettraux, M., Weissert, H. & Homewood, P. An oxygen-minimum palaeoceanographic signal from Early Toarcian cavity fills. *J. Geol. Soc.* **146**, 333–344, https://doi.org/10.1144/gsjgs.146.2.0333 (1989).
422. Meyer, V. D., Max, L., Hefter, J., Tiedemann, R. & Mollenhauer, G. Glacial-to-Holocene evolution of sea surface temperature and surface circulation in the subarctic northwest Pacific and the Western Bering Sea. *Paleoceanography* **31**, 916–927, https://doi.org/10.1002/2015pa002877 (2016).
423. Middleton, P. D., Marshall, J. D. & Brenchley, P. J. Evidence for isotopic change associated with Late Ordovician glaciation, from brachiopods and marine cements of Central Sweden. In Barnes, C. R. & Williams, S. H. (eds.) *Advances in Ordovician Geology*, vol. 90-9, 336, https://doi.org/10.4095/132198 (Geological Survey of Canada Papers, Vancouver, B.C, 1991).
424. Mii, H., Grossman, E. L. & Yancey, T. E. Stable carbon and oxygen isotope shifts in Permian seas of West Spitsbergen-Global change or diagenetic artifact? *Geology* **25**, 227, 10.1130/0091-7613(1997)025<0227:scaois>2.3.co;2 (1997).
425. Mii, H., Grossman, E. L. & Yancey, T. E. Carboniferous isotope stratigraphies of North America: Implications for Carboniferous paleoceanography and Mississippian glaciation. *Geological Society of America Bulletin* **111**, 960–973, 10.1130/0016-7606(1999)111<0960:cisona>2.3.co;2 (1999).
426. Mii, H.-S., Grossman, E. L., Yancey, T. E., Chuvashov, B. & Egorov, A. Isotopic records of brachiopod shells from the Russian Platform — evidence for the onset of mid-Carboniferous glaciation. *Chem. Geol.* **175**, 133–147, https://doi.org/10.1016/s0009-2541(00)00366-1 (2001).

427. Mii, H., Shi, G., Cheng, C. & Chen, Y. Permian Gondwanaland paleoenvironment inferred from carbon and oxygen isotope records of brachiopod fossils from Sydney Basin, southeast Australia. *Chem. Geol.* **291**, 87–103, https://doi.org/10.1016/j.chemgeo.2011.10.002 (2012).
428. Mii, H., Shi, G. & Wang, C. Late Paleozoic middle-latitude Gondwana environment-stable isotope records from Western Australia. *Gondwana Res.* **24**, 125–138, https://doi.org/10.1016/j.gr.2012.10.013 (2013).
429. Mitchell, L., Fallick, A. E. & Curry, G. B. Stable carbon and oxygen isotope compositions of mollusc shells from Britain and New Zealand. *Palaeogeography, Palaeoclimatology, Palaeoecology* **111**, 207–216, https://doi.org/10.1016/0031-0182(94)90063-9 (1994).
430. Montañez, I. P. *et al.* Carboniferous climate teleconnections archived in coupled bioapatite $\delta^{18}O_{PO4}$ and $^{87}Sr/^{86}Sr$ records from the epicontinental Donets Basin, Ukraine. *Earth Planet. Sci. Lett.* **492**, 89–101, https://doi.org/10.1016/j.epsl.2018.03.051 (2018).
431. Morante, R. Permian and early Triassic isotopic records of carbon and strontium in Australia and a scenario of events about the Permian-Triassic boundary. *Historical Biol.* **11**, 289–310, https://doi.org/10.1080/10292389609380546 (1996).
432. Morrison, J. O. *Cretaceous marine invertebrates: A geochemical perspective*. Ph.D. thesis, University of Ottawa (1991).
433. Moriya, K., Wilson, P. A., Friedrich, O., Erbacher, J. & Kawahata, H. Testing for ice sheets during the mid-Cretaceous greenhouse using glassy foraminiferal calcite from the mid-Cenomanian tropics on Demerara Rise. *Geology* **35**, 615, https://doi.org/10.1130/g23589a.1 (2007).
434. Müller, J. *et al.* Cordilleran ice-sheet growth fueled primary productivity in the Gulf of Alaska, northeast Pacific Ocean. *Geology* **46**, 307–310, https://doi.org/10.1130/g39904.1 (2018).
435. Murphy, M. & Kennett, J. Development of latitudinal thermal gradients during the Oligocene: Oxygen-isotope evidence from the Southwest Pacific. In *Initial Reports of the Deep Sea Drilling Project*, 90, https://doi.org/10.2973/dsdp.proc.90.140.1986 (U.S. Government Printing Office, 1986).
436. Mutterlose, J., Malkoc, M., Schouten, S., Sinninghe Damsté, J. S. & Forster, A. TEX_{86} and stable $\delta^{18}O$ paleothermometry of early Cretaceous sediments: Implications for belemnite ecology and paleotemperature proxy application. *Earth Planet. Sci. Lett.* **298**, 286–298, https://doi.org/10.1016/j.epsl.2010.07.043 (2010).
437. Mutterlose, J., Malkoc, M., Schouten, S. & Sinninghe Damsté, J. S. Reconstruction of vertical temperature gradients in past oceans — Proxy data from the Hauterivian–early Barremian (Early Cretaceous) of the Boreal Realm. *Palaeogeography, Palaeoclimatology, Palaeoecology* **363-364**, 135–143, https://doi.org/10.1016/j.palaeo.2012.09.006 (2012).
438. Mutterlose, J., Bottini, C., Schouten, S. & Sinninghe Damsté, J. S. High sea-surface temperatures during the early Aptian Oceanic Anoxic Event 1a in the Boreal Realm. *Geology* **42**, 439–442, https://doi.org/10.1130/g35394.1 (2014).
439. Naafs, B. D. A. *et al.* Late Pliocene changes in the North Atlantic Current. *Earth Planet. Sci. Lett.* **298**, 434–442, https://doi.org/10.1016/j.epsl.2010.08.023 (2010).
440. Naafs, B. & Pancost, R. Sea-surface temperature evolution across Aptian Oceanic Anoxic Event 1a. *Geology* **44**, 959–962, https://doi.org/10.1130/g38575.1 (2016).
441. Naafs, B. D. A., Voelker, A. H. L., Karas, C., Andersen, N. & Sierro, F. J. Repeated near-collapse of the Pliocene sea surface temperature gradient in the North Atlantic. *Paleoceanogr. Paleoclimatol.* **35**, https://doi.org/10.1029/2020pa003905 (2020).
442. Nairn, M. G., Lear, C. H., Sosdian, S. M., Bailey, T. R. & Beavington-Penney, S. Tropical sea surface temperatures following the middle Miocene climate transition from laser-ablation ICP-MS analysis of glassy foraminifera. *Paleoceanogr. Paleoclimatol.* **36**, https://doi.org/10.1029/2020pa004165 (2021).
443. Nakashima, R., Suzuki, A. & Watanabe, T. Life history of the Pliocene scallop *Fortipecten*, based on oxygen and carbon isotope profiles. *Palaeogeography, Palaeoclimatology, Palaeoecology* **211**, 299–307, https://doi.org/10.1016/j.palaeo.2004.05.011 (2004).
444. Narkiewicz, M., Narkiewicz, K., Krzenińska, E. & Kruchek, S. A. Oxygen isotopic composition of conodont apatite in the equatorial epeiric Belarussian basin (Eifelian)–Relationship to fluctuating seawater salinity and temperature. *PALAIOS* **32**, 439–447, https://doi.org/10.2110/palo.2016.059 (2017).
445. Nascimento, R. *et al.* Tropical Atlantic stratification response to late Quaternary precessional forcing. *Earth Planet. Sci. Lett.* **568**, 117030, https://doi.org/10.1016/j.epsl.2021.117030 (2021).
446. Nathan, S. A. & Leckie, R. M. Early history of the Western Pacific Warm Pool during the middle to late Miocene (13.2–5.8 Ma): Role of sea-level change and implications for equatorial circulation. *Palaeogeography, Palaeoclimatology, Palaeoecology* **274**, 140–159, https://doi.org/10.1016/j.palaeo.2009.01.007 (2009).
447. Nelson, C., Hendy, C. & Dudley, W. Quaternary isotope stratigraphy of Hole 593, Challenger Plateau, South Tasman Sea: Preliminary observations based on foraminifers and calcareous nannofossils. In *Initial Reports of the Deep Sea Drilling Project*, **90**, https://doi.org/10.2973/dsdp.proc.90.143.1986 (U.S. Government Printing Office, 1986).
448. Nelson, C., Hendy, C., Cuthbertson, A. & Jarrett, G. Late Quaternary carbonate and isotope stratigraphy, Subantarctic Site 594, Southwest Pacific. In *Initial Reports of the Deep Sea Drilling Project*, 90, https://doi.org/10.2973/dsdp.proc.90.144.1986 (U.S. Government Printing Office, 1986).
449. Niebuhr, B. & Joachimski, M. M. Stable isotope and trace element geochemistry of Upper Cretaceous carbonates and belemnite rostra (Middle Campanian, north Germany). *Geobios* **35**, 51–64, https://doi.org/10.1016/s0016-6995(02)00009-8 (2002).
450. Nori, L. & Lathuilière, B. Form and environment of *Gryphaea arcuata*. *Lethaia* **36**, 83–96, https://doi.org/10.1080/00241160310003081 (2003).
451. Norris, R., Corfield, R. & Cartlidge, J. Evolutionary ecology of *Globorotalia* (*Globoconella*) (planktic foraminifera). *Mar. Micropaleontology* **23**, 121–145, https://doi.org/10.1016/0377-8398(94)90004-3 (1994).
452. Nunn, E. V., Price, G. D., Hart, M. B., Page, K. N. & Leng, M. J. Isotopic signals from Callovian–Kimmeridgian (Middle–Upper Jurassic) belemnites and bulk organic carbon, Staffin Bay, Isle of Skye, Scotland. *J. Geol. Soc.* **166**, 633–641, https://doi.org/10.1144/0016-76492008-067 (2009).
453. Nunn, E. V. & Price, G. D. Late Jurassic (Kimmeridgian–Tithonian) stable isotopes ($\delta^{18}O$, $\delta^{13}C$) and Mg/Ca ratios: New palaeoclimate data from Helmsdale, northeast Scotland. *Palaeogeography, Palaeoclimatology, Palaeoecology* **292**, 325–335, https://doi.org/10.1016/j.palaeo.2010.04.015 (2010).
454. Nützel, A., Joachimski, M. & Correa, M. L. Seasonal climatic fluctuations in the Late Triassic tropics–High-resolution oxygen isotope records from aragonitic bivalve shells (Cassian Formation, Northern Italy). *Palaeogeography, Palaeoclimatology, Palaeoecology* **285**, 194–204, https://doi.org/10.1016/j.palaeo.2009.11.011 (2010).
455. O'Brien, C. L. *et al.* High sea surface temperatures in tropical warm pools during the Pliocene. *Nat. Geosci.* **7**, 606–611, https://doi.org/10.1038/ngeo2194 (2014).
456. O'Brien, C. L. *et al.* The enigma of Oligocene climate and global surface temperature evolution. *Proc. Natl Acad. Sci.* **117**, 25302–25309, https://doi.org/10.1073/pnas.2003914117 (2020).
457. OConnor, L. K. *et al.* Late Cretaceous temperature evolution of the southern high latitudes: A TEX_{86} perspective. *Paleoceanogr. Paleoclimatol.* **34**, 436–454, https://doi.org/10.1029/2018pa003546 (2019).
458. Ohta, S., Kaiho, K. & Takei, T. Relationship between surface-water temperature and ice-sheet expansion during the middle Miocene. *Palaeogeography, Palaeoclimatology, Palaeoecology* **201**, 307–320, https://doi.org/10.1016/s0031-0182(03)00617-5 (2003).
459. Padden, M. *Late Jurassic paleoceanography: Evidence from stable isotopes and carbonate sedimentology*. Ph.D. thesis, ETH Zurich. https://doi.org/10.3929/ethz-a-004200330 (2001).
460. Pagani, M., Liu, Z., LaRiviere, J. & Ravelo, A. C. High Earth-system climate sensitivity determined from Pliocene carbon dioxide concentrations. *Nat. Geosci.* **3**, 27–30, https://doi.org/10.1038/ngeo724 (2009).

461. Pahnke, K., Zahn, R., Elderfield, H. & Schulz, M. 340,000-year centennial-scale marine record of southern hemisphere climatic oscillation. *Science* **301**, 948–952, https://doi.org/10.1126/science.1084451 (2003).
462. Pardo, A., Keller, G., Molina, E. & Canudo, J. Planktic foraminiferal turnover across the Paleocene-Eocene transition at DSDP Site 401, Bay of Biscay, North Atlantic. *Mar. Micropaleontology* **29**, 129–158, https://doi.org/10.1016/s0377-8398(96)00035-7 (1997).
463. Parvizi, T., Bahrami, A., Königshof, P. & Kaiser, S. Conodont biostratigraphy of Upper Devonian–Lower Carboniferous deposits in eastern Alborz (Mighan section), North Iran. *Palaeoworld* https://doi.org/10.1016/j.palwor.2021.01.008 (2021).
464. Pearson, P. & Shackleton, N. Neogene multispecies planktonic foraminifer stable isotope record, Site 871, Limalok Guyot. In *Proceedings of the Ocean Drilling Program, 144 Scientific Results*, https://doi.org/10.2973/odp.proc.sr.144.054.1995 (Ocean Drilling Program, 1995).
465. Pearson, P., Shackleton, N., Weedon, G. & Hall, M. Multispecies planktonic foraminifer stable isotope stratigraphy through Oligocene/Miocene boundary climatic cycles, Site 926. In *Proceedings of the Ocean Drilling Program*, https://doi.org/10.2973/odp.proc.sr.154.118.1997 (Ocean Drilling Program, 1997).
466. Pearson, P. N. *et al*. Warm tropical sea surface temperatures in the Late Cretaceous and Eocene epochs. *Nature* **413**, 481–487, https://doi.org/10.1038/35097000 (2001).
467. Pearson, P. N. *et al*. Stable warm tropical climate through the Eocene Epoch. *Geology* **35**, 211, https://doi.org/10.1130/g23175a.1 (2007).
468. Pearson, P. N. *et al*. Extinction and environmental change across the Eocene-Oligocene boundary in Tanzania. *Geology* **36**, 179, https://doi.org/10.1130/g24308a.1 (2008).
469. Pearson, P. N. & Wade, B. S. Taxonomy and stable isotope paleoecology of well-preserved planktonic foraminifera from the uppermost Oligocene of Trinidad. *J. Foraminifer. Res.* **39**, 191–217, https://doi.org/10.2113/gsjfr.39.3.191 (2009).
470. Penman, D. E., Hönisch, B., Zeebe, R. E., Thomas, E. & Zachos, J. C. Rapid and sustained surface ocean acidification during the Paleocene-Eocene Thermal Maximum. *Paleoceanography* **29**, 357–369, https://doi.org/10.1002/2014pa002621 (2014).
471. Peterson, L. *et al*. Late Quaternary stratigraphy and sedimentation at Site 1002, Cariaco Basin (Venezuela). In *Proceedings of the Ocean Drilling Program, 165 Scientific Results*, https://doi.org/10.2973/odp.proc.sr.165.017.2000 (Ocean Drilling Program, 2000).
472. Petrick, B. *et al*. Oceanographic and climatic evolution of the southeastern subtropical Atlantic over the last 3.5 Ma. *Earth Planet. Sci. Lett.* **492**, 12–21, https://doi.org/10.1016/j.epsl.2018.03.054 (2018).
473. Petrick, B. *et al*. Glacial Indonesian Throughflow weakening across the Mid-Pleistocene Climatic Transition. *Scientific Reports* **9**, https://doi.org/10.1038/s41598-019-53382-0 (2019).
474. Petrizzo, M. R., Huber, B. T., Wilson, P. A. & MacLeod, K. G. Late Albian paleoceanography of the western subtropical North Atlantic. *Paleoceanography* **23**, https://doi.org/10.1029/2007pa001517 (2008).
475. Pfuhl, H. A. & Shackleton, N. J. Changes in coiling direction, habitat depth and abundance in two menardellid species. *Mar. Micropaleontology* **50**, 3–20, https://doi.org/10.1016/s0377-8398(03)00063-x (2004).
476. Picard, S. *et al*. δ^{18}O values of coexisting brachiopods and fish: Temperature differences and estimates of paleo–water depths. *Geology* **26**, 975, 10.1130/0091-7613(1998)026<0975:ovocba>2.3.co;2 (1998).
477. Pierre, C., Saliege, J., Urrutiaguer, M. & Giraudeau, J. Stable isotope record of the last 500 k.y. at Site 1087 (Southern Cape Basin). In *Proceedings of the Ocean Drilling Program*, https://doi.org/10.2973/odp.proc.sr.175.230.2001 (Ocean Drilling Program, 2001).
478. Pirrie, D. & Marshall, J. D. High-paleolatitude Late Cretaceous paleotemperatures: New data from James Ross Island, Antarctica. *Geology* **18**, 31, 10.1130/0091-7613(1990)018<0031:hplcpn>2.3.co;2 (1990).
479. Pirrie, D., Doyle, P., Marshall, J. D. & Ellis, G. Cool Cretaceous climates: new data from the Albian of western Australia. *J. Geol. Soc.* **152**, 739–742, https://doi.org/10.1144/gsjgs.152.5.0739 (1995).
480. Pirrie, D., Marshall, J., Doyle, P. & Riccardi, A. Cool early Albian climates: new data from Argentina. *Cretac. Res.* **25**, 27–33, https://doi.org/10.1016/j.cretres.2003.10.002 (2004).
481. Plancq, J., Mattioli, E., Pittet, B., Simon, L. & Grossi, V. Productivity and sea-surface temperature changes recorded during the late Eocene–early Oligocene at DSDP Site 511 (south atlantic). *Palaeogeography, Palaeoclimatology, Palaeoecology* **407**, 34–44, https://doi.org/10.1016/j.palaeo.2014.04.016 (2014).
482. Plancq, J. *et al*. Multi-proxy constraints on sapropel formation during the late Pliocene of central Mediterranean (southwest Sicily). *Earth Planet. Sci. Lett.* **420**, 30–44, https://doi.org/10.1016/j.epsl.2015.03.031 (2015).
483. Podlaha, O. G., Mutterlose, J. & Veizer, J. Preservation of δ^{18}O and δ^{13}C in belemnite rostra from the Jurassic/Early Cretaceous successions, https://doi.org/10.2475/ajs.298.4.324 (1998).
484. Polik, C. A., Elling, F. J. & Pearson, A. Impacts of paleoecology on the TEX_{86} sea surface temperature proxy in the Pliocene-Pleistocene Mediterranean Sea. *Paleoceanogr. Paleoclimatol.* **33**, 1472–1489, https://doi.org/10.1029/2018pa003494 (2018).
485. Poore, R. & Matthews, R. Oxygen isotope ranking of late Eocene and Oligocene planktonic foraminifers: Implications for Oligocene sea-surface temperatures and global ice-volume. *Mar. Micropaleontology* **9**, 111–134, https://doi.org/10.1016/0377-8398(84)90007-0 (1984).
486. Popp, B. N., Anderson, T. F. & Sandberg, P. A. Brachiopods as indicators of original isotopic compositions in some Paleozoic limestones. *Geol. Soc. Am. Bull.* **97**, 1262–1269, https://doi.org/10.1130/0016-7606(1986)97 (1986).
487. Prentice, M., Freiz, J., Simonds, G. & Matthews, R. Neogene trends in planktonic foraminifer δ^{18}O from Site 807: Implications for global ice volume and western equatorial Pacific sea-surface temperatures. In *Proceedings of the Ocean Drilling Program, 130 Scientific Results*, https://doi.org/10.2973/odp.proc.sr.130.029.1993 (Ocean Drilling Program, 1993).
488. Price, G. & Sellwood, B. Palaeotemperatures indicated by Upper Jurassic (Kimmeridgian-Tithonian) fossils from Mallorca determined by oxygen isotope composition. *Palaeogeography, Palaeoclimatology, Palaeoecology* **110**, 1–10, https://doi.org/10.1016/0031-0182(94)90106-6 (1994).
489. Price, G. & Sellwood, B. "Warm" palaeotemperatures from high Late Jurassic palaeolatitudes (Falkland Plateau): Ecological, environmental or diagenetic controls? *Palaeogeography, Palaeoclimatology, Palaeoecology* **129**, 315–327, https://doi.org/10.1016/s0031-0182(96)00058-2 (1997).
490. Price, G. D., Sellwood, B. W., Corfield, R. M., Clarke, L. & Cartlidge, J. E. Isotopic evidence for palaeotemperatures and depth stratification of Middle Cretaceous planktonic foraminifera from the Pacific Ocean. *Geol. Mag.* **135**, 183–191, https://doi.org/10.1017/s0016756898008334 (1998).
491. Price, G. D., Ruffell, A. H., Jones, C. E., Kalin, R. M. & Mutterlose, J. Isotopic evidence for temperature variation during the early Cretaceous (late Ryazanian–mid-Hauterivian). *J. Geol. Soc.* **157**, 335–343, https://doi.org/10.1144/jgs.157.2.335 (2000).
492. Price, G. D. & Gröcke, D. R. Strontium-isotope stratigraphy and oxygen- and carbon-isotope variation during the Middle Jurassic–Early Cretaceous of the Falkland Plateau, South Atlantic. *Palaeogeography, Palaeoclimatology, Palaeoecology* **183**, 209–222, https://doi.org/10.1016/s0031-0182(01)00486-2 (2002).
493. Price, G. & Hart, M. Isotopic evidence for Early to mid-Cretaceous ocean temperature variability. *Mar. Micropaleontology* **46**, 45–58, https://doi.org/10.1016/s0377-8398(02)00043-9 (2002).
494. Price, G. & Mutterlose, J. Isotopic signals from late Jurassic–early Cretaceous (Volgian–Valanginian) sub-Arctic belemnites, Yatria River, Western Siberia. *J. Geol. Soc.* **161**, 959–968, https://doi.org/10.1144/0016-764903-169 (2004).
495. Price, G. D. & Page, K. N. A carbon and oxygen isotopic analysis of molluscan faunas from the Callovian-Oxfordian boundary at Redcliff Point, Weymouth, Dorset: implications for belemnite behaviour. *Proc. Geologists' Assoc.* **119**, 153–160, https://doi.org/10.1016/s0016-7878(08)80315-x (2008).

496. Price, G. D., Twitchett, R. J., Smale, C. & Marks, V. Isotopic analysis of the life and history of the enigmatic squid *Spirula spirula*, with implications for studies of fossil cephalopods. *PALAIOS* **24**, 273–279, https://doi.org/10.2110/palo.2008.p08-067r (2009).
497. Price, G. D. Carbon-isotope stratigraphy and temperature change during the Early–Middle Jurassic (Toarcian–Aalenian), Raasay, Scotland, UK. *Palaeogeography, Palaeoclimatology, Palaeoecology* **285**, 255–263, https://doi.org/10.1016/j.palaeo.2009.11.018 (2010).
498. Price, G. D. & Teece, C. Reconstruction of Jurassic (Bathonian) palaeosalinity using stable isotopes and faunal associations. *J. Geol. Soc.* **167**, 1199–1208, https://doi.org/10.1144/0016-76492010-029 (2010).
499. Price, G., Főzy, I., Janssen, N. & Pálfy, J. Late Valanginian–Barremian (Early Cretaceous) palaeotemperatures inferred from belemnite stable isotope and Mg/Ca ratios from Bersek Quarry (Gerecse Mountains, Transdanubian Range, Hungary). *Palaeogeography, Palaeoclimatology, Palaeoecology* **305**, 1–9, https://doi.org/10.1016/j.palaeo.2011.02.007 (2011).
500. Price, G. D., Twitchett, R. J., Wheeley, J. R. & Buono, G. Isotopic evidence for long term warmth in the Mesozoic. *Scientific Reports* **3**, https://doi.org/10.1038/srep01438 (2013).
501. Qing, H. & Veizer, J. Oxygen and carbon isotopic composition of Ordovician brachiopods: Implications for coeval seawater. *Geochim. Cosmochim. Acta* **58**, 4429–4442, https://doi.org/10.1016/0016-7037(94)90345-X (1994).
502. Quillévéré, F., Aubry, M.-P., Norris, R. D. & Berggren, W. A. Paleocene oceanography of the eastern subtropical Indian Ocean. *Palaeogeography, Palaeoclimatology, Palaeoecology* **184**, 371–405, https://doi.org/10.1016/s0031-0182(02)00275-4 (2002).
503. Quinton, P. C. & MacLeod, K. G. Oxygen isotopes from conodont apatite of the midcontinent, US: Implications for Late Ordovician climate evolution. *Palaeogeography, Palaeoclimatology, Palaeoecology* **404**, 57–66, https://doi.org/10.1016/j.palaeo.2014.03.036 (2014).
504. Quinton, P. C. *et al*. Testing the early Late Ordovician cool-water hypothesis with oxygen isotopes from conodont apatite. *Geol. Mag.* **155**, 1727–1741, https://doi.org/10.1017/s0016756817000589 (2017).
505. Quinton, P. C., Speir, L., Miller, J., Ethington, R. & MacLeod, K. G. Extreme heat in the early Ordovician. *PALAIOS* **33**, 353–360, https://doi.org/10.2110/palo.2018.031 (2018).
506. Raitzsch, M. *et al*. Atmospheric carbon dioxide variations across the middle Miocene climate transition. *Clim. Past.* **17**, 703–719, https://doi.org/10.5194/cp-17-703-2021 (2021).
507. Rao, C. P. Elemental composition of marine calcite from modern temperate shelf brachiopods, bryozoans and bulk carbonates, eastern Tasmania, Australia. *Carbonates Evaporites* **11**, 1–18, https://doi.org/10.1007/bf03175781 (1996).
508. Rasmussen, C. M. *et al*. Onset of main Phanerozoic marine radiation sparked by emerging Mid Ordovician icehouse. *Sci. Rep.* **6**, 1–9, https://doi.org/10.1038/srep18884 (2016).
509. Riboulleau, A. *et al*. Evolution de la paléotempérature des eaux de la plate-forme Russe au cours du Jurassique Supérieur. *Comptes Rendus de. l'Académie des. Sciences-Series IIA-Earth Planet. Sci.* **326**, 239–246, https://doi.org/10.1016/S1251-8050(97)86813-9 (1998).
510. Richey, J. N., Hollander, D. J., Flower, B. P. & Eglinton, T. I. Merging late Holocene molecular organic and foraminiferal-based geochemical records of sea surface temperature in the Gulf of Mexico. *Paleoceanography* **26**, https://doi.org/10.1029/2010pa002000 (2011).
511. Riding, J. B., Leng, M. J., Kender, S., Hesselbo, S. P. & Feist-Burkhardt, S. Isotopic and palynological evidence for a new Early Jurassic environmental perturbation. *Palaeogeography, Palaeoclimatology, Palaeoecology* **374**, 16–27, https://doi.org/10.1016/j.palaeo.2012.10.019 (2013).
512. Rigo, M. & Joachimski, M. M. Palaeoecology of Late Triassic conodonts: Constraints from oxygen isotopes in biogenic apatite. *Acta Palaeontologica Polonica* **55**, 471–478, https://doi.org/10.4202/app.2009.0100 (2010).
513. Roark, A. *et al*. Brachiopod geochemical records from across the Carboniferous seas of North America: Evidence for salinity gradients, stratification, and circulation patterns. *Palaeogeography, Palaeoclimatology, Palaeoecology* **485**, 136–153, https://doi.org/10.1016/j.palaeo.2017.06.009 (2017).
514. Robinson, S. A. *et al*. Early Jurassic North Atlantic sea-surface temperatures from TEX_{86} palaeothermometry. *Sedimentology* **64**, 215–230, https://doi.org/10.1111/sed.12321 (2016).
515. Robinson, S. A. *et al*. Southern Hemisphere sea-surface temperatures during the Cenomanian–Turonian: Implications for the termination of Oceanic Anoxic Event 2. *Geology* **47**, 131–134, https://doi.org/10.1130/g45842.1 (2019).
516. Romano, C. *et al*. Climatic and biotic upheavals following the end-Permian mass extinction. *Nat. Geosci.* **6**, 57–60, https://doi.org/10.1038/ngeo1667 (2012).
517. Rommerskirchen, F., Condon, T., Mollenhauer, G., Dupont, L. & Schefuss, E. Miocene to Pliocene development of surface and subsurface temperatures in the Benguela Current system. *Paleoceanography* **26**, https://doi.org/10.1029/2010pa002074 (2011).
518. Rosales, I., Quesada, S. & Robles, S. Primary and diagenetic isotopic signals in fossils and hemipelagic carbonates: the Lower Jurassic of northern Spain. *Sedimentology* **48**, 1149–1169, https://doi.org/10.1046/j.1365-3091.2001.00412.x (2001).
519. Rosales, I. *et al*. Isotope records (C-O-Sr) of late Pliensbachian-early Toarcian environmental perturbations in the westernmost Tethys (Majorca Island, Spain). *Palaeogeography, Palaeoclimatology, Palaeoecology* **497**, 168–185, https://doi.org/10.1016/j.palaeo.2018.02.016 (2018).
520. Rosell-Melé, A., Martnez-Garcia, A. & McClymont, E. L. Persistent warmth across the Benguela upwelling system during the Pliocene Epoch. *Earth Planet. Sci. Lett.* **386**, 10–20, https://doi.org/10.1016/j.epsl.2013.10.041 (2014).
521. Rosenau, N. A., Herrmann, A. D. & Leslie, S. A. Conodont apatite $\delta^{18}O$ values from a platform margin setting, Oklahoma, USA: Implications for initiation of Late Ordovician icehouse conditions. *Palaeogeography, Palaeoclimatology, Palaeoecology* **315-316**, 172–180, https://doi.org/10.1016/j.palaeo.2011.12.003 (2012).
522. Rosenau, N. A., Tabor, N. J. & Herrmann, A. D. Assessing the paleoenvironmental significance of middle–late Pennsylvanian conodont apatite $\delta^{18}O$ values in the Illinois Basin. *PALAIOS* **29**, 250–265, https://doi.org/10.2110/palo.2013.112 (2014).
523. Rousselle, G., Beltran, C., Sicre, M.-A., Raffi, I. & Rafélis, M. D. Changes in sea-surface conditions in the equatorial Pacific during the middle Miocene–Pliocene as inferred from coccolith geochemistry. *Earth Planet. Sci. Lett.* **361**, 412–421, https://doi.org/10.1016/j.epsl.2012.11.003 (2013).
524. Ruebsam, W., Reolid, M., Sabatino, N., Masetti, D. & Schwark, L. Molecular paleothermometry of the early Toarcian climate perturbation. *Glob. Planet. Change* **195**, 103351, https://doi.org/10.1016/j.gloplacha.2020.103351 (2020).
525. Russon, T. *et al*. Inter-hemispheric asymmetry in the early Pleistocene Pacific warm pool. *Geophys. Res. Lett.* **37**, https://doi.org/10.1029/2010gl043191 (2010).
526. Russon, T. *et al*. The mid-Pleistocene transition in the subtropical southwest Pacific. *Paleoceanography* **26**, https://doi.org/10.1029/2010pa002019 (2011).
527. Sabino, M. *et al*. The response of water column and sedimentary environments to the advent of the Messinian salinity crisis: Insights from an onshore deep-water section (Govone, NW Italy. *Geol. Mag.* **158**, 825–841, https://doi.org/10.1017/s0016756820000874 (2020).
528. Salocchi, A. C. *et al*. Biomarker constraints on Mediterranean climate and ecosystem transitions during the Early-Middle Miocene. *Palaeogeography, Palaeoclimatology, Palaeoecology* **562**, 110092, https://doi.org/10.1016/j.palaeo.2020.110092 (2021).
529. Saltzman, E. & Barron, E. Deep circulation in the Late Cretaceous: Oxygen isotope paleotemperatures from *Inoceramus* remains in DSDP cores. *Palaeogeography, Palaeoclimatology, Palaeoecology* **40**, 167–181, https://doi.org/10.1016/0031-0182(82)90088-8 (1982).

530. Samtleben, C., Munnecke, A., Bickert, T. & Pätzold, J. The Silurian of Gotland (Sweden): Facies interpretation based on stable isotopes in brachiopod shells. *Geol. Rundsch.* **85**, 278–292, https://doi.org/10.1007/bf02422234 (1996).
531. Sánchez-Montes, M. L. *et al*. Late Pliocene Cordilleran Ice Sheet development with warm northeast Pacific sea surface temperatures. *Clim. Past.* **16**, 299–313, https://doi.org/10.5194/cp-16-299-2020 (2020).
532. Sangiorgi, F. *et al*. Southern Ocean warming and Wilkes Land ice sheet retreat during the mid-Miocene. *Nature Communications* **9**, https://doi.org/10.1038/s41467-017-02609-7 (2018).
533. Sangiorgi, F., Quaijtaal, W., Donders, T. H., Schouten, S. & Louwye, S. Middle Miocene temperature and productivity evolution at a Northeast Atlantic shelf site (IODP U1318, Porcupine Basin): Global and regional changes. *Paleoceanogr. Paleoclimatol.* **36**, https://doi.org/10.1029/2020PA004059 (2021).
534. Sato, K. *et al*. Establishment of the western Pacific warm pool during the Pliocene: Evidence from planktic foraminifera, oxygen isotopes, and Mg/Ca ratios. *Palaeogeography, Palaeoclimatology, Palaeoecology* **265**, 140–147, https://doi.org/10.1016/j.palaeo.2008.05.003 (2008).
535. Savin, S. M., Douglas, R. G. & Stehli, F. G. Tertiary marine paleotemperatures. *Geological Society of America Bulletin* **86**, 1499, 10.1130/0016-7606(1975)86<1499:tmp>2.0.co;2 (1975).
536. Scasso, R. A. *et al*. A high-resolution record of environmental changes from a Cretaceous-Paleogene section of Seymour Island, Antarctica. *Palaeogeography, Palaeoclimatology, Palaeoecology* **555**, 109844, https://doi.org/10.1016/j.palaeo.2020.109844 (2020).
537. Schefuß, E., Sinninghe Damsté, J. S. & Jansen, J. H. F. Forcing of tropical Atlantic sea surface temperatures during the mid-Pleistocene transition. *Paleoceanography* **19**, https://doi.org/10.1029/2003pa000892 (2004).
538. Schefuß, E., Kuhlmann, H., Mollenhauer, G., Prange, M. & Pätzold, J. Forcing of wet phases in southeast Africa over the past 17,000 years. *Nature* **480**, 509–512, https://doi.org/10.1038/nature10685 (2011).
539. Scheiner, F., Holcová, K., Milovský, R. & Kuhnert, H. Temperature and isotopic composition of seawater in the epicontinental sea (Central Paratethys) during the Middle Miocene Climate Transition based on Mg/Ca, $\delta^{18}O$ and $\delta^{13}C$ from foraminiferal tests. *Palaeogeography, Palaeoclimatology, Palaeoecology* **495**, 60–71, https://doi.org/10.1016/j.palaeo.2017.12.027 (2018).
540. Schneider, R. R., Müller, P. J. & Ruhland, G. Late Quaternary surface circulation in the east equatorial South Atlantic: Evidence from alkenone sea surface temperatures. *Paleoceanography* **10**, 197–219, https://doi.org/10.1029/94pa03308 (1995).
541. Schneider, R. R. *et al*. Late Quaternary surface temperatures and productivity in the east-equatorial South Atlantic: Response to changes in trade/monsoon wind forcing and surface water advection. In *The South Atlantic*, 527–551 https://doi.org/10.1007/978-3-642-80353-6_27 (Springer Berlin Heidelberg, 1996).
542. Schobben, M., Joachimski, M. M., Korn, D., Leda, L. & Korte, C. Palaeotethys seawater temperature rise and an intensified hydrological cycle following the end-Permian mass extinction. *Gondwana Res.* **26**, 675–683, https://doi.org/10.1016/j.gr.2013.07.019 (2014).
543. Schönfeld, J., Sirocko, F. & Jørgensen, N. Oxygen isotope composition of Upper Cretaceous chalk at Lägerdorf (NW Germany): its original environmental signal and palaeotemperature interpretation. *Cretac. Res.* **12**, 27–46, https://doi.org/10.1016/0195-6671(91)90025-8 (1991).
544. Schoon, P. L., Heilmann-Clausen, C., Schultz, B. P., Sinninghe Damsté, J. S. & Schouten, S. Warming and environmental changes in the eastern North Sea Basin during the Paleocene–Eocene Thermal Maximum as revealed by biomarker lipids. *Org. Geochem.* **78**, 79–88, https://doi.org/10.1016/j.orggeochem.2014.11.003 (2015).
545. Schouten, S. *et al*. Extremely high sea-surface temperatures at low latitudes during the middle Cretaceous as revealed by archaeal membrane lipids. *Geology* **31**, 1069, https://doi.org/10.1130/g19876.1 (2003).
546. Scott, G., Nelson, C. & Stone, H. Planktic foraminiferal events in early Miocene Zones N.6 and N.7 at southwest Pacific DSDP Site 593: Relation with climatic changes in oxygen isotope zone Milb. *Mar. Micropaleontology* **25**, 29–45, https://doi.org/10.1016/0377-8398(94)00025-i (1995).
547. Seki, O. *et al*. Alkenone and boron-based Pliocene pCO_2 records. *Earth Planet. Sci. Lett.* **292**, 201–211, https://doi.org/10.1016/j.epsl.2010.01.037 (2010).
548. Seki, O. *et al*. Paleoceanographic changes in the eastern equatorial Pacific over the last 10 Myr. *Paleoceanography* **27**, https://doi.org/10.1029/2011pa002158 (2012).
549. Shackleton, N. The deep-sea sediment record of climate variability. *Prog. Oceanography* **11**, 199–218, https://doi.org/10.1016/0079-6611(82)90008-8 (1982).
550. Shackleton, N., Hall, M. & Boersma, A. Oxygen and carbon isotope data from Leg 74 foraminifers. In *Initial Reports of the Deep Sea Drilling Project*, https://doi.org/10.2973/dsdp.proc.74.115.1984 (U.S. Government Printing Office, 1984).
551. Shackleton, N. & Hall, M. The late Miocene stable isotope record, Site 926. In *Proceedings of the Ocean Drilling Program*, https://doi.org/10.2973/odp.proc.sr.154.119.1997 (Ocean Drilling Program, 1997).
552. Shen, S.-Z. *et al*. A sudden end-Permian mass extinction in South China. *Geol. Soc. Am. Bull.* **131**, 205–223, https://doi.org/10.1130/b31909.1 (2018).
553. Shenton, B. J. *et al*. Clumped isotope thermometry in deeply buried sedimentary carbonates: The effects of bond reordering and recrystallization. *Geological Society of America Bulletin* B31169.1, https://doi.org/10.1130/b31169.1 (2015).
554. Shevenell, A. E., Kennett, J. P. & Lea, D. W. Middle Miocene Southern Ocean cooling and Antarctic cryosphere expansion. *Science* **305**, 1766–1770, https://doi.org/10.1126/science.1100061 (2004).
555. Shevenell, A. E., Ingalls, A. E., Domack, E. W. & Kelly, C. Holocene Southern Ocean surface temperature variability west of the Antarctic Peninsula. *Nature* **470**, 250–254, https://doi.org/10.1038/nature09751 (2011).
556. Shields, G. A. *et al*. Sr, C, and O isotope geochemistry of Ordovician brachiopods: A major isotopic event around the Middle-Late Ordovician transition. *Geochim. Cosmochim. Acta* **67**, 2005–2025, https://doi.org/10.1016/s0016-7037(02)01116-x (2003).
557. Shintani, T., Yamamoto, M. & Chen, M.-T. Paleoenvironmental changes in the northern South China Sea over the past 28,000 years: A study of TEX_{86}-derived sea surface temperatures and terrestrial biomarkers. *J. Asian Earth Sci.* **40**, 1221–1229, https://doi.org/10.1016/j.jseaes.2010.09.013 (2011).
558. Si, W. & Aubry, M.-P. Vital effects and ecologic adaptation of photosymbiont-bearing planktonic foraminifera during the Paleocene-Eocene Thermal Maximum, implications for paleoclimate. *Paleoceanogr. Paleoclimatol.* **33**, 112–125, https://doi.org/10.1002/2017pa003219 (2018).
559. Simon, M. H. *et al*. A late Pleistocene dataset of Agulhas Current variability. *Scientific Data* **7**, https://doi.org/10.1038/s41597-020-00689-7 (2020).
560. Sinninghe Damsté, J. S., van Bentum, E. C., Reichart, G.-J., Pross, J. & Schouten, S. ACO_2 decrease-driven cooling and increased latitudinal temperature gradient during the mid-Cretaceous Oceanic Anoxic Event 2. *Earth Planet. Sci. Lett.* **293**, 97–103, https://doi.org/10.1016/j.epsl.2010.02.027 (2010).
561. Śliwińska, K., Mets, A. & Schouten, S. Data report: distribution and sources of tetraether lipids in Oligocene deposits from the western North Atlantic, IODP Sites U1406 and U1411. In *Proceedings of the IODP*, https://doi.org/10.2204/iodp.proc.342.205.2017 (Integrated Ocean Drilling Program, 2017).
562. Śliwińska, K. K., Thomsen, E., Schouten, S., Schoon, P. L. & Heilmann-Clausen, C. Climate- and gateway-driven cooling of Late Eocene to earliest Oligocene sea surface temperatures in the North Sea Basin. *Scientific Reports* **9**, https://doi.org/10.1038/s41598-019-41013-7 (2019).
563. Sluijs, A. *et al*. Environmental precursors to rapid light carbon injection at the Paleocene/Eocene boundary. *Nature* **450**, 1218–1221, https://doi.org/10.1038/nature06400 (2007).

564. Sluijs, A. *et al*. Arctic late Paleocene-early Eocene paleoenvironments with special emphasis on the Paleocene-Eocene Thermal Maximum (Lomonosov Ridge, Integrated Ocean Drilling Program Expedition 302). *Paleoceanography* **23**, https://doi.org/10.1029/2007pa001495 (2008).
565. Sluijs, A. *et al*. Warming, euxinia and sea level rise during the Paleocene–Eocene Thermal Maximum on the Gulf Coastal Plain: Implications for ocean oxygenation and nutrient cycling. *Clim. Past.* **10**, 1421–1439, https://doi.org/10.5194/cp-10-1421-2014 (2014).
566. Smith, V. *et al*. Life and death in the Chicxulub impact crater: A record of the Paleocene–Eocene Thermal Maximum. *Clim. Past.* **16**, 1889–1899, https://doi.org/10.5194/cp-16-1889-2020 (2020).
567. Smith, R. A. *et al*. Plio-Pleistocene Indonesian Throughflow variability drove eastern Indian Ocean sea surface temperatures. *Paleoceanogr. Paleoclimatol.* **35**, https://doi.org/10.1029/2020pa003872 (2020).
568. Söderlund, U. *Stable isotopic analyses of Turritellidae and Conidae shells from the Mississippi area during late Eocene and early Oligocene*. Master's thesis, Gothenburg University (2000).
569. Sosdian, S. M., Babila, T. L., Greenop, R., Foster, G. L. & Lear, C. H. Ocean carbon storage across the middle Miocene: A new interpretation for the Monterey Event. *Nature Communications* **11**, https://doi.org/10.1038/s41467-019-13792-0 (2020).
570. Sosdian, S. M. & Lear, C. H. Initiation of the Western Pacific Warm Pool at the Middle Miocene Climate Transition? *Paleoceanogr. Paleoclimatol.* **35**, https://doi.org/10.1029/2020pa003920 (2020).
571. Sprovieri, M. *et al*. Ba/Ca evolution in water masses of the Mediterranean late Neogene. *Paleoceanography* **23**, https://doi.org/10.1029/2007pa001469 (2008).
572. Stanton, R. J., Jeffery, D. L. & Ahr, W. M. Early Mississippian climate based on oxygen isotope compositions of brachiopods, Alamogordo Member of the Lake Valley Formation, south-central New Mexico. *Geological Society of America Bulletin* **114**, 4–11, 10.1130/0016-7606(2002)114<0004:emcboo>2.0.co;2 (2002).
573. Stein, R. *et al*. Evidence for ice-free summers in the late Miocene central Arctic Ocean. *Nature Communications* **7**, https://doi.org/10.1038/ncomms11148 (2016).
574. Steinig, S. *et al*. Evidence for a regional warm bias in the Early Cretaceous TEX_{86} record. *Earth Planet. Sci. Lett.* **539**, 116184, https://doi.org/10.1016/j.epsl.2020.116184 (2020).
575. Steinke, S., Groeneveld, J., Johnstone, H. & Rendle-Bühring, R. East Asian summer monsoon weakening after 7.5 Ma: Evidence from combined planktonic foraminifera Mg/Ca and $\delta^{18}O$ (ODP Site 1146: northern South China Sea). *Palaeogeography, Palaeoclimatology, Palaeoecology* **289**, 33–43, https://doi.org/10.1016/j.palaeo.2010.02.007 (2010).
576. Steph, S. *Pliocene stratigraphy and the impact of Panama uplift on changes in Caribbean and tropical east Pacific upper ocean stratification (6-2.5 Ma)*. Ph.D. thesis, Christian-Albrechts Universität Kiel (2005).
577. Steph, S., Tiedemann, R., Groeneveld, J., Sturm, A. & Nürnberg, D. Pliocene changes in tropical east Pacific upper ocean stratification: Response to tropical gateways? In *Proceedings of the Ocean Drilling Program, 202 Scientific Results*, https://doi.org/10.2973/odp.proc.sr.202.211.2006 (Ocean Drilling Program, 2006).
578. Stephenson, M. *et al*. Abrupt environmental and climatic change during the deposition of the Early Permian Haushi limestone, Oman. *Palaeogeography, Palaeoclimatology, Palaeoecology* **270**, 1–18, https://doi.org/10.1016/j.palaeo.2008.08.008 (2008).
579. Steuber, T. Isotopic and chemical intra-shell variations in low-Mg calcite of rudist bivalves (Mollusca-Hippuritacea): disequilibrium fractionations and late Cretaceous seasonality. *Int. J. Earth Sci.* **88**, 551–570, https://doi.org/10.1007/s005310050284 (1999).
580. Steuber, T., Rauch, M., Masse, J.-P., Graaf, J. & Malkoč, M. Low-latitude seasonality of Cretaceous temperatures in warm and cold episodes. *Nature* **437**, 1341–1344, https://doi.org/10.1038/nature04096 (2005).
581. Stevens, K., Mutterlose, J. & Schweigert, G. Belemnite ecology and the environment of the Nusplingen Plattenkalk (Late Jurassic, southern Germany): Evidence from stable isotope data. *Lethaia* **47**, 512–523, https://doi.org/10.1111/let.12076 (2014).
582. Stewart, D. R., Pearson, P. N., Ditchfield, P. W. & Singano, J. M. Miocene tropical Indian Ocean temperatures: Evidence from three exceptionally preserved foraminiferal assemblages from Tanzania. *J. Afr. Earth Sci.* **40**, 173–189, https://doi.org/10.1016/j.jafrearsci.2004.09.001 (2004).
583. Stewart, J. A., James, R. H., Anand, P. & Wilson, P. A. Silicate weathering and carbon cycle controls on the Oligocene-Miocene transition glaciation. *Paleoceanography* **32**, 1070–1085, https://doi.org/10.1002/2017pa003115 (2017).
584. Stokke, E. W., Jones, M. T., Tierney, J. E., Svensen, H. H. & Whiteside, J. H. Temperature changes across the Paleocene-Eocene Thermal Maximum – a new high-resolution TEX_{86} temperature record from the Eastern North Sea Basin. *Earth Planet. Sci. Lett.* **544**, 116388, https://doi.org/10.1016/j.epsl.2020.116388 (2020).
585. Stott, L. & Kennett, J. The paleoceanographic and paleoclimatic signature of the Cretaceous/Paleogene boundary in the Antarctic: Stable isotopic results from ODP Leg 113. In *Proceedings of the Ocean Drilling Program, 113 Scientific Reports*, https://doi.org/10.2973/odp.proc.sr.113.158.1990 (Ocean Drilling Program, 1990).
586. Stott, L., Kennett, J., Shackleton, N. & Corfield, R. The evolution of Antarctic surface waters during the Paleogene: Inferences from the stable isotopic composition of planktonic foraminifers, ODP Leg 113. In *Proceedings of the Ocean Drilling Program, 113 Scientific Reports*, https://doi.org/10.2973/odp.proc.sr.113.187.1990 (Ocean Drilling Program, 1990).
587. Stott, L. D., Sinha, A., Thiry, M., Aubry, M.-P. & Berggren, W. A. Global $\delta^{13}C$ changes across the Paleocene-Eocene boundary: criteria for terrestrial-marine correlations. *Geol. Society, London, Spec. Publ.* **101**, 381–399, https://doi.org/10.1144/gsl.sp.1996.101.01.19 (1996).
588. Suan, G., Mattioli, E., Pittet, B., Mailliot, S. & Lécuyer, C. Evidence for major environmental perturbation prior to and during the Toarcian (Early Jurassic) oceanic anoxic event from the Lusitanian Basin, Portugal. *Paleoceanography* **23**, https://doi.org/10.1029/2007pa001459 (2008).
589. Suan, G. *et al*. Secular environmental precursors to Early Toarcian (Jurassic) extreme climate changes. *Earth Planet. Sci. Lett.* **290**, 448–458, https://doi.org/10.1016/j.epsl.2009.12.047 (2010).
590. Sun, Y. *et al*. Lethally hot temperatures during the Early Triassic greenhouse. *Science* **338**, 366–370, https://doi.org/10.1126/science.1224126 (2012).
591. Sun, Y. *et al*. Climate warming, euxinia and carbon isotope perturbations during the Carnian (Triassic) Crisis in South China. *Earth Planet. Sci. Lett.* **444**, 88–100, https://doi.org/10.1016/j.epsl.2016.03.037 (2016).
592. Sun, Y., Orchard, M., Kocsis, Á. & Joachimski, M. Carnian–Norian (Late Triassic) climate change: Evidence from conodont oxygen isotope thermometry with implications for reef development and Wrangellian tectonics. *Earth Planet. Sci. Lett.* **534**, 116082, https://doi.org/10.1016/j.epsl.2020.116082 (2020).
593. Super, J. R. *et al*. North Atlantic temperature and pCO_2 coupling in the early-middle Miocene. *Geology* **46**, 519–522, https://doi.org/10.1130/g40228.1 (2018).
594. Super, J. R. *et al*. Miocene evolution of North Atlantic sea surface temperature. *Paleoceanogr. Paleoclimatol.* **35**, https://doi.org/10.1029/2019pa003748 (2020).
595. Suttner, T. J. *et al*. Paleotemperature record of the Middle Devonian Kačák Episode. *Scientific Reports* **11**, https://doi.org/10.1038/s41598-021-96013-3 (2021).
596. Tangunan, D. *et al*. Strong glacial-interglacial variability in upper ocean hydrodynamics, biogeochemistry, and productivity in the southern Indian Ocean. *Commun. Earth Environ.* **2**, https://doi.org/10.1038/s43247-021-00148-0 (2021).
597. Tao, K. & Grossman, E. L. Origin of high productivity in the Pliocene of the Florida platform: Evidence from stable isotopes and trace elements. *PALAIOS* **25**, 796–806, https://doi.org/10.2110/palo.2010.p10-058r (2010).

598. Tapia, R. *et al*. Glacial differences of Southern Ocean intermediate waters in the central South Pacific. *Quaternary Sci. Rev.* **208**, 105–117, https://doi.org/10.1016/j.quascirev.2019.01.016 (2019).
599. Taylor, A. K. *et al*. Plio-Pleistocene continental hydroclimate and Indian Ocean sea surface temperatures at the southeast African margin. *Paleoceanogr. Paleoclimatol.* **36**, https://doi.org/10.1029/2020pa004186 (2021).
600. Teichert, B. & Luppold, F. Glendonites from an Early Jurassic methane seep — climate or methane indicators. *Palaeogeography, Palaeoclimatology, Palaeoecology* **390**, 81–93, https://doi.org/10.1016/j.palaeo.2013.03.001 (2013).
601. Thomas, E. & Shackleton, N. J. The Paleocene-Eocene benthic foraminiferal extinction and stable isotope anomalies. *Geol. Society, London, Spec. Publ.* **101**, 401–441, https://doi.org/10.1144/gsl.sp.1996.101.01.20 (1996).
602. Thomas, D. J., Bralower, T. J. & Zachos, J. C. New evidence for subtropical warming during the Late Paleocene Thermal Maximum: Stable isotopes from Deep Sea Drilling Project Site 527, Walvis Ridge. *Paleoceanography* **14**, 561–570, https://doi.org/10.1029/1999pa900031 (1999).
603. Thomas, D. J., Zachos, J. C., Bralower, T. J., Thomas, E. & Bohaty, S. Warming the fuel for the fire: Evidence for the thermal dissociation of methane hydrate during the Paleocene-Eocene Thermal Maximum. *Geology* **30**, 1067, 10.1130/0091-7613(2002)030<1067:wtfftf>2.0.co;2 (2002).
604. Thomas, E. K. *et al*. Temperature and leaf wax δ^2H records demonstrate seasonal and regional controls on Asian monsoon proxies. *Geology* **42**, 1075–1078, https://doi.org/10.1130/g36289.1 (2014).
605. Thomas, E. *et al*. Early Eocene Thermal Maximum 3: Biotic response at Walvis Ridge (SE Atlantic Ocean). *Paleoceanogr. Paleoclimatol.* **33**, 862–883, https://doi.org/10.1029/2018pa003375 (2018).
606. Thompson, E. I. & Schmitz, B. Barium and the Late Paleocene δ^{13}C maximum: Evidence of increased marine surface productivity. *Paleoceanography* **12**, 239–254, https://doi.org/10.1029/96pa03331 (1997).
607. Tian, J. *et al*. Late Pliocene monsoon linkage in the tropical South China Sea. *Earth and Planetary Science Letters* **252**, 72-81, https://doi.org/10.1016/j.epsl.2006.09.028 (2006).
608. Tibbett, E. J. *et al*. Late Eocene record of hydrology and temperature from Prydz Bay, East Antarctica. *Paleoceanogr. Paleoclimatol.* **36**, https://doi.org/10.1029/2020pa004204 (2021).
609. Tiedemann, R. *Acht Millionen Jahre Klimageschichte von Nordwest Afrika und Paläo-Ozeanographie des angrenzenden Atlantiks: Hochauflösende Zeitreihen von ODP-Sites 658-661*. Ph.D. thesis, Christian-Albrechts-Universität Kiel (1991).
610. Tiedemann, R., Sturm, A., Steph, S., Lund, S. & Stoner, J. Astronomically calibrated timescales from 6 to 2.5 Ma and benthic isotope stratigraphies, Sites 1236, 1237, 1239, and 1241. In *Proceedings of the Ocean Drilling Program, 202 Scientific Results*, https://doi.org/10.2973/odp.proc.sr.202.210.2007 (Ocean Drilling Program, 2007).
611. Tierney, J. E., Pausata, F. S. R. & deMenocal, P. Deglacial Indian monsoon failure and North Atlantic stadials linked by Indian Ocean surface cooling. *Nat. Geosci.* **9**, 46–50, https://doi.org/10.1038/ngeo2603 (2016).
612. Trela, W., Krzemińska, E., Jewuła, K. & Czupyt, Z. Oxygen isotopes from apatite of Middle and Late Ordovician conodonts in Peri-Baltica (the Holy Cross Mountains, Poland) and their climatic implications. *Geosciences* **12**, https://doi.org/10.3390/geosciences12040165 (2022).
613. Tripati, A. & Zachos, J. Late Eocene tropical sea surface temperatures: A perspective from Panama. *Paleoceanography* **17**, 4-1–4-14, https://doi.org/10.1029/2000pa000605 (2002).
614. Tripati, A. K. *et al*. Tropical sea-surface temperature reconstruction for the early Paleogene using Mg/Ca ratios of planktonic foraminifera. *Paleoceanography* **18**, https://doi.org/10.1029/2003pa000937 (2003).
615. Tripati, A. K. & Elderfield, H. Abrupt hydrographic changes in the equatorial Pacific and subtropical Atlantic from foraminiferal Mg/Ca indicate greenhouse origin for the Thermal Maximum at the Paleocene-Eocene Boundary. *Geochem. Geophys. Geosyst.* **5**, https://doi.org/10.1029/2003gc000631 (2004).
616. Trotter, J. A., Williams, I. S., Barnes, C. R., Lécuyer, C. & Nicoll, R. S. Did cooling oceans trigger Ordovician biodiversification? Evidence from conodont thermometry. *Science* **321**, 550–554, https://doi.org/10.1126/science.1155814 (2008).
617. Trotter, J. A., Williams, I. S., Nicora, A., Mazza, M. & Rigo, M. Long-term cycles of Triassic climate change: a new δ^{18}O record from conodont apatite. *Earth Planet. Sci. Lett.* **415**, 165–174, https://doi.org/10.1016/j.epsl.2015.01.038 (2015).
618. Trotter, J. A., Williams, I. S., Barnes, C. R., Männik, P. & Simpson, A. New conodont δ^{18}O records of Silurian climate change: Implications for environmental and biological events. *Palaeogeography, Palaeoclimatology, Palaeoecology* **443**, 34–48, https://doi.org/10.1016/j.palaeo.2015.11.011 (2016).
619. Tzanova, A. & Herbert, T. D. Regional and global significance of Pliocene sea surface temperatures from the Gulf of Cadiz (Site U1387) and the Mediterranean. *Glob. Planet. Change* **133**, 371–377, https://doi.org/10.1016/j.gloplacha.2015.07.001 (2015).
620. Ullmann, C. V. *et al*. Partial diagenetic overprint of Late Jurassic belemnites from New Zealand: Implications for the preservation potential of δ^7Li values in calcite fossils. *Geochim. Cosmochim. Acta* **120**, 80–96, https://doi.org/10.1016/j.gca.2013.06.029 (2013).
621. Ullmann, C., Campbell, H., Frei, R. & Korte, C. Geochemical signatures in Late Triassic brachiopods from New Caledonia. *N. ZealJ. Geol. Geophysics* **57**, 420–431, https://doi.org/10.1080/00288306.2014.958175 (2014).
622. Ullmann, C. V., Campbell, H. J., Frei, R. & Korte, C. Oxygen and carbon isotope and Sr/Ca signatures of high-latitude Permian to Jurassic calcite fossils from New Zealand and New Caledonia. *Gondwana Res.* **38**, 60–73, https://doi.org/10.1016/j.gr.2015.10.010 (2016).
623. van de Schootbrugge, B., Föllmi, K. B., Bulot, L. G. & Burns, S. J. Paleoceanographic changes during the early Cretaceous (Valanginian–Hauterivian): evidence from oxygen and carbon stable isotopes. *Earth Planet. Sci. Lett.* **181**, 15–31, https://doi.org/10.1016/S0012-821X(00)00194-1 (2000).
624. van de Schootbrugge, B. *et al*. Toarcian oceanic anoxic event: An assessment of global causes using belemnite C isotope records. *Paleoceanography* **20**, https://doi.org/10.1029/2004pa001102 (2005).
625. van de Schootbrugge, B. *et al*. Early Jurassic climate change and the radiation of organic-walled phytoplankton in the Tethys Ocean. *Paleobiology* **31**, 73–97, 10.1666/0094-8373(2005)031<0073:ejccat>2.0.co;2 (2005).
626. van de Schootbrugge, B. *et al*. End-Triassic calcification crisis and blooms of organic-walled 'disaster species'. *Palaeogeography, Palaeoclimatology, Palaeoecology* **244**, 126–141, https://doi.org/10.1016/j.palaeo.2006.06.026 (2007).
627. van der Weijst, C. M. H. *et al*. A fifteen-million-year surface- and subsurface-integrated TEX_{86} temperature record from the eastern equatorial Atlantic. *Clim. Past* https://doi.org/10.5194/cp-2021-92 (2021).
628. van Eijden, A. & Ganssen, G. An Oligocene multi-species foraminiferal oxygen and carbon isotope record from ODP Hole 758A (Indian Ocean): Paleoceanographic and paleo-ecologic implications. *Mar. Micropaleontology* **25**, 47–65, https://doi.org/10.1016/0377-8398(94)00028-l (1995).
629. van Geldern, R. *et al*. Carbon, oxygen and strontium isotope records of Devonian brachiopod shell calcite. *Palaeogeography, Palaeoclimatology, Palaeoecology* **240**, 47–67, https://doi.org/10.1016/j.palaeo.2006.03.045 (2006).
630. van Helmond, N. A. G. M. *et al*. A perturbed hydrological cycle during Oceanic Anoxic Event 2. *Geology* **42**, 123–126, https://doi.org/10.1130/g34929.1 (2013).
631. van Helmond, N. A. G. M. *et al*. Freshwater discharge controlled deposition of Cenomanian–Turonian black shales on the NW European epicontinental shelf (Wunstorf, northern Germany. *Clim. Past.* **11**, 495–508, https://doi.org/10.5194/cp-11-495-2015 (2015).
632. Veizer, J. & Hoefs, J. The nature of ^{18}O/^{16}O and ^{13}C/^{12}C secular trends in sedimentary carbonate rocks. *Geochim. Cosmochim. Acta* **40**, 1387–1395, https://doi.org/10.1016/0016-7037(76)90129-0 (1976).

633. Veizer, J., Fritz, P. & Jones, B. Geochemistry of brachiopods: Oxygen and carbon isotopic records of Paleozoic oceans. *Geochim. Cosmochim. Acta* **50**, 1679–1696, https://doi.org/10.1016/0016-7037(86)90130-4 (1986).
634. Veizer, J. *et al.* $^{87}Sr/^{86}Sr$, $\delta^{13}C$ and $\delta^{18}O$ evolution of Phanerozoic seawater. *Chem. Geol.* **161**, 59–88, https://doi.org/10.1016/s0009-2541(99)00081-9 (1999).
635. Vellekoop, J. *et al.* Rapid short-term cooling following the Chicxulub impact at the Cretaceous-Paleogene boundary. *Proc. Natl Acad. Sci.* **111**, 7537–7541, https://doi.org/10.1073/pnas.1319253111 (2014).
636. Vellekoop, J. *et al.* Evidence for Cretaceous-Paleogene boundary bolide "impact winter" conditions from New Jersey, USA. *Geology* **44**, 619–622, https://doi.org/10.1130/g37961.1 (2016).
637. Venti, N. L. & Billups, K. Surface water hydrography of the Kuroshio extension during the Pliocene–Pleistocene climate transition. *Mar. Micropaleontology* **101**, 106–114, https://doi.org/10.1016/j.marmicro.2013.02.004 (2013).
638. Venti, N. L., Billups, K. & Herbert, T. D. Paleoproductivity in the northwestern Pacific Ocean during the Pliocene-Pleistocene climate transition (3.0–1.8ma). *Paleoceanography* **32**, 92–103, https://doi.org/10.1002/2016pa002955 (2017).
639. Venz, K. A., Hodell, D. A., Stanton, C. & Warnke, D. A. A 1.0 Myr record of Glacial North Atlantic Intermediate Water variability from ODP Site 982 in the northeast Atlantic. *Paleoceanography* **14**, 42–52, https://doi.org/10.1029/1998pa900013 (1999).
640. Vickers, M. L. *et al.* Unravelling Middle to Late Jurassic palaeoceanographic and palaeoclimatic signals in the Hebrides Basin using belemnite clumped isotope thermometry. *Earth Planet. Sci. Lett.* **546**, 116401, https://doi.org/10.1016/j.epsl.2020.116401 (2020).
641. Vincent, E., Killingley, J. S. & Berger, W. H. Miocene oxygen and carbon isotope stratigraphy of the tropical Indian Ocean. In *Geological Society of America Memoirs*, 103–130, https://doi.org/10.1130/mem163-p103 (Geological Society of America, 1985).
642. Vincent, E., Shackleton, N. & Hall, M. Miocene oxygen and carbon isotope stratigraphy of planktonic foraminifers at Sites 709 and 758, tropical Indian Ocean. In *Proceedings of the Ocean Drilling Program, 121 Scientific Results*, https://doi.org/10.2973/odp.proc.sr.121.134.1991 (Ocean Drilling Program, 1991).
643. Voigt, S. Stable oxygen and carbon isotopes from brachiopods of southern England and northwestern Germany: Estimation of Upper Turonian palaeotemperatures. *Geol. Mag.* **137**, 687–703, https://doi.org/10.1017/s0016756800004696 (2000).
644. Voigt, S., Wilmsen, M., Mortimore, R. N. & Voigt, T. Cenomanian palaeotemperatures derived from the oxygen isotopic composition of brachiopods and belemnites: evaluation of Cretaceous palaeotemperature proxies. *Int. J. Earth Sci.* **92**, 285–299, https://doi.org/10.1007/s00531-003-0315-1 (2003).
645. Wade, B. S. & Kroon, D. Middle Eocene regional climate instability: Evidence from the western North Atlantic. *Geology* **30**, 1011, 10.1130/0091-7613(2002)030<1011:mercie>2.0.co;2 (2002).
646. Wade, B. S. & Pearson, P. N. Planktonic foraminiferal turnover, diversity fluctuations and geochemical signals across the Eocene/Oligocene boundary in Tanzania. *Mar. Micropaleontology* **68**, 244–255, https://doi.org/10.1016/j.marmicro.2008.04.002 (2008).
647. Wade, B. S. *et al.* Multiproxy record of abrupt sea-surface cooling across the Eocene-Oligocene transition in the Gulf of Mexico. *Geology* **40**, 159–162, https://doi.org/10.1130/g32577.1 (2012).
648. Wadleigh, M. A. & Veizer, J. $^{18}O/^{16}O$ and $^{13}C/^{12}C$ in lower Paleozoic articulate brachiopods: Implications for the isotopic composition of seawater. *Geochim. Cosmochim. Acta* **56**, 431–443, https://doi.org/10.1016/0016-7037(92)90143-7 (1992).
649. Wagner, T. *et al.* Rapid warming and salinity changes of Cretaceous surface waters in the subtropical North Atlantic. *Geology* **36**, 203, https://doi.org/10.1130/g24523a.1 (2008).
650. Wallace, Z. A. & Elrick, M. Early Mississippian orbital-scale glacio-eustasy detected from high-resolution oxygen isotopes of marine apatite (conodonts). *J. Sediment. Res.* **84**, 816–824, https://doi.org/10.2110/jsr.2014.69 (2014).
651. Wang, W. *et al.* A high-resolution Middle to Late Permian paleotemperature curve reconstructed using oxygen isotopes of well-preserved brachiopod shells. *Earth Planet. Sci. Lett.* **540**, 116245, https://doi.org/10.1016/j.epsl.2020.116245 (2020).
652. Wang, M. *et al.* Late Miocene-Pliocene Asian summer monsoon variability linked to both tropical Pacific temperature and Walker Circulation. *Earth Planet. Sci. Lett.* **561**, 116823, https://doi.org/10.1016/j.epsl.2021.116823 (2021).
653. Wara, M. W., Ravelo, A. C. & Delaney, M. L. Permanent El Niño-like conditions during the Pliocene warm period. *Science* **309**, 758–761, https://doi.org/10.1126/science.1112596 (2005).
654. Weinerová, H. *et al.* Oxygen and carbon stable isotope records of the Lochkovian-Pragian boundary interval from the Prague Basin (Lower Devonian, Czech Republic). *Palaeogeography, Palaeoclimatology, Palaeoecology* **560**, 110036, https://doi.org/10.1016/j.palaeo.2020.110036 (2020).
655. Weirauch, D., Billups, K. & Martin, P. Evolution of millennial-scale climate variability during the mid-Pleistocene. *Paleoceanography* **23**, https://doi.org/10.1029/2007pa001584 (2008).
656. Wells, P., Wells, G., Cali, J. & Chivas, A. Response of deep-sea benthic foraminifera to Late Quaternary climate changes, southeast Indian Ocean, offshore Western Australia. *Mar. Micropaleontology* **23**, 185–229, https://doi.org/10.1016/0377-8398(94)90013-2 (1994).
657. Wenzel, B. & Joachimski, M. M. Carbon and oxygen isotopic composition of Silurian brachiopods (Gotland/Sweden): Palaeoceanographic implications. *Palaeogeography, Palaeoclimatology, Palaeoecology* **122**, 143–166, https://doi.org/10.1016/0031-0182(95)00094-1 (1996).
658. Wenzel, B., Lécuyer, C. & Joachimski, M. M. Comparing oxygen isotope records of Silurian calcite and phosphate—$\delta^{18}O$ compositions of brachiopods and conodonts. *Geochim. Cosmochim. Acta* **64**, 1859–1872, https://doi.org/10.1016/s0016-7037(00)00337-9 (2000).
659. Wheeley, J. R., Smith, M. P. & Boomer, I. Oxygen isotope variability in conodonts: implications for reconstructing Palaeozoic palaeoclimates and palaeoceanography. *J. Geol. Soc.* **169**, 239–250, https://doi.org/10.1144/0016-76492011-048 (2012).
660. Wheeley, J. R., Jardine, P. E., Raine, R. J., Boomer, I. & Smith, M. P. Paleoecologic and paleoceanographic interpretation of $\delta^{18}O$ variability in Lower Ordovician conodont species. *Geology* **46**, 467–470, https://doi.org/10.1130/g40145.1 (2018).
661. Whitman, J. M. & Berger, W. Pliocene-Pleistocene oxygen isotope record Site 586, Ontong Java Plateau. *Mar. Micropaleontology* **18**, 171–198, https://doi.org/10.1016/0377-8398(92)90012-9 (1992).
662. Wierzbowski, H. Detailed oxygen and carbon isotope stratigraphy of the Oxfordian in Central Poland. *Int. J. Earth Sci.* **91**, 304–314, https://doi.org/10.1007/s005310100217 (2002).
663. Wierzbowski, H. Carbon and oxygen isotope composition of Oxfordian–Early Kimmeridgian belemnite rostra: Palaeoenvironmental implications for Late Jurassic seas. *Palaeogeography, Palaeoclimatology, Palaeoecology* **203**, 153–168, https://doi.org/10.1016/s0031-0182(03)00673-4 (2004).
664. Wierzbowski, H. & Joachimski, M. Reconstruction of late Bajocian–Bathonian marine palaeoenvironments using carbon and oxygen isotope ratios of calcareous fossils from the Polish Jura Chain (central Poland). *Palaeogeography, Palaeoclimatology, Palaeoecology* **254**, 523–540, https://doi.org/10.1016/j.palaeo.2007.07.010 (2007).
665. Wierzbowski, H., Dembicz, K. & Praszkier, T. Oxygen and carbon isotope composition of Callovian–Lower Oxfordian (Middle–Upper Jurassic) belemnite rostra from central Poland: A record of a late Callovian global sea-level rise. *Palaeogeography, Palaeoclimatology, Palaeoecology* **283**, 182–194, https://doi.org/10.1016/j.palaeo.2009.09.020 (2009).
666. Wierzbowski, H. Seawater temperatures and carbon isotope variations in central European basins at the Middle-Late Jurassic transition (Late Callovian-Early Kimmeridgian). *Palaeogeography, Palaeoclimatology, Palaeoecology* **440**, 506–523, https://doi.org/10.1016/j.palaeo.2015.09.020 (2015).
667. Wierzbowski, H., Szaniawski, H. & Błażejowski, B. Structural, chemical and isotope evidence for secondary phosphate mineralization of grasping spines of Early Palaeozoic chaetognaths. *Lethaia* **54**, 245–259, https://doi.org/10.1111/let.12400 (2021).

668. Wilf, P., Johnson, K. R. & Huber, B. T. Correlated terrestrial and marine evidence for global climate changes before mass extinction at the Cretaceous-Paleogene boundary. *Proc. Natl Acad. Sci.* **100**, 599–604, https://doi.org/10.1073/pnas.0234701100 (2003).
669. Wilson, P. A., Norris, R. D. & Cooper, M. J. Testing the Cretaceous greenhouse hypothesis using glassy foraminiferal calcite from the core of the Turonian tropics on Demerara Rise. *Geology* **30**, 607, 10.1130/0091-7613(2002)030<0607:ttcghu>2.0.co;2 (2002).
670. Windler, G., Tierney, J. E., DiNezio, P. N., Gibson, K. & Thunell, R. Shelf exposure influence on Indo-Pacific Warm Pool climate for the last 450,000 years. *Earth Planet. Sci. Lett.* **516**, 66–76, https://doi.org/10.1016/j.epsl.2019.03.038 (2019).
671. Wittkopp, F. *et al. Sea Surf. Temp. estimates sediment. cores Jpn. Sea* https://doi.org/10.1594/PANGAEA.879742 (2017).
672. Wittkopp, F. *Org. geochemical investigation Sediment. Jpn. Sea: Track. paleoceanographic paleoclimatic changes mid-Miocene* https://doi.org/10.1594/PANGAEA.881046 (2017).
673. Woelders, L. *et al.* Latest Cretaceous climatic and environmental change in the South Atlantic region. *Paleoceanography* **32**, 466–483, https://doi.org/10.1002/2016pa003007 (2017).
674. Woelders, L. *et al.* Robust multi-proxy data integration, using late Cretaceous paleotemperature records as a case study. *Earth Planet. Sci. Lett.* **500**, 215–224 (2018).
675. Wojcieszek, D. & Dekens, P. *South. Atl. Ocean. Oxyg. isotope Mg/Ca data last 5 Ma* https://www.ncdc.noaa.gov/paleo-search/study/20325 (2010).
676. Woodruff, F. & Savin, S. Mid-Miocene isotope stratigraphy in the deep sea: High-resolution correlations, paleoclimatic cycles, and sediment preservation. *Paleoceanography* **6**, 755–806, https://doi.org/10.1029/91pa02561 (1991).
677. Wu, Y. *et al.* Evolution of the upper ocean stratification in the Japan Sea since the last glacial. *Geophys. Res. Lett.* **47**, https://doi.org/10.1029/2020gl088255 (2020).
678. Wu, B. *et al.* Roadian-Wordian (Middle Permian) conodont biostratigraphy, sedimentary facies and paleotemperature evolution at the Shuixiakou Section, Xikou Area, Southeastern Qinling Region, China. *J. Earth Sci.* **32**, 534–553, https://doi.org/10.1007/s12583-020-1099-y (2021).
679. Yamamoto, M., Kishizaki, M., Oba, T. & Kawahata, H. Intense winter cooling of the surface water in the northern Okinawa Trough during the last glacial period. *J. Asian Earth Sci.* **69**, 86–92, https://doi.org/10.1016/j.jseaes.2012.06.011 (2013).
680. Yamamoto, M., Sai, H., Chen, M.-T. & Zhao, M. The East Asian winter monsoon variability in response to precession during the past 150,000 yr. *Clim. Past.* **9**, 2777–2788, https://doi.org/10.5194/cp-9-2777-2013 (2013).
681. Yamamoto, M. & Kobayashi, D. Surface ocean cooling in the subarctic North Pacific during the late Pliocene suggests an atmospheric reorganization prior to extensive Northern Hemisphere glaciation. *Deep. Sea Res. Part. II: Topical Stud. Oceanography* **125-126**, 177–183, https://doi.org/10.1016/j.dsr2.2015.03.005 (2016).
682. Yao, L. *et al.* Global cooling initiated the Middle-Late Mississippian biodiversity crisis. *Glob. Planet. Change* **215**, 103852, https://doi.org/10.1016/j.gloplacha.2022.103852 (2022).
683. Zachos, J. C., Stott, L. D. & Lohmann, K. C. Evolution of Early Cenozoic marine temperatures. *Paleoceanography* **9**, 353–387, https://doi.org/10.1029/93pa03266 (1994).
684. Zachos, J. C. *et al.* A transient rise in tropical sea surface temperature during the Paleocene-Eocene Thermal Maximum. *Science* **302**, 1551–1554, https://doi.org/10.1126/science.1090110 (2003).
685. Zachos, J. *et al.* Extreme warming of mid-latitude coastal ocean during the Paleocene-Eocene Thermal Maximum: Inferences from TEX_{86} and isotope data. *Geology* **34**, 737, https://doi.org/10.1130/g22522.1 (2006).
686. Žák, K. *et al.* Comparison of carbonate C and O stable isotope records across the Jurassic/Cretaceous boundary in the Tethyan and Boreal Realms. *Palaeogeography, Palaeoclimatology, Palaeoecology* **299**, 83–96, https://doi.org/10.1016/j.palaeo.2010.10.038 (2011).
687. Zakharov, Y. D., Ignatyev, A. V., Ukhaneva, N. G. & Afanasyeva, T. Cretaceous ammonoid succession in the Far East (South Sakhalin). *Bull. Inst. R. Sci. Natur. Belgique* **66**, 109–127 (1996).
688. Zakharov, Y. D. *et al.* Palaeotemperature curve for the Late Cretaceous of the northwestern circum-Pacific. *Cretac. Res.* **20**, 685–697, https://doi.org/10.1006/cres.1999.0175 (1999).
689. Zakharov, Y. D. *et al.* Seasonal temperature fluctuations in the high northern latitudes during the Cretaceous Period: Isotopic evidence from Albian and Coniacian shallow-water invertebrates of the Talovka River Basin, Koryak Upland, Russian Far East. *Cretac. Res.* **26**, 113–132, https://doi.org/10.1016/j.cretres.2004.11.005 (2005).
690. Zakharov, Y. D. *et al.* Late Barremian–early Aptian climate of the northern middle latitudes: Stable isotope evidence from bivalve and cephalopod molluscs of the Russian Platform. *Cretac. Res.* **44**, 183–201, https://doi.org/10.1016/j.cretres.2013.04.007 (2013).
691. Zhang, Y. G., Pagani, M., Liu, Z., Bohaty, S. M. & DeConto, R. A 40-million-year history of atmospheric CO_2. *Phil. Trans. R. Soc. A.* **371**, 20130096, https://doi.org/10.1098/rsta.2013.0096 (2013).
692. Zhang, Y. G., Pagani, M. & Liu, Z. A 12-million-year temperature history of the tropical Pacific Ocean. *Science* **344**, 84–87, https://doi.org/10.1126/science.1246172 (2014).
693. Zhang, X., Joachimski, M. M. & Gong, Y. Late Devonian greenhouse-icehouse climate transition: New evidence from conodont $\delta^{18}O$ thermometry in the eastern Palaeotethys (Lali section, South China). *Chem. Geol.* **581**, 120383, https://doi.org/10.1016/j.chemgeo.2021.120383 (2021).
694. Zhuang, G., Pagani, M. & Zhang, Y. G. Monsoonal upwelling in the western Arabian Sea since the middle Miocene. *Geology* **45**, 655–658, https://doi.org/10.1130/g39013.1 (2017).
695. Žigaitė, Ž., Joachimski, M. M., Lehnert, O. & Brazauskas, A. $\delta^{18}O$ composition of conodont apatite indicates climatic cooling during the Middle Pridoli. *Palaeogeography, Palaeoclimatology, Palaeoecology* **294**, 242–247, https://doi.org/10.1016/j.palaeo.2010.03.033 (2010).
696. O'Brien, C. L. *et al.* Cretaceous sea-surface temperature evolution: Constraints from TEX_{86} and planktonic foraminiferal oxygen isotopes. *Earth-Sci. Rev.* **172**, 224–247, https://doi.org/10.1016/j.earscirev.2017.07.012 (2017).
697. Evans, D. *et al.* Eocene greenhouse climate revealed by coupled clumped isotope-Mg/Ca thermometry. *Proc. Natl Acad. Sci.* **115**, 1174–1179, https://doi.org/10.1073/pnas.1714744115 (2018).
698. Jonkers, L. *et al.* Integrating palaeoclimate time series with rich metadata for uncertainty modelling: Strategy and documentation of the palmod 130k marine palaeoclimate data synthesis. *Earth Syst. Sci. Data* **12**, 1053–1081, https://doi.org/10.5194/essd-12-1053-2020 (2020).
699. Kaufman, D. *et al.* A global database of Holocene paleotemperature records. *Sci. Data* **7**, 1–34, https://doi.org/10.1038/s41597-020-0445-3 (2020).
700. Osman, M. B. *et al.* Globally resolved surface temperatures since the Last Glacial Maximum. *Nature* **599**, 239–244, https://doi.org/10.1038/s41586-021-03984-4 (2021).
701. Seton, M. *et al.* A global data set of present–day oceanic crustal age and seafloor spreading parameters. *Geochemistry, Geophysics, Geosystems* **21**, https://doi.org/10.1029/2020GC009214 (2020).
702. Popp, B. N., Anderson, T. F. & Sandberg, P. A. Textural, elemental, and isotopic variations among constituents in Middle Devonian limestones, North America. *J. Sediment. Res.* **56**, 715–727, https://doi.org/10.1306/212F8A26-2B24-11D7-8648000102C1865D (1986).
703. Rejebian, V. A., Harris, A. G. & Huebner, J. S. Conodont color and textural alteration: An index to regional metamorphism, contact metamorphism, and hydrothermal alteration. *Geol. Soc. Am. Bull.* **99**, 471–479, https://doi.org/10.1130/0016-7606(1987)99 (1987).
704. Kim, J.-H. *et al.* New indices and calibrations derived from the distribution of crenarchaeal isoprenoid tetraether lipids: Implications for past sea surface temperature reconstructions. *Geochim. Cosmochim. Acta* **74**, 4639–4654, https://doi.org/10.1016/j.gca.2010.05.027 (2010).

705. Inglis, G. N. & Tierney, J. E. *The $TEX_{8}6$ Paleotemperature Proxy*. Elements in Geochemical Tracers in Earth System Science (Cambridge University Press, 2020).
706. LeGrande, A. N. & Schmidt, G. A. Global gridded data set of the oxygen isotopic composition in seawater. *Geophysical research letters* **33** (2006).
707. Scotese, C. R. & Wright, N. PALEOMAP paleodigital elevation models (PaleoDEMS) for the Phanerozoic. https://www.earthbyte.org/paleodem-resource-scotese-and-wright-2018 (2018).
708. Peters, S. E., Husson, J. M. & Czaplewski, J. Macrostrat: A platform for geological data integration and deep-time Earth crust research. *Geochemistry, Geophysics, Geosystems* **19**, 1393–1409, https://doi.org/10.1029/2018GC007467 (2018).
709. Alroy, J. *et al*. Effects of sampling standardization on estimates of Phanerozoic marine diversification. *Proc. Natl Acad. Sci.* **98**, 6261–6266, https://doi.org/10.1073/pnas.111144698 (2001).
710. Gradstein, F. M., Ogg, J. G., Schmitz, M. D. & Ogg, G. M. *Geologic Time Scale 2020* (Elsevier, 2020).
711. Rontani, J.-F., Volkman, J. K., Prahl, F. & Wakeham, S. G. Biotic and abiotic degradation of alkenones and implications for $U^{K'}_{37}$ paleoproxy applications: A review. *Org. Geochem.* **59**, 95–113, https://doi.org/10.1016/j.orggeochem.2013.04.005 (2013).
712. Wycech, J. B. *et al*. Comparison of $\delta^{18}O$ analyses on individual planktic foraminifer (Orbulina universa) shells by SIMS and gas-source mass spectrometry. *Chem. Geol.* **483**, 119–130, https://doi.org/10.1016/j.chemgeo.2018.02.028 (2018).
713. Brand, U. & Morrison, J. Paleoscene# 6. Biogeochemistry of fossil marine invertebrates. *Geosci. Can.* **14**, 85–107 (1987).
714. Morrison, J. & Brand, U. Paleoscene# 5. Geochemistry of recent marine invertebrates. *Geosci. Can.* **13**, 237–254 (1986).
715. Brown, S. J. & Elderfield, H. Variations in Mg/Ca and Sr/Ca ratios of planktonic foraminifera caused by postdepositional dissolution: Evidence of shallow Mg-dependent dissolution. *Paleoceanography* **11**, 543–551, https://doi.org/10.1029/96PA01491 (1996).
716. Rosenthal, Y. *et al*. Interlaboratory comparison study of Mg/Ca and Sr/Ca measurements in planktonic foraminifera for paleoceanographic research. *Geochemistry, Geophysics, Geosystems* **5**, https://doi.org/10.1029/2003GC000650 (2004).
717. Hopmans, E. C. *et al*. A novel proxy for terrestrial organic matter in sediments based on branched and isoprenoid tetraether lipids. *Earth Planet. Sci. Lett.* **224**, 107–116, https://doi.org/10.1016/j.epsl.2004.05.012 (2004).
718. Zhang, Y. G. *et al*. Methane Index: A tetraether archaeal lipid biomarker indicator for detecting the instability of marine gas hydrates. *Earth Planet. Sci. Lett.* **307**, 525–534, https://doi.org/10.1016/j.epsl.2011.05.031 (2011).
719. Zhang, Y. G., Pagani, M. & Wang, Z. Ring Index: A new strategy to evaluate the integrity of TEX_{86} paleothermometry. *Paleoceanography* **31**, 220–232, https://doi.org/10.1002/2015PA002848 (2016).
720. Filippova, A., Kienast, M., Frank, M. & Schneider, R. R. Alkenone paleothermometry in the North Atlantic: A review and synthesis of surface sediment data and calibrations. *Geochemistry, Geophysics, Geosystems* **17**, 1370–1382, https://doi.org/10.1002/2015GC006106 (2016).
721. Wang, K. J. *et al*. Group 2i Isochrysidales produce characteristic alkenones reflecting sea ice distribution. *Nat. Commun.* **12**, 15, https://doi.org/10.1038/s41467-020-20187-z (2021).
722. Urey, H. C. The thermodynamic properties of isotopic substances. *Journal of the Chemical Society (Resumed)* 562–581 (1947).
723. Brassell, S. C. Climatic influences on the Paleogene evolution of alkenones. *Paleoceanography* **29**, 255–272, https://doi.org/10.1002/2013PA002576 (2014).
724. Schrag, D. P. Effects of diagenesis on the isotopic record of late Paleogene tropical sea surface temperatures. *Chem. Geol.* **161**, 215–224 (1999).
725. Walker, L. J., Wilkinson, B. H. & Ivany, L. C. Continental drift and Phanerozoic carbonate accumulation in shallow-shelf and deep-marine settings. *J. Geol.* **110**, 75–87, https://doi.org/10.1086/324318 (2002).
726. Haq, B. U. & Al-Qahtani, A. M. Phanerozoic cycles of sea-level change on the Arabian Platform. *GeoArabia* **10**, 127–160, https://doi.org/10.2113/geoarabia1002127 (2005).
727. Mackenzie, F. & Pigott, J. Tectonic controls of Phanerozoic sedimentary rock cycling. *J. Geol. Soc.* **138**, 183–196, https://doi.org/10.1144/gsjgs.138.2.0183 (1981).
728. Clark, D. L. Extinction of conodonts. *Journal of Paleontology* 652–661 (1983).
729. Müller, R. D. *et al*. GPlates: Building a virtual Earth through deep time. *Geochemistry, Geophysics, Geosystems* **19**, 2243–2261, https://doi.org/10.1029/2018GC007584 (2018).
730. Raja, N. B. *et al*. Colonial history and global economics distort our understanding of deep-time biodiversity. *Nature Ecology & Evolution* https://doi.org/10.1038/s41559-021-01608-8 (2021).
731. Veizer, J. & Prokoph, A. Temperatures and oxygen isotopic composition of Phanerozoic oceans. *Earth-Sci. Rev.* **146**, 92–104, https://doi.org/10.1016/j.earscirev.2015.03.008 (2015).
732. Jaffrés, J. B., Shields, G. A. & Wallmann, K. The oxygen isotope evolution of seawater: A critical review of a long-standing controversy and an improved geological water cycle model for the past 3.4 billion years. *Earth-Sci. Rev.* **83**, 83–122, https://doi.org/10.1016/j.earscirev.2007.04.002 (2007).
733. Montañez, I. P. & Poulsen, C. J. The Late Paleozoic Ice Age: An evolving paradigm. *Annu. Rev. Earth Planet. Sci.* **41**, 629–656, https://doi.org/10.1146/annurev.earth.031208.100118 (2013).
734. Bemis, B. E., Spero, H. J., Bijma, J. & Lea, D. W. Reevaluation of the oxygen isotopic composition of planktonic foraminifera: Experimental results and revised paleotemperature equations. *Paleoceanography* **13**, 150–160, https://doi.org/10.1029/98PA00070 (1998).
735. Grossman, E. L. & Ku, T.-L. Oxygen and carbon isotope fractionation in biogenic aragonite: temperature effects. *Chem. Geology: Isotope Geosci. Sect.* **59**, 59–74, https://doi.org/10.1016/0168-9622(86)90057-6 (1986).
736. Kim, S.-T. & O'Neil, J. R. Equilibrium and nonequilibrium oxygen isotope effects in synthetic carbonates. *Geochimica et. cosmochimica acta* **61**, 3461–3475, https://doi.org/10.1016/S0016-7037(97)00169-5 (1997).
737. Grossman, E. L. Applying oxygen isotope paleothermometry in deep time. *Paleontological Soc. Pap.* **18**, 39–68, https://doi.org/10.1017/S1089332600002540 (2012).
738. Pucéat, E. *et al*. Revised phosphate-water fractionation equation reassessing paleotemperatures derived from biogenic apatite. *Earth Planet. Sci. Lett.* **298**, 135–142, https://doi.org/10.1016/j.epsl.2010.07.034 (2010).
739. Anand, P., Elderfield, H. & Conte, M. H. Calibration of Mg/Ca thermometry in planktonic foraminifera from a sediment trap time series. *Paleoceanography* **18**, https://doi.org/10.1029/2002PA000846 (2003).
740. Schouten, S., Hopmans, E. C., Schefuß, E. & Damste, J. S. S. Distributional variations in marine crenarchaeotal membrane lipids: a new tool for reconstructing ancient sea water temperatures. *Earth Planet. Sci. Lett.* **204**, 265–274, https://doi.org/10.1016/S0012-821X(02)00979-2 (2002).
741. Müller, P. J., Kirst, G., Ruhland, G., Von Storch, I. & Rosell-Melé, A. Calibration of the alkenone paleotemperature index $U^{K'}_{37}$ based on core-tops from the eastern South Atlantic and the global ocean (60°N-60°S). *Geochim. Cosmochim. Acta* **62**, 1757–1772, https://doi.org/10.1016/S0016-7037(98)00097-0 (1998).
742. Conte, M. H. *et al*. Global temperature calibration of the alkenone unsaturation index ($U^{K'}_{37}$) in surface waters and comparison with surface sediments. *Geochemistry, Geophysics, Geosystems* **7**, https://doi.org/10.1029/2005GC001054 (2006).

Acknowledgements
The authors would like to acknowledge the numerous researchers who generated the original data, many of whom kindly provided additional metadata upon request. EJJ was supported by the PhanTASTIC Postdoctoral Fellowship, funded by Roland and Debra Sauermann. JET was supported by grant #2016-015 from the Heising-Simons Foundation. Additional funding support was provided by: NERC NE/N015045/1 to HLF, GCRF Royal Society Dorothy Hodgkin Fellowship DHF\ R1\191178 to GNI, the Schlanger Ocean Drilling Fellowship to RR, NSF OCE-2202760 to WS, the Student Awards Agency Scotland to MLS, and the University of Arizona Technology and Research Initiative Fund to KT.

Author contributions
Authorship is subdivided into three tiers. The first tier (E.J.J., J.E.T., B.T.H., S.L.W. & D.J.L.) reflects the core PhanTASTIC team; i.e., those who conceived of, supervised, and/or carried out the execution of the broader PhanSST project. B.T.H. and S.L.W. conceived the project and acquired funding. E.J.J. and J.E.T. spearheaded the data collection and developed the metadata structure. E.J.J. performed the database statistics analyses and drafted the manuscript. All first tier authors contributed edits to the initial draft of the manuscript. The second tier (listed alphabetically: H.L.F., G.N.I., E.L.M., C.L.O., R.R., W.S., M.L.S., K.T.) are those who contributed substantially to the database by: entering >15 of records into the template and/or quality control checking >25 records. The third tier (listed alphabetically: E.A., M.J.C., R.R.D., D.E., W.R.G., E.L.G., M.J.H., B.N.H., K.G.M., L.K.O., M.L.S.M., H.S., Y.G.Z.) includes everyone else who, at a minimum, entered at least one record into the database template. All authors reviewed the manuscript.

Competing interests
The authors declare no competing interests.

Additional information
Correspondence and requests for materials should be addressed to E.J.J.

Reprints and permissions information is available at www.nature.com/reprints.

Publisher's note Springer Nature remains neutral with regard to jurisdictional claims in published maps and institutional affiliations.